THERMODYNAMIC STUDIES OF HYDRIDE- AND PROTON-DONOR ABILITIES OF HETEROLEPTIC TRANSITION METAL COMPLEXES CONTAINING TRIPHOSPHINE AND MONOPHOSPHINE LIGANDS

_____

A Thesis

Presented to

The Faculty of the Department of Chemistry

Sam Houston State University

_____

In Partial Fulfillment

of the Requirements for the Degree of

Master of Science

_____

by

William Fernandez

August, 2020

THERMODYNAMIC STUDIES OF HYDRIDE- AND PROTON-DONOR ABILITIES OF HETEROLEPTIC TRANSITION METAL COMPLEXES CONTAINING TRIPHOSPHINE AND MONOPHOSPHINE LIGANDS

by

William Fernandez

_____

APPROVED:

Christopher M. Zall, PhD
Thesis Director

Benny E. Arney, PhD
Committee Member

Richard E. Norman, PhD
Committee Member

John B. Pascarella, PhD
Dean, College of Science and Engineering Technology

DEDICATION

I dedicate the time, work, and research efforts of this thesis to my mom, sister, brother and the rest of my family. All of the consultations I have had with my family has helped pushed me through this and better appreciate all the little things in life. I would definitely not be where I am if not for my family and all the help and wisdom, they provide me to push through and continue.

ABSTRACT

Fernandez, William, *Thermodynamic studies of hydride- and proton-donor abilities of heteroleptic transition metal complexes containing triphosphine and monophosphine ligands.* Master of Science (Chemistry), August, 2020, Sam Houston State University, Huntsville, Texas.

Transition metal hydrides are reactive intermediates in many catalytic reactions, including the hydrogenation of carbon dioxide. These intermediates can react as proton donors or as hydride donors, characterized by thermodynamic parameters such as pK_a and $\Delta G°_{H-}$, for acidities and hydricities, respectively. In this study, the reactivity of a series of transition metal hydride complexes containing a combination of triphosphine (PP_2) and monophosphine (PR_3) ligands was studied to identify promising catalysts for CO_2 hydrogenation. The structures and energies of group 9 and 10 transition metal hydrides were determined by density functional theory (DFT) calculations to estimate the pK_a, $\Delta G°_{H-}$, and the free energy of H_2 activation ($\Delta G°_{H_2}$) of these species. The DFT-calculated structures are largely similar to those of the analogous bis(diphosphine) complexes, with the notable exception of the Pd(II) and Pt(II) hydride cations. The structures of the Pd(II) and Pt(II) hydrides were virtually four-coordinate and square planar, resulting from dissociation of one of the terminal phosphines of the triphosphine ligand from the metal center. Based on the energies of the calculated species, rhodium and cobalt complexes containing trialkyl or alkyldiarylphosphines were identified as promising catalysts for CO_2 hydrogenation. The monohydride complexes with these ligand combinations have sufficient hydricity to reduce CO_2 to formate ($\Delta G°_{H-} \leq 44$ kcal/mol), the metal(I) cations have free energies for H_2 activation that are thermally accessible at low H_2 pressures ($\Delta G°_{H_2} \lesssim 0$), and the metal(III) dihydride complexes with these ligands have pK_a values between 19 and 27, allowing them to be deprotonated by a range of bases commonly used

for CO_2 hydrogenation. Based on these promising leads, the rhodium(I) complexes $[Rh(PP_2)(PPh_3)]^+$, $[Rh(PP_2)(L^{PhenH})]^+$, $[Rh(PP_2)(L^{Phen+})]^{2+}$, $[HRh(PP_2)(PPh_3)]$, and $[HRh(PP_2)(L^{PhenH})]$ were synthesized, where L^{PhenH} and L^{Phen+} are diphenylethylphosphine ligands with an embedded phenanthridinium-based organic hydride donor in its reduced and oxidized forms. Studies of H_2 activation and hydride transfer were conducted using these complexes, giving a preliminary experimental estimate for the hydricity of $[HRh(PP_2)(PPh_3)]$, ($\Delta G°_{H-}$ = 39.5 kcal/mol). Preliminary catalytic studies of $[Rh(PP_2)(L^{PhenH})]^+$ showed it was active for CO_2 hydrogenation under very mild conditions, with an initial turnover frequency (TOF) as high as 90 h^{-1} at 1.8 atm H_2/CO_2 at ambient temperature.

KEY WORDS: Acidity, Hydricity, Heteroleptic, Triphosphine, Monophosphine, Reactivity, Thermodynamic

ACKNOWLEDGEMENTS

I would like to thank everyone who has been a part of my life during my six years at Sam Houston State University. To the friends that graduated and the friends currently present, you have been so supportive and always right there when I needed you. Thank you for giving me a shoulder to lean on and providing insightful and helpful discussions. Thank you to the professors that believed in me and guided me in the right direction, without you I would not be striving for the best and know all the knowledge you have driven into me. Special thanks to my committee members, Dr. Richard Norman and Dr. Benny Arney who have helped make this an enjoyable experience. Especially Dr. Christopher Zall who welcomed me into the group with open arms and taught me what it means to be a synthetic inorganic chemist. Words alone cannot convey my appreciation and the amount of respect I have for you. Thank you for all the discussions and feedback you provided, it will all be taken to heart and a lasting memory I will never forget. All of it has been a good experience and I would not change it. Lastly, thank you Ashley for being the gear that keeps me going and keep my sanity throughout the whole experience.

TABLE OF CONTENTS

Page

DEDICATION iii

ABSTRACT iv

ACKNOWLEDGEMENTS vi

TABLE OF CONTENTS vii

LIST OF TABLES ix

LIST OF FIGURES xi

CHAPTER I: INTRODUCTION 1

1.1 CO_2 hydrogenation 1

1.2 Catalysis 2

1.3 Catalysts used for CO_2 hydrogenation 3

1.4 Objectives 13

CHAPTER II: COMPUTATIONAL STUDY AND CALCULATIONS ON TRANSITION METAL HYDRIDES 15

2.1 Introduction 15

2.2 Geometric and structural analysis 22

2.3 Acidity and hydricity analysis 44

2.4 Conclusion 55

2.5 Experimental 56

CHAPTER III: SYNTHESIS AND CHARACTERIZATION OF RHODIUM METAL HYDRIDES 57

3.1 Introduction 57

3.2 Synthesis of mixed triphosphine-, monophosphine-ligated Rh(I) complexes..... 63

3.3 Stoichiometric reactivity studies of rhodium(I) triphosphine complexes..... 67

3.4 Preliminary studies of catalytic CO_2 hydrogenation using $Rh(PP_2)(L^{PhenH})]^+$ 71

3.5 Conclusion 76

3.6 Experimental..... 77

REFERENCES 87

APPENDIX A..... 94

VITA..... 126

LIST OF TABLES

Table **Page**

1 Selected bond distances and sum of electronic and thermal free energies for group 9 metal(III) dihydride cations 23

2 Selected bond angles for group 9 metal(III) dihydride cations (Degrees) 24

3 Selected bond distances and sum of electronic and thermal free energies for group 9 metal(III) monohydride dications 25

4 Selected bond angles for group 9 metal(III) monohydride dication complexes (Degrees) 26

5 Selected bond distances and sum of electronic and thermal free energies for group 9 metal(III) trications 27

6 Selected bond angles for group 9 metal(III) trications (Degrees) 28

7 Selected bond distances and sum of electronic and thermal free energies along with τ_5 for group 9 metal(I) monohydride complexes 30

8 Selected bond angles for group 9 metal(I) monohydride complexes (Degrees) ... 31

9 Selected bond distances and sum of electronic and thermal free energies along with τ_4 for group 9 metal(I) cations 32

10 Selected bond angles for group 9 metal(I) cations (Degrees) 33

11 Selected bond distances and sum of electronic and thermal free energies along with τ_5 for nickel(II) hydride complexes 34

12 Selected bond angles for nickel(II) hydride complexes (Degrees) 34

13 Selected bond distances and sum of electronic and thermal free energies along with τ_5 for palladium hydride and platinum hydride complexes 37

14 Selected bond angles for palladium hydride and platinum hydride complexes (Degrees) 38

15 Selected bond distances and sum of electronic and thermal free energies along with τ_4 for nickel(II) dication complexes 39

16 Selected bond angles for nickel(II) dication complexes (Degrees) 40

17 Selected bond distances and sum of electronic and thermal free energies along with τ_4 for palladium and platinum dication complexes 40

18 Selected bond angles for palladium and platinum dication complexes (Degrees) 40

19 Selected bond distances and sum of electronic and thermal free energies along with τ_4 for nickel(0) complexes 42

20 Selected bond angles for nickel(0) complexes (Degrees) 42

21 Selected bond distances and sum of electronic and thermal free energies along with τ_4 for palladium(0) and platinum(0) complexes 43

22 Selected bond angles for palladium(0) and platinum(0) complexes (Degrees) 43

23 DFT-Calculated and experimental pK_a values of known bis(diphosphine) complexes 46

24 DFT-Calculated and experimental hydricity values of known bis(diphosphine) complexes 47

25 DFT-Calculated pK_a values for metal triphosphine complexes 48

26 DFT-Calculated hydricity values for metal triphosphine complexes 52

27 Free energy of the reaction of a metal(I) cation with H_2 to form a metal(III) dihydride 60

LIST OF FIGURES

Figure **Page**

1 Reactions involved in hydrogenation of CO_2 to formic acid or methanol..... 2

2 General mechanism for CO_2 hydrogenation using a rhodium(I) catalyst..... 4

3 General mechanism for CO_2 hydrogenation using a ruthenium(II) catalyst..... 4

4 Acidity half-reaction for a metal(II)-hydride and thermodynamic relationship to pK_a 7

5 Hydricity half-reaction for a metal(II) hydride..... 7

6 Thermodynamic cycle for the free energy relationships for the oxidative addition of H_2 to a metal cation and the acidity and hydricity half-reactions..... 8

7 Thermodynamic relationship between hydricity and CO_2 reduction..... 9

8 Free energy for heterolytic H_2 activation in the presence of a base, as a function of pK_a and hydricity..... 10

9 Example structures of metal(triphosphine)(monophosphine) complexes..... 11

10 Example structures of metal(triphosphine)(monophosphine) complexes containing $L^{Phen+}$and L^{PhenH}..... 12

11 Labeling scheme for M and P atoms and formula for τ_4 and τ_5..... 19

12 Optimized structure of $[H_2Co(PP_2)(PPh_3)]^+$. Hydrogen atoms, other than the metal hydrides have been omitted..... 23

13 Optimized structure of $[HCo(PP_2)(PPh_3)]$. Hydrogen atoms, other than the metal hydrides have been omitted..... 30

14 Optimized structure of $[HPd(PP_2)(PMe_3)]^+$. Hydrogen atoms, other than the metal hydrides have been omitted..... 36

15 Optimized structure of $[HPd(PP_2)(PPh_2C_2H_5)]^+$. Hydrogen atoms, other than the metal hydrides have been omitted. 36

16 Optimized structure of $[HPd(PP_2)(PPh_3)]^+$. Hydrogen atoms, other than the metal hydrides have been omitted. 37

17 Optimized structure of $[Ni(PP_2)(PPh_3)]^{2+}$. Hydrogen atoms, other than the metal hydrides have been omitted. 39

18 Optimized structure of $[Ni^0(PP_2)(PPh_3)]$. Hydrogen atoms, other than the metal hydrides have been omitted. 42

19 Relationship between acidity of target M–H species and proton transfer with a reference M–H species of known acidity 44

20 Relationship between hydricity of target M-H species and hydride transfer with a reference M-H species of known hydricity 45

21 Example calculation for the acidity determination of $[HNi(dmpe)_2]^+$ 46

22 Example calculation for the hydricity determination for $[HNi(dmpe)_2]^+$ 47

23 Proposed catalytic cycle for CO_2 hydrogenation using the novel rhodium(triphosphine)(monophosphine) complexes 58

24 Thermodynamic cycle to calculate the free energy of H_2 activation by Method A 59

25 Thermodynamic cycle to calculate the free energy of H_2 activation by Method B 60

26 Synthesis of $[Rh(PP_2)(PPh_3)][SbF_6]$ 64

27 Synthesis of $[Rh(PP_2)(MeCN)][BF_4]$ 66

28 Synthesis of $[Rh(PP_2)(PPh_3)][BF_4]$ 66

29 Reaction to synthesize the [$HRh(PP_2)(PPh_3)$] complex 66

30 Protonation and H_2 elimination from [$HRh(PP_2)(L^{PhenH})$] 68

31 H_2 heterolysis reactions and K_{eq} values using various bases 69

32 Bases used for H_2 heterolysis and their conjugate acids 69

33 Oxidation of the L^{PhenH} ligand by a tritylium salt 71

34 Catalytic reaction and conditions for CO_2 hydrogenation 72

35 Reaction progress for the catalytic hydrogenation of CO_2 using 5 mol % $[Rh(PP_2)(L^{PhenH})]^+$ relative to DBU under 1.8 atm H_2/CO_2 (1:1, ambient temperature, CD_3CN solvent), as measured by ^1H NMR spectroscopy 73

36 Reaction progress for the catalytic hydrogenation of CO_2 using 1 mol % $[Rh(PP2)(L^{PhenH})]^+$ relative to Verkade's base under 1.8 atm H_2/CO_2 (1:1, ambient temperature, THF solvent), as measured by ^{31}P NMR spectroscopy..... 74

CHAPTER I

INTRODUCTION

1.1 CO_2 hydrogenation

A significant challenge for the 21st century is to develop technologies to generate, store, and utilize energy in an environmentally responsible manner. Global energy use is projected to more than double this century as the world's population grows. Most energy in the U.S and globally, is derived from fossil fuels that produce CO_2 and other pollutants. Renewable energy sources like wind and solar have become cheap and abundant, but they produce energy intermittently and unreliably.[1] Storing the energy from these sources, by using it to produce renewable chemical fuels, is an attractive alternative. H_2 can be produced electrocatalytically by electrolysis of water, and carbon-based fuels can be generated through the catalytic hydrogenation of CO_2, forming molecules like formic acid and methanol.[2–4] These processes require the development of efficient and cheap catalysts. This work describes the synthesis and thermodynamic studies of transition metal complexes that contain triphosphine and monophosphine ligands and the evaluation of their suitability towards catalytic CO_2 hydrogenation. The focus is on the ability of these novel catalysts to facilitate H_2 activation. These new catalysts are analogous to metal bis(diphosphine) complexes that have been extensively studied and used in stoichiometric and catalytic H_2 activation and CO_2 reduction reactions.[5,6] For these new complexes, thermodynamic and structural analyses were pursued to identify periodic trends and structure reactivity relationships to determine key aspects pertaining to their development into efficient catalysts.

1.2 Catalysis

Formation of formic acid from CO_2 and H_2 (eq. 1) is a thermodynamically unfavorable reaction. However, in the presence of a base, which yields the formate salt, the reaction becomes thermodynamically favorable (eq. 2). The favorability of eq. 2 depends on the choice of base and solvent and is most favorable with a strong base and a more polar solvent. The hydrogenation of CO_2 to methanol (eq. 3) is thermodynamically favorable at 298 K. However, neither reaction takes place at an appreciable rate without a catalyst.[7,8]

$$CO_{2\,(g)} + H_{2\,(g)} \longrightarrow HCOOH\ (aq) \qquad \Delta G_{298} = 7.6\ kcal \qquad \text{eq. 1}$$

$$CO_{2\,(g)} + H_{2\,(g)} + Base \longrightarrow HCO_2^- + HBase^+ \qquad \text{eq. 2}$$

$$CO_{2\,(g)} + 3\,H_{2\,(g)} \longrightarrow CH_3OH\ (l) + H_2O\ (l) \qquad \Delta G_{298} = -2.1\ kcal \qquad \text{eq. 3}$$

Figure 1. *Reactions involved in hydrogenation of CO_2 to formic acid or methanol*

Metal hydrides are key intermediates in catalytic CO_2 hydrogenation. Optimal catalysts have high catalytic activity, involve low cost metals, and operate under mild conditions. The catalytic activity is usually assessed based on the turnover number (TON) and frequency (TOF). The TON is defined as mol of product per mol of catalyst, and the higher the value the better the catalyst. The TOF is calculated as TON per unit time, and a higher value correlates to a faster catalyst. Typically, effective catalysts involve expensive metals such as ruthenium[9] and iridium.[10] Finding alternative and cheaper metals to use for catalytic reactions is most desired. Some catalysts are most effective in the presence of high temperature or pressure, but catalysts better suited for ambient temperature or pressure are more convenient.

In transition metal-catalyzed CO_2 hydrogenation, the metal must activate H_2, forming metal hydride intermediates, which then react with and reduce CO_2. In the

hydrogenation of CO_2 to formate (eq. 2), this typically involves deprotonation of a M–H bond of a metal dihydride by the base and hydride transfer from the resulting metal monohydride species to CO_2, producing formate. Quantification of the reaction energies for each step, using thermodynamic parameters such as the hydricity or pK_a of a metal hydride, can help tune a specific complex for the hydrogenation of CO_2, allowing the reaction to work at lower temperatures and pressures. Thermodynamic optimization does not guarantee that a complex will be an effective catalyst, as kinetic and mechanistic issues may lower the reaction rate. However, complexes that have mismatched thermodynamic properties, such as an unfavorable hydride transfer step between the metal hydride and CO_2, will either be inactive altogether or will require harsh conditions, such as high pressures of CO_2, to drive catalysis. A thermodynamically optimized catalyst should be capable of operating efficiently under mild conditions.

1.3 Catalysts used for CO_2 hydrogenation

The first reports of CO_2 hydrogenation using transition-metal catalysts used a series of late-transition metals with phosphine-based ligands like triphenylphosphine (PPh_3) and bis(diphenylphosphino)ethane (dppe). These catalysts were complexes of Pd, Ru, Ir, and Rh, such as $[Ru(PPh_3)_4H_2]$ and $[Rh(PPh_3)_3Cl]$.[11] For the next few decades, most of the work was done using similar Rh and Ru monophosphine complexes. In general, these catalysts follow one of two mechanisms based on the method of H_2 activation (Figure 2 and 3, respectively).[4]

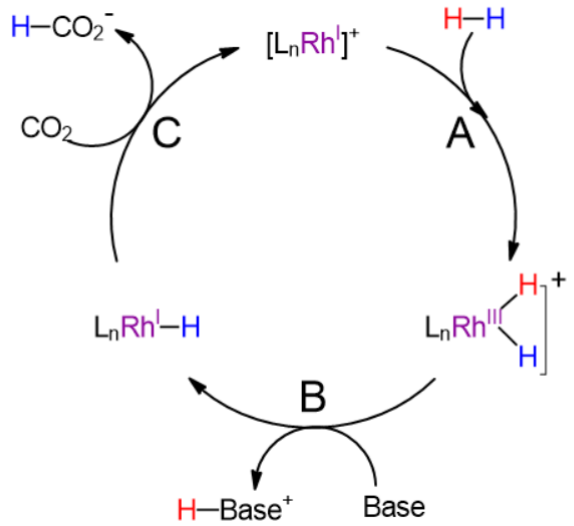

Figure 2. *General mechanism for CO_2 hydrogenation using a rhodium(I) catalyst*

Rhodium(I) phosphine complexes can undergo direct oxidative addition of H_2 to form a Rh^{III} dihydride (step A). Deprotonation of the catalyst forms a more nucleophilic Rh^{I} monohydride (step B), which can then hydride transfer to CO_2 to produce formate and regenerate the original Rh^{I} catalyst (step C).

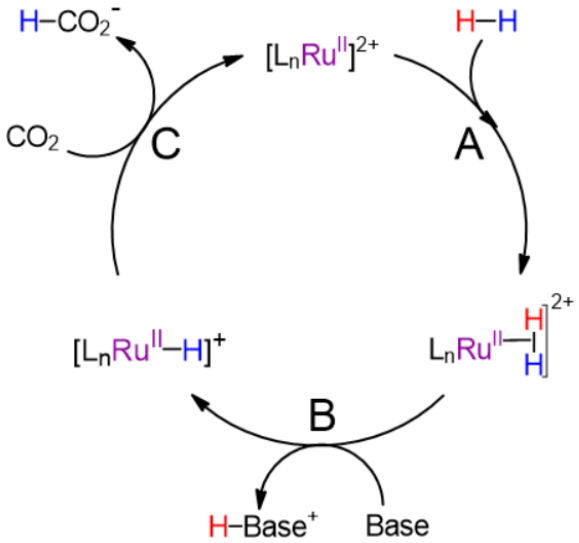

Figure 3. *General mechanism for CO_2 hydrogenation using a ruthenium(II) catalyst*

Ru^{II} catalysts do not undergo direct oxidative addition of H_2, because the resulting Ru^{IV} dihydrides would be in an unfavorable oxidation state. Instead, they bind H_2, forming a non-classical dihydrogen complex (step A), which is deprotonated by an

exogenous base, producing the Ru^{II} monohydride (step B). In both mechanisms, CO_2 reduction occurs through net hydride transfer from the metal hydride to CO_2, producing formate. This can occur as a discrete step (shown as Step C) or as a stepwise insertion of CO_2 into the metal hydride bond, followed by dissociation of formate.[4]

More recently, catalysts with tridentate pincer ligands have been developed,[12] which contain three donor ligands bound in a meridional fashion. Currently the most active catalysts are Ir and Ru pincer complexes.[13–15] These are believed to go through oxidative addition and heterolytic mechanisms, respectively. The role of the pincer ligand is primarily to confer stability, through the chelate effect, allowing these catalysts to operate under very harsh conditions of temperature and pressure with minimal catalyst decomposition.

Goals of current research are to develop catalysts for CO_2 hydrogenation that can operate under milder conditions and to develop catalysts based on inexpensive first row metals like Fe, Ni, and Co. Both goals depend on the identification of transition metal complexes with favorable reactivities, which can be quantified in terms of thermodynamic proton and hydride donor abilities, or acidities and hydricities, respectively. To operate under mild conditions, a catalyst must be tuned so that each step in the mechanism takes place as favorably as possible. In general, first-row metal hydrides are less reactive, and therefore a more careful attention to proton and hydride donor abilities is necessary when evaluating these catalysts. One highly successful example is a cobalt hydride, $[HCo(dmpe)_2]$, reported by Jeletic *et al*.[16] This complex was identified as a promising catalyst based on predictions of its hydride donor ability and acidity made by using density functional theory calculations.[17] Subsequent experimental

studies of CO_2 hydrogenation using this complex showed it to be an extraordinarily active catalyst, giving an extremely high TOF of 3,400 h^{-1} even at ambient temperatures and very low (1 atm) pressures of H_2/CO_2. This rate is competitive with those of the fastest second- and third-row transition metal catalysts, despite operating under much milder conditions. The disadvantage is that, because the Co(I) hydride is such a strong hydride donor, regeneration of $[HCo(dmpe)_2]$ by deprotonating the Co(III) dihydride, $[H_2Co(dmpe)_2]^+$, requires a very strong base. By contrast, the rhodium-analogue of this catalyst, $[HRh(dmpe)_2]$, is a much less active catalyst. Even though it is an even stronger hydride donor, its corresponding dihydride, $[H_2Rh(dmpe)_2]^+$, is too weakly acidic to be deprotonated efficiently even when using a very strong base. Taken together, these results demonstrate that highly effective catalysts, including those based on first-row transition metal hydrides, can be developed by paying careful attention to the thermodynamic favorability of the key steps in the mechanism. However, the thermodynamic properties must be balanced so that no step in the reaction mechanism is strongly disfavored.

Catalytic intermediates should be similar in energy so that the free energy changes in each step are near zero. If any step of the catalytic cycle is significantly uphill, it adds a thermodynamic barrier on top of the activation barrier for that step. If any step is significantly downhill, it forces a subsequent step of the cycle to be uphill. In other words, a step being very favorable means that step involves an unstable intermediate that will be difficult to regenerate in the catalytic cycle. The free energies of each step in the mechanisms described above can be estimated if the thermodynamic hydride donor abilities and acidities of the metal hydride intermediates are known.

The acidity is quantified using the usual pK_a parameter,[18] which can be converted to a free energy for proton dissociation in units of kcal/mol, for a reaction at 298 K, shown in Figure 4 and eq. 4, by rewriting the usual relationship shown in eq. 5. The acidity half-reaction results in a formal reduction of the metal center by two electrons because the elections in the metal hydride species are formally assigned to the hydride ligand. When this bond is cleaved heterolytically to give H^+, the electrons are assigned to the metal ion in the conjugate base.

$$[M\text{-}H]^+ \rightleftharpoons M^0 + H^+ \quad \Delta G^\circ_{H^+} = 1.364 pK_a \quad \text{eq. 4}$$

$$\Delta G^\circ_{H^+} = -RT \ln K_a \quad \text{eq. 5}$$

Figure 4. *Acidity half-reaction for a metal(II)-hydride and thermodynamic relationship to pK_a*

A similar parameter, known as hydricity (ΔG_{H^-}), has been established to quantify hydride donor abilities shown in Figure 5. It is the free energy for heterolytically cleaving the metal hydride bond to give free metal cation and hydride ions (eq. 6).[19] Since the electrons in the metal hydride bond are formally assigned to hydrogen, heterolytic cleavage to form H^- does not result in a change in oxidation state of the metal.

$$[M\text{-}H]^+ \rightleftharpoons M^{II} + H^- \quad \Delta G^\circ_{H^-} \quad \text{eq. 6}$$

Figure 5. *Hydricity half-reaction for a metal(II) hydride*

Both acidities and hydricities are important in the hydrogenation of CO_2. For example, the free energy of Step A in Figure 2, namely oxidative addition of H_2 at a metal center to form a metal dihydride, can be quantified based on the hydricity of the metal hydride and the acidity of the metal dihydride species, as shown in the thermodynamic cycle in Figure 6.. The free energy for heterolytic cleavage of H_2 into H^+

and H^- has been established as 76 kcal/mol in MeCN.[20] Stepwise addition of the resulting H^- and H^+ ions to the metal center is a function of the acidity of the dihydride (eq. 8) and hydricity of the monohydride (eq. 9), and the overall free energy of H_2 addition is therefore given by eq. 11.

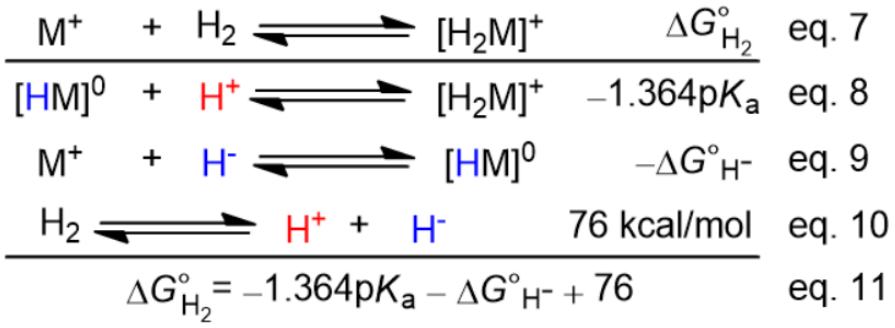

Figure 6. *Thermodynamic cycle for the free energy relationships between the oxidative addition of H_2 to a metal cation and the acidity and hydricity half-reactions*

In Step B of the catalytic cycle in Figure 2, the metal(III) dihydride must be deprotonated by a base to form the active metal(I) hydride species. To drive this reaction, the conjugate acid of the base must have a pK_a (referred to as pK_{aH} for the base) that is greater than that of the dihydride complex. Therefore, the lower the pK_a of the dihydride complex, the more favorable the deprotonation step, or the weaker the base necessary to give a favorable deprotonation.

The free energy for the key CO_2 reduction step in catalysis (Step C in Figure 2 and 3 and eq. 12 in Figure 7) is also directly related to the hydride donor ability of the metal hydride species, as shown in Figure 7 (eq. 13). The free energy for formation of formate from CO_2 and solvated hydride ion (eq. 14) was determined to be -44 kcal/mol in acetonitrile solvent[21,22] and therefore, hydride transfer from a metal ion to CO_2 requires a metal hydride with a $\Delta G^o_{H^-}$ value of $\leq$ 44 kcal.

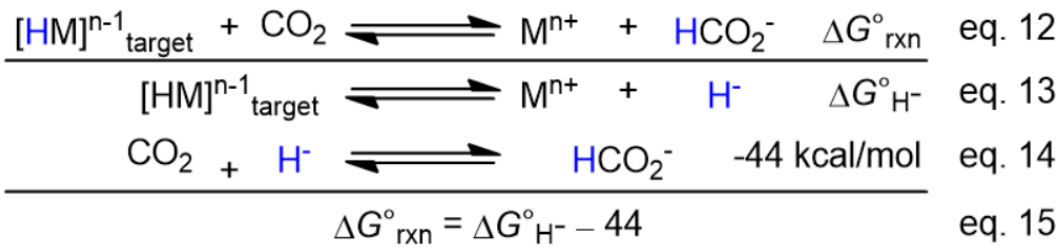

Figure 7. *Thermodynamic relationship between hydricity and CO_2 reduction*

Thus, there is a balance of thermodynamics, where a catalyst that is a stronger hydride donor will be more reactive towards CO_2 reduction but will be harder to regenerate. If the hydricity is too great (very low value of $\Delta G^{o}_{H^-}$), either the H_2 addition step or the deprotonation of the resulting metal dihydride or dihydrogen complex will be unfavorable. This was observed in studies of rhodium bis(diphosphine) catalysts for CO_2 hydrogenation, where although [HRh(dmpe)$_2$] ($\Delta G^{o}_{H^-} \approx 26.6$ kcal/mol)[23] was a much stronger hydride donor than [HCo(dmpe)$_2$] ($\Delta G^{o}_{H^-} \approx 36.3$ kcal/mol),[17] the pK_a of the rhodium(III) dihydride (36.7 in MeCN)[23] is too high to be efficiently deprotonated by even the strongest bases typically used in catalytic reactions, whereas the pK_a of the cobalt(III) dihydride, [H_2Co(dmpe)$_2$]$^+$ (33.7 in MeCN)[24] is well matched to that of the proazaphosphatrane base known as Verkade's base (2,8,9-triisopropyl-2,5,8,9-tetraaza-1-phosphabicyclo[3.3.3]undecane, or Vkd), whose conjugate acid has a pK_{aH} of 33.6.[25]

For catalysts that operate through the heterolytic H_2 activation mechanism, such as the ruthenium phosphine complexes mentioned above, no oxidative addition step occurs, and the free energy for forming the active metal hydride can be defined as shown in Figure 8. The free energy for heterolytic H_2 cleavage to form a metal hydride using a given base depends on the hydricity of the metal hydride and the basicity of the base. The relationship between these parameters is given in eq. 20.

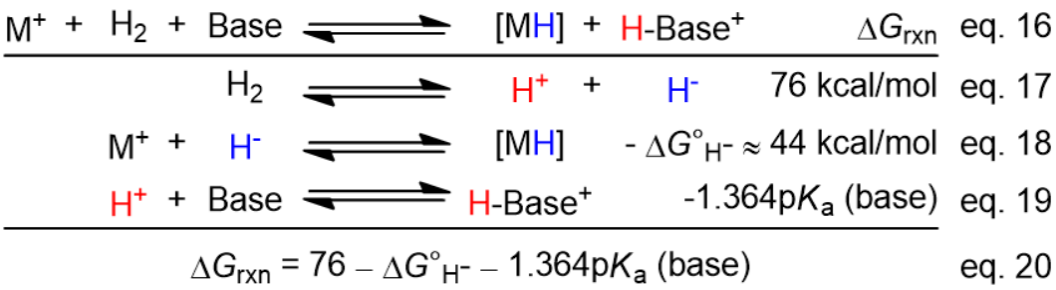

Figure 8. *Free energy for heterolytic H_2 activation in the presence of a base, as a function of pK_a and hydricity*

The most extensive studies of acidities and hydricities for transition metal hydrides are for metal bis(diphosphine) complexes with the formula $[HM(diphosphine)_2]^{n+}$. For example, nickel bis(diphosphine) complexes have hydricities between 49 – 65 kcal/mol,[19] and are ineffective at CO_2 hydrogenation, lacking sufficient hydride donor ability to reduce CO_2 to formate. However, cobalt(I) bis(diphosphines), whose hydricities are between 36 – 50 kcal/mol can be highly active.[17] Rh complexes such as $[HRh(dmpe)_2]$, have even lower values of $\Delta G^{o}_{H^-}$ and are stronger hydride donors.[23] The choice of transition metal is therefore a key factor in the hydricity and acidity, with group 9 metal hydrides typically being better hydride donors and weaker acids than group 10 metals. The analogous series of metal-tetraphosphine complexes containing one monophosphine and one triphosphine ligand have not been studied, even though the triphosphine ligand is similar to the pincer complexes that are well-established catalysts for CO_2 hydrogenation.

Research in the Zall group is focused on developing catalysts for reactions, like CO_2 hydrogenation, that are important for energy storage and conversion. Many of the catalyst designs use a combination of monophosphine and triphosphine ligands. The most commonly used triphosphine ligand in these studies is bis(2-

diphenylphosphinoethyl)phenylphosphine (PP_2), which is commercially available and air-stable. This ligand can coordinate in a flexible tridentate fashion that can support the six-coordinate, five-coordinate, and four-coordinate structures expected for the metal dihydrides, monohydrides, and their conjugate free metal ions, as shown in Figure 9. Using this ligand as a consistent and versatile supporting group, the monophosphine ligand can be extensively varied to include strongly electron-donating trialkylphosphines and less donating triarylphosphines like PPh_3, and other ligands. Understanding the effect of the metal and ligand variation on the pK_a and hydricity values of these metal hydrides is crucial to their utility as catalysts.

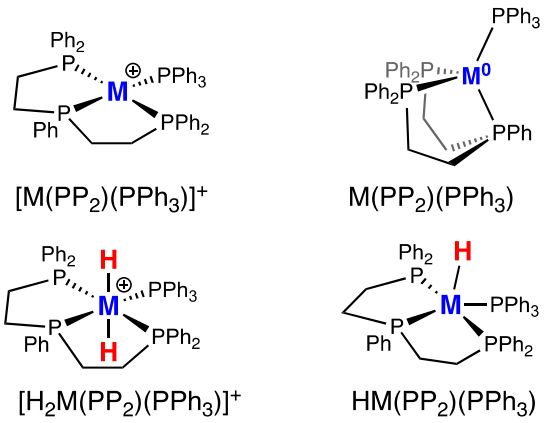

Figure 9. *Example structures of metal(triphosphine)(monophosphine) complexes*

One class of ligands used in the Zall group is a monophosphine containing a redox-active heterocycle tethered to a diphenylphosphine group by a flexible alkyl linker. These groups are analogues of the biological cofactor NADH that can donate or accept a hydride ion, corresponding to reduced (LH) and oxidized (L^+) forms.[26] In the context of hydrogenation catalysis, these are designed to work cooperatively with a reduced metal ion to heterolytically activate H_2 to form a ligand-based hydride and metal-based proton

in the form of an acidic metal-hydride group. The best studied example in the Zall group is the phenanthridinium-containing ligand shown in Figure 10.

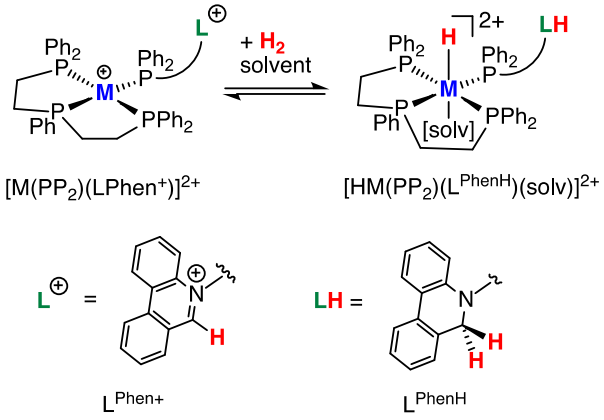

Figure 10. *Example structures of metal(triphosphine)(monophosphine) complexes containing* L^{Phen+} *and* L^{PhenH}

Proton transfer from a metal hydride, such as $[HM(PP_2)(L)_n]^{n+}$, generates a reduced metal complex, $[M(PP_2)(L)_n]^{n-1}$. Hydride transfer from the same metal hydride generates an ion in the same oxidation state, $[M(PP_2)(L)_n]^{n+1}$, but with one fewer strongly donating hydride ligand as shown in Figure 10. Therefore, the product of the acidity half-reaction is more electron-rich and the product of the hydricity half-reaction is less electron-rich. As a result, ligands that contain more electron-donating substituents, like trialkylphosphines, should make a metal hydride more hydridic and less acidic, and for less donating substituents like triarylphosphines the trend is the reverse. These trends have been confirmed in studies of metal bis(diphosphine complexes), where, for example, $[HCo(dmpe)_2]$ ($\Delta G°_{H^-}$ 36.3 kcal/mol)[17] is more hydridic than $[HCo(dppe)_2]$ ($\Delta G°_{H^-}$ = 49.9 kcal/mol)[27] but the corresponding hydride is significantly less acidic (pK_a 33.7 for $[H_2Co(dmpe)_2]^+$; 22.8 for $[H_2Co(dppe)_2]^+$).[24,27] In addition, structural rearrangements between the species in these half-reactions can create dramatic changes in

the hydricities and acidities, depending on the steric bulk and conformational flexibilities of the ligands.[28] For example, deprotonation of a nickel(II) hydride, such as $[HNi(dmpe)_2]^+$, generates a neutral Ni(0) species, $[Ni^0(dmpe)_2]$, which has an essentially tetrahedral geometry. However, H^- transfer from $[HNi(dmpe)_2]^+$, generates a $[Ni(dmpe)_2]^{2+}$, which is a Ni(II) ion with an essentially square planar geometry. Bulky substituents, like the phenyl groups in $[HNi(dppe)_2]^+$, can destabilize the sterically more crowded square planar geometry and favor the tetrahedral structure, thereby making the hydride more acidic and less hydridic.[5] Not only the steric bulk of the substituents but also the bite angle of the diphosphine backbone can significantly affect these values.[29] Diphosphine ligands with larger backbones and therefore larger bite angles between the phosphorus donor atoms similarly create sterically congested square planar complexes and therefore decreased hydricity. However, analogous relationships for the mixed (triphosphine)(monophosphine) complexes in this study have not been established and are a major focus of this study.

1.4 Objectives

In this project, metal-hydrides with mixed triphosphine and monophosphine ligand complexes are studied to evaluate their potential in CO_2 hydrogenation. Computational studies are performed, with the use of density functional theory (DFT) methods, to estimate the structures and thermodynamic acidities and hydricities of a wide variety of group 9 and 10 metal complexes. These values are analyzed to identify complexes that showed the most promise as catalysts for CO_2 hydrogenation. The selected complexes are studied experimentally to validate the computationally-

determined thermodynamic parameters and to demonstrate their reactivity towards H_2 activation and catalytic CO_2 hydrogenation.

The primary objectives for this research are to:

1. Determine hydricity values for a series of group 9 and 10 transition metal hydride complexes that contain mixed triphosphine and monophosphine ligands through density functional theory (DFT) studies that model hydride transfer between the geometry-optimized structures of the metal hydrides and their conjugate hydride acceptor ions.
2. Determine acidities of analogous group 9 and 10 metal hydride ions through analogous DFT studies that model proton transfer between the geometry-optimized structures of the metal hydrides and their conjugate bases.
3. Analyze the values to find periodic trends between the metal complexes, compare the values and trends to those of bis(diphosphines), and understand the structural and electronic factors that determine these values.
4. Perform experimental measurements of hydricity and acidity for complexes whose DFT-predicted values were most ideal for CO_2 hydrogenation.
5. Assess the catalytic activity of complexes described above in the catalytic hydrogenation of CO_2.

CHAPTER II

Computational Study and Calculations on Transition Metal Hydrides

2.1 Introduction

The primary goal of this research was to determine the thermodynamic hydricities and acidities of transition metal hydrides containing a combination of triphosphine and monophosphine ligands and evaluate their suitability for the catalytic hydrogenation of CO_2. These studies began with density functional theory calculations to determine the geometry-optimized structures of a variety of metal(triphosphine)(monophosphine) complexes. The specific complexes chosen for study were those that appear as reactants and products in the pK_a and $\Delta G°_H$- half-reactions. The estimated pK_a or $\Delta G°_H$- value for each hydride was then determined using the DFT-calculated energies of these species in a thermodynamic cycle modeling proton or hydride transfer to a reference metal ion whose conjugate hydride has a known acidity or hydricity value, respectively. These studies began with geometry calculations to determine the structures and energies of the relevant metal complexes. Since these species, in nearly all cases, have not been previously reported in the literature, their structures are of considerable interest and are fundamental to understanding their stability and reactivity.

pK_a and hydricity values were calculated for cationic metal(III) dihydrides of the group 9 metals Co and Rh, because metal bis(diphosphine) complexes of these metals, such as $[Co(dmpe)_2]^+$, are known to be effective catalysts for CO_2 hydrogenation.[16,30] The first step in these reactions is the oxidative addition of H_2 to form a metal(III) dihydride, such as $[H_2Co(dmpe)_2]^+$. The catalytic activity of the catalysts depends strongly on the free energy for this H_2 activation step (ΔG_{H_2}, eq. 21).

$$[M^{I}(PP_2)(PR_3)]^{+} + H_2 \leftrightharpoons [H_2M^{III}(PP_2)(PR_3)]^{+} \quad \text{eq. 21}$$

The details of relating ΔG_{H2} to these ΔG_{H}- and pK_a values are discussed in Ch 3. They depend on the energies of a variety of species, including the metal(I) cation, the metal(III) dihydride cation, metal(III) monohydride dication, metal(III) trication, and metal(I) hydride complexes.

As six-coordinate, d^6 metal ions, an approximately octahedral geometry was expected for metal(III) dihydride complexes. The acidity of these species is defined by the usual pK_a half-reaction, which in this case generates a neutral metal(I) monohydride species (eq. 22) that is itself a key catalytic intermediate.

$$[H_2M^{III}(PP_2)(PR_3)]^{+} \leftrightharpoons H^{+} + [HM^{I}(PP_2)(PR_3)] \quad \text{eq. 22}$$

The hydricity of the metal(III) dihydride, on the other hand, is defined by H^{-} transfer from this ion. The product of this half-reaction is a metal(III) monohydride that, as a d^6 ion, will bind another ligand to remain six-coordinate and therefore be electronically and coordinatively saturated. The additional ligand was modeled as MeCN, because the relevant H^{+} and H^{-} transfer equilibria are usually studied in MeCN solvent. The relevant hydricity half-reaction is therefore shown in eq. 23.

$$[H_2M^{III}(PP_2)(PR_3)]^{+} + MeCN \leftrightharpoons H^{-} + [HM^{III}(PP_2)(PR_3)(MeCN)]^{2+} \quad \text{eq. 23}$$

The free MeCN ligand in eq. 24 was not explicitly modeled using DFT calculations, because eq. 23 itself was not directly calculated in the methodology of these studies. Instead, the hydricity studies were determined by modeling H^{-} transfer to a reference hydride acceptor in an equilibrium in which the additional MeCN ligand is exchanged along with the hydride ion.

$$[H_2M_1^{III}(PP_2)(PR_3)]^+ + [HM_2^{III}(P_2)_2(MeCN)]^{2+} \leftrightharpoons$$

$$[HM_1^{III}(PP_2)(PR_3)(MeCN)]^{2+} + [H_2M_2^{III}(P_2)_2]^+ \quad \text{eq.24}$$

Similarly, the hydricity of the metal(III) monohydride dication is defined by H^- transfer from this ion, which is accompanied by binding of a second MeCN ligand, forming a metal(III) disolvate trication shown in eq. 25.

$$[HM^{III}(PP_2)(PR_3)(MeCN)]^{2+} + MeCN \leftrightharpoons H^- + [M^{III}(PP_2)(PR_3)(MeCN)_2]^{3+} \quad \text{eq. 25}$$

On the other hand, the acidity of the metal(III) monohydride is defined by the half-reaction in eq. 26, in which the product is a d^8 metal(I) cation that is a stable 16-electron complex upon the expected dissociation of MeCN. This species is the same as the product of eq. 27, for the hydricity half-reaction of the metal(I) hydride.

$$[HM^{III}(PP_2)(PR_3)(MeCN)]^{2+} \leftrightharpoons H^+ + [M^{I}(PP_2)(PR_3)]^+ + MeCN \quad \text{eq. 26}$$

The metal(I) monohydride is the species predicted to react with CO_2, and the favorability of this key reaction step depends on the hydride donor ability of the hydride complex (eq. 27).

$$[HM^{I}(PP_2)(PR_3)] \leftrightharpoons H^- + [M^{I}(PP_2)(PR_3)]^+ \quad \text{eq. 27}$$

The metal(I) cations are expected to have approximately square planar geometries, which are typical for four-coordinate d^8 metal ions, but studies of the analogous metal bis(diphosphine) complexes have shown that sterically bulky phosphine ligands can cause distortions towards a tetrahedral geometry. These distortions dramatically affect the H^- donor abilities, with bulkier ligands and ligands with larger chelate bite angles that leads to weaker hydride donor abilities (greater $\Delta G°_{H^-}$). The effect is attributed to lowering of the energy of the $d_{x^2-y^2}$ orbital as the structure becomes more tetrahedrally distorted.[5,28,29] This is the lowest unoccupied molecular orbital in a square

planar geometry, and thus the orbital into which the electron pair from the H^- ion is formally added when forming the metal(I) hydride complex from the square planar cation. Because this orbital is at a lower energy in a tetrahedral geometry, and this geometry relieves the steric strain between ligand substituents, these distortions stabilize the metal hydride relative to the free metal ion and therefore lower the hydride donor ability. This effect has been observed for nickel, palladium, platinum, cobalt, and rhodium monohydrides and appears to be a consistent property of d^8 metal-hydride complexes with diphosphine ligands.[5,28,29,31,32] For bis(diphosphine) complexes, the distortion is typically characterized by the dihedral angles between the diphosphine ligands. These dihedral angles increase, indicating a more tetrahedrally distorted structure, with bulkier substituents on the phosphine donor atoms (e.g. dppe vs. dmpe) and with increased ligand bite angle (e.g. dppe vs. dppp). This structural effect is in addition to the electronic effects discussed in Ch 1, where electron-withdrawing substituents on the phosphines make the hydrides more acidic and electron-donating substituents make them more hydridic. Such structural factors are not established for the mixed-ligand metal(triphosphine)(monophosphine) complexes, and therefore the structures of the geometry-optimized complexes were of interest, potentially allowing new structure-reactivity relationships to be developed.

For the structures in this study, the ligand bite angle was expected to be essentially constant, as the same triphosphine ligand is used in the various complexes, and there is no well-defined dihedral angle to use in a similar fashion. Instead, the degree to which each four-coordinate structure is square planar or tetrahedral is characterized by the τ_4 parameter, defined by the formula shown in Figure 11, which uses the two greatest

metal-ligand bond angles (α and β, respectively) in each structure. A perfectly square planar structure (α = β = 180°) would give $\tau_4 = 0$, and a perfectly tetrahedral structure (α = β = 109.5°) would give $\tau_4 = 1$.[33]

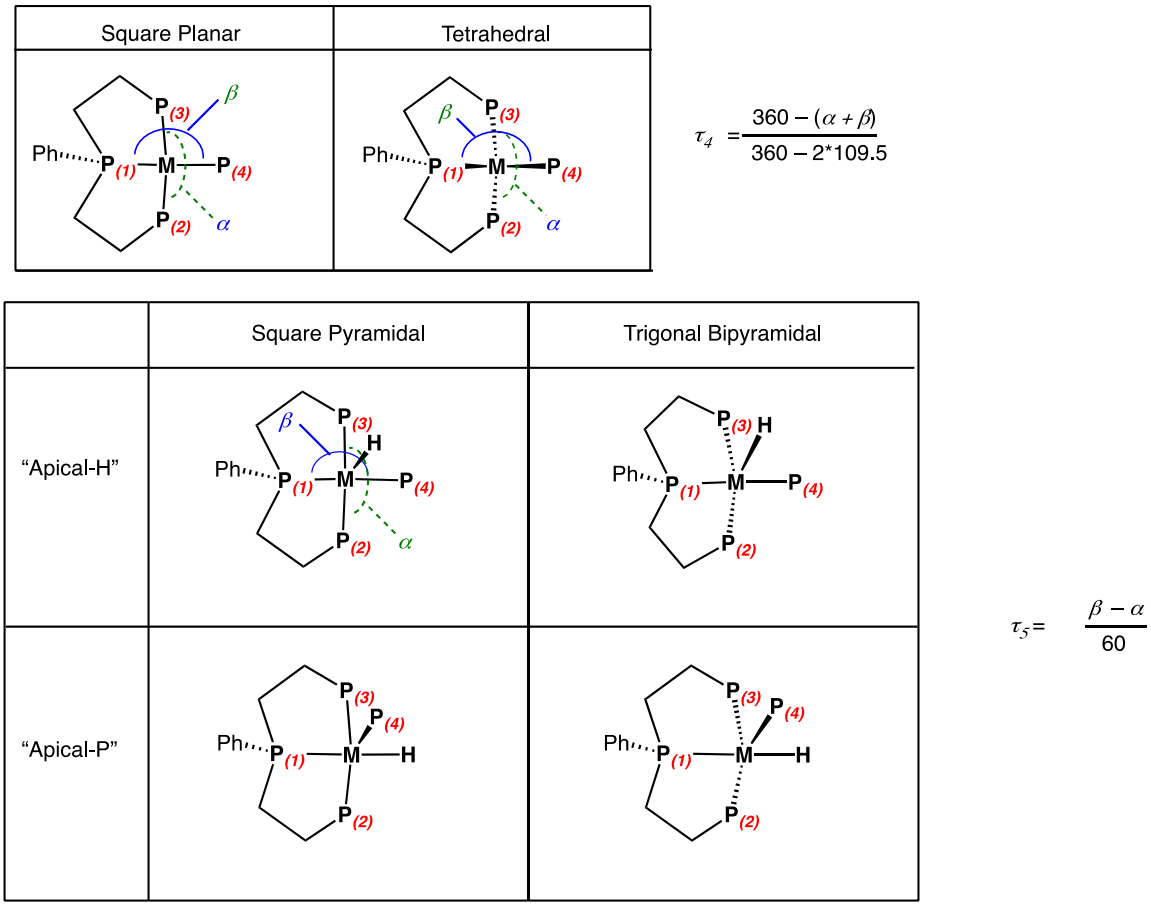

Figure 11. *Labeling scheme for M and P atoms and formula for τ_4 and τ_5*

For clarity, only the phenyl group on the central phosphorus atom of the triphosphine ligand is shown.

Similarly, the five-coordinate metal(I) hydride complexes can adopt either a square pyramidal or trigonal bipyramidal geometry. These can be distinguished using a similar parameter, known as τ_5, whose formula is given in Figure 11. A perfectly square pyramidal geometry (α = β = 180°) would give $\tau_5 = 0$, and a trigonal bipyramidal geometry (α = 120°, β = 180°) would give $\tau_5 = 1$.[34]

Both square pyramidal and trigonal bipyramidal input geometries were tested in the calculation of the metal(I) hydride species, but these inputs gave essentially identical structures after geometry optimization. However, an additional, very important factor in the structures of these five-coordinate hydrides was the arrangement of the hydride and monophosphine ligands with respect to the triphosphine ligand. As shown in Figure 11, two starting configurations are possible, each of which can optimize to a square pyramidal or trigonal bipyramidal geometry, but which cannot interconvert with each other. It is convenient to refer to the square pyramidal arrangement, in which the three donor groups in the triphosphine (P_1-P_3) occupy three of the four positions within the base of the square pyramid. The remaining basal position can, in one configuration, be occupied by the monophosphine ligand, therefore putting the hydride in the apical position ("apical-H"). The other option ("apical-P") places the monophosphine in the apical position and the hydride in the basal position.

In these square pyramidal geometries, the phenyl substituent on the central phosphorus atom (P_1) of the triphosphine ligand points up, towards the apex of the square pyramid. This places the substituent on the same face of the metal center as the apical ligand (P_4 or H). The P_4-M-H unit can rotate with respect to the triphosphine, and therefore the square pyramidal initial geometries are capable of rotating to achieve a trigonal bipyramidal geometry and *vice versa*. However, an apical-H structure cannot rotate to give an apical-P structure or *vice versa*. For all five-coordinate monohydride complexes, initial structures with both apical-H and apical-P configurations were optimized and compared. In addition, the monophosphine can rotate so that its substituents are arranged in either a staggered or eclipsed conformation with respect to

the central phosphorus atom across the metal center from it. For each $[HM(PP_2)(PPh_3)]$ complex, both conformations were compared.

Similar studies were performed for the group 10 metal complexes. For these species, the hydricities and acidities of the d^8 monohydrides, i.e. eq. 28 and 29, respectively, were the relevant half-reactions.

$$[HM(PP_2)(PR_3)]^+ \leftrightharpoons H^- + [M^{II}(PP_2)(PR_3)]^{2+} \qquad \text{eq. 28}$$

$$[HM(PP_2)(PR_3)]^+ \leftrightharpoons H^+ + [M^0(PP_2)(PR_3)] \qquad \text{eq. 29}$$

Calculations involving d^6 metal ions, such as $[H_2M(PP_2)(PR_3)]^{2+}$, $[HM(PP_2)(PR_3)]^{3+}$, and $[M(PP_2)(PR_3)]^{4+}$, were not studied, as their excessively high M(IV) oxidation states make them unlikely to be viable intermediates during catalysis.

The metal(II) dications in eq. 28 are expected to be approximately square planar d^8 ions, subject to the same structural effects discussed for the d^8 group 9 cations. On the other hand, the metal(0) complexes in eq. 29 are d^{10} metal centers that should favor a tetrahedral geometry. As a result, the hydricities, but not the acidities, of these group 10 metal(II) hydrides were expected to show a measurable dependence on the steric properties of the ligands.

Studies for each metal were performed with either PPh_3 or PMe_3 as the monophosphine ligand. PMe_3 is significantly more electron-donating, which was expected to increase the hydride donor ability and decrease the acidity relative to the PPh_3 complexes; however, PPh_3 is also considerably more sterically bulky. Based on the precedent for bis(diphosphine) complexes, this steric difference was expected to decrease the hydricity (raise the value of ΔG_H-) but not to significantly affect the acidity.[5,29]

Altogether, the PMe_3 complexes were expected to be considerably stronger hydride donors and to be somewhat less acidic.

Studies were also performed for a Pd complex containing a PPh_2Et ligand, which is intermediate in bulk and electron donor ability and is a truncated model for other monophosphine ligands studied by the Zall group. These ligands contain a diphenyl(alkyl)phosphine donor group tethered to a redox-active heterocycle that can act as an organic hydride donor. Another set of studies was performed for a rhodium complex using a complete model of one of these ligands, abbreviated PPh_2PhenH, or L^{PhenH}, in which the hydride donor is a dihydrophenanthridinium group. The rhodium complex with this ligand, $[Rh(PP_2)(L^{PhenH})]^+$, is an important, catalytically active species (see Ch 3).

2.2 Geometric and structural analysis

As expected, the optimized structures of the group 9 metal(III) dihydrides showed essentially octahedral geometries. As an example, the structure of $[H_2Co(PP_2)(PPh_3)]^+$, is shown in Figure 12. Selected bond distances are given in Table 1 and bond angles in Table 2. Notably, the substituents on P_1 and P_4 adopt a staggered conformation. The two M–H bonds, placed in a *trans* arrangement due to the expected steric preference for a *trans* arrangement of P1 and P4, have H-M-H angles nearly equal to 180° in each structure, and the M-H distances are nearly identical within each structure. However, the bond angles are not equal: the P_1-M-H_1 angles, for the hydride on the opposite face from the phenyl substituent on P_1, are less than 90° in each structure, whereas the P1-M-H2 angles, for the hydride on the same face as the phenyl substituent, is between 97-98° in each structure, meaning the H-M-H unit is linear and tilted away from this phenyl

substituent. The P1-M-P2 and P1-M-P3 angles, corresponding to the chelate bite angle, are slightly larger for the PMe_3 complexes than the PPh_3 or L^{PhenH} complexes and slightly larger for the $[H_2Co]^+$ structures than for the $[H_2Rh]^+$ structures: the more sterically crowded complexes and smaller metal ion give smaller bite angles. But, comparing the P1-M-P2 angles for the PMe_3 case, the Co complex has a larger bite angle (85.4° vs 84.2°).

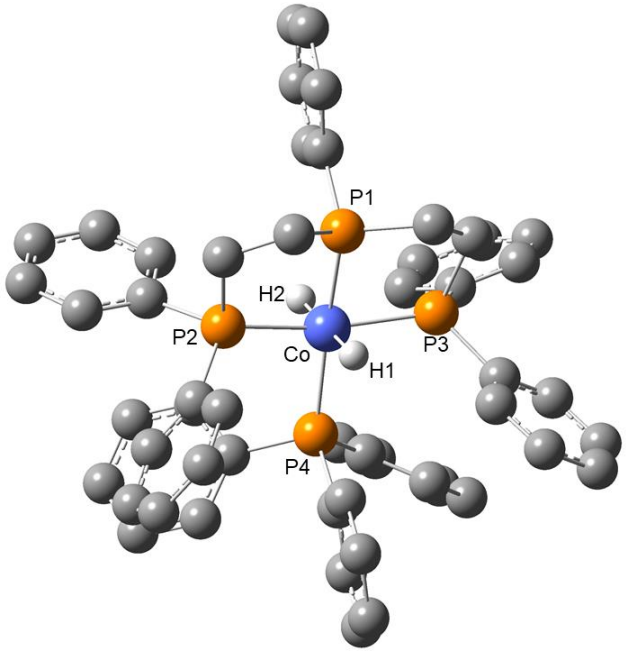

Figure 12. *Optimized structure of $[H_2Co(PP_2)(PPh_3)]^+$. Hydrogen atoms, other than the metal hydrides have been omitted.*

Table 1: *Selected bond distances and sum of electronic and thermal free energies for group 9 metal(III) dihydride cations*

Distances (Å)	$[H_2Co(PP_2)(PMe_3)]^+$	$[H_2Co(PP_2)(PPh_3)]^+$	$[H_2Rh(PP_2)(PMe_3)]^+$	$[H_2Rh(PP_2)(L^{PhenH})]^+$	$[H_2Rh(PP_2)(PPh_3)]^+$
M–P1	2.24	2.25	2.34	2.34	2.35
M–P2	2.27	2.31	2.38	2.39	2.40
M–P3	2.27	2.31	2.38	2.40	2.42
M–P4	2.27	2.32	2.38	2.42	2.43

(continued)

M–H1	1.53	1.53	1.65	1.65	1.64
M–H2	1.52	1.52	1.64	1.64	1.64
Energy (Hartree)	-1612.21592	-2188.88179	-1576.71259	-2557.58430	-2153.37340

Table 2: *Selected bond angles for group 9 metal(III) dihydride cations (Degrees)*

		$[H_2Co(PP_2)(PMe_3)]^+$			
P1–Co–P2	85.4	P3–Co–P4	94.3	H1–Co–H2	180.0
P1–Co–P3	85.4	H1–Co–P1	82.6	H2–Co–P1	97.5
P1–Co–P4	175.3	H1–Co–P2	86.2	H2–Co–P2	93.8
P2–Co–P3	168.8	H1–Co–P3	86.2	H2–Co–P3	93.8
P2–Co–P4	94.3	H1–Co–P4	92.7	H2–Co–P4	87.3
		$[H_2Co(PP_2)(PPh_3)]^+$			
P1–Co–P2	84.1	P3–Co–P4	95.5	H1–Co–H2	178.4
P1–Co–P3	84.3	H1–Co–P1	80.4	H2–Co–P1	98.0
P1–Co–P4	173.7	H1–Co–P2	86.5	H2–Co–P2	93.2
P2–Co–P3	168.0	H1–Co–P3	88.7	H2–Co–P3	91.4
P2–Co–P4	95.8	H1–Co–P4	93.3	H2–Co–P4	88.2
		$[H_2Rh(PP_2)(PMe_3)]^+$			
P1–Rh–P2	84.2	P3–Rh–P4	95.5	H1–Rh–H2	179.0
P1–Rh–P3	84.2	H1–Rh–P1	83.0	H2–Rh–P1	98.1
P1–Rh–P4	174.6	H1–Rh–P2	85.8	H2–Rh–P2	94.3
P2–Rh–P3	166.3	H1–Rh–P3	85.8	H2–Rh–P3	94.3
P2–Rh–P4	95.5	H1–Rh–P4	91.6	H2–Rh–P4	97.3
		$[H_2Rh(PP_2)(L^{PhenH})]^+$			
P1–Rh–P2	82.9	P3–Rh–P4	97.9	H1–Rh–H2	179.4
P1–Rh–P3	83.5	H1–Rh–P1	82.9	H2–Rh–P1	97.1
P1–Rh–P4	172.9	H1–Rh–P2	84.2	H2–Rh–P2	95.2
P2–Rh–P3	165.5	H1–Rh–P3	89.1	H2–Rh–P3	91.5
P2–Rh–P4	94.9	H1–Rh–P4	90.2	H2–Rh–P4	89.9
		$[H_2Rh(PP_2)(PPh_3)]^+$			
P1–Rh–P2	82.9	P3–Rh–P4	98.4	H1–Rh–H2	178.2
P1–Rh–P3	83.1	H1–Rh–P1	88.7	H2–Rh–P1	90.1
P1–Rh–P4	173.3	H1–Rh–P2	82.0	H2–Rh–P2	96.5
P2–Rh–P3	161.6	H1–Rh–P3	85.8	H2–Rh–P3	95.4
P2–Rh–P4	96.9	H1–Rh–P4	97.9	H2–Rh–P4	83.2

The geometries of the metal(III) monohydride dications are similar to those of the dihydrides, where the MeCN ligand replaces the hydride located at H2. Alternative structures in which the MeCN ligand replaces H1 were examined but found to have higher energy. Structures in which the MeCN or hydride were placed *trans* to P1 were not examined, due to the strong steric repulsion expected upon placing P4 *cis* to the other phosphines in these structures. The M-H bond distances are longer in the dihydride structures than in the monohydrides. This is expected, since the more highly-charged cation should have a smaller atomic radius. However, the trend for the M-P bond distances is the opposite: these bonds are consistently longer for the monohydrides than the dihydrides, reflecting weaker metal-ligand back bonding in the less electron-rich monohydride dications. Although the removal of the hydride ligand, as a σ-donor, should not directly affect the energies of the orbitals involved in M-P backbonding, the increased positive charge and the resulting lower overall electron density should lower the energy of the d_π orbitals involved in backbonding and therefore indirectly weaken their ability to donate into the π-acceptor orbitals on the ligands. The selected bond distances are given in Table 3 and angles in Table 4.

Table 3: *Selected bond distances and sum of electronic and thermal free energies for group 9 metal(III) monohydride dications*

Distances (Å)	$[HCo(PP_2)(PMe_3)(MeCN)]^{2+}$	$[HCo(PP_2)(PPh_3)(MeCN)]^{2+}$	$[HRh(PP_2)(PMe_3)(MeCN)]^{2+}$	$[HRh(PP_2)(L^{PhenH})(MeCN)]^{2+}$	$[HRh(PP_2)(PPh_3)(MeCN)]^{2+}$
M–P1	2.31	2.30	2.40	2.38	2.38
M–P2	2.33	2.35	2.43	2.45	2.46
M–P3	2.32	2.36	2.42	2.44	2.45
M–P4	2.32	2.38	2.42	2.48	2.48
M–H	1.47	1.45	1.56	1.54	1.55

(continued)

M–N	1.93	1.95	2.14	2.16	2.16
Energy (Hartree)	-1744.54989	-2321.20906	-1709.04725	-2689.91553	-2285.71189

Table 4: *Selected bond angles for group 9 metal(III) monohydride dication complexes (Degrees)*

		$[HCo(PP_2)(PMe_3)(MeCN)]^{2+}$			
P1–Co–P2	84.7	P3–Co–P4	95.6	H–Co–N	178.9
P1–Co–P3	84.2	H–Co–P1	86.6	N–Co–P1	93.4
P1–Co–P4	175.2	H–Co–P2	78.2	N–Co–P2	102.8
P2–Co–P3	154.5	H–Co–P3	78.3	N–Co–P3	100.7
P2–Co–P4	93.7	H–Co–P4	88.6	N–Co–P4	91.3
		$[HCo(PP_2)(PPh_3)(MeCN)]^{2+}$			
P1–Co–P2	82.5	P3–Co–P4	96.2	H–Co–N	178.7
P1–Co–P3	84.2	H–Co–P1	92.4	N–Co–P1	88.8
P1–Co–P4	178.0	H–Co–P2	87.0	N–Co–P2	92.9
P2–Co–P3	165.6	H–Co–P3	88.3	N–Co–P3	92.1
P2–Co–P4	97.1	H–Co–P4	86.4	N–Co–P4	92.3
		$[HRh(PP_2)(PMe_3)(MeCN)]^{2+}$			
P1–Rh–P2	83.4	P3–Rh–P4	94.9	H–Rh–N	178.7
P1–Rh–P3	82.9	H–Rh–P1	87.0	N–Rh–P1	94.2
P1–Rh–P4	174.0	H–Rh–P2	80.0	N–Rh–P2	100.8
P2–Rh–P3	156.0	H–Rh–P3	79.6	N–Rh–P3	99.8
P2–Rh–P4	94.7	H–Rh–P4	87.1	N–Rh–P4	91.7
		$[HRh(PP_2)(L^{PhenH})(MeCN)]^{2+}$			
P1–Rh–P2	82.8	P3–Rh–P4	95.9	H–Rh–N	177.3
P1–Rh–P3	83.4	H–Rh–P1	83.3	N–Rh–P1	95.4
P1–Rh–P4	171.4	H–Rh–P2	83.3	N–Rh–P2	94.1
P2–Rh–P3	161.0	H–Rh–P3	82.2	N–Rh–P3	100.1
P2–Rh–P4	95.9	H–Rh–P4	88.1	N–Rh–P4	93.2
		$[HRh(PP_2)(PPh_3)(MeCN)]^{2+}$			
P1–Rh–P2	82.5	P3–Rh–P4	96.3	H–Rh–N	178.3
P1–Rh–P3	82.6	H–Rh–P1	81.5	N–Rh–P1	99.0
P1–Rh–P4	168.2	H–Rh–P2	82.5	N–Rh–P2	99.1
P2–Rh–P3	161.6	H–Rh–P3	84.7	N–Rh–P3	93.8
P2–Rh–P4	96.0	H–Rh–P4	86.7	N–Rh–P4	92.7

The trends are similar for the metal(III) trication disolvate complexes: the geometries, as with the other d^6 metal complexes, are octahedral, with shorter M-N distances for the two MeCN ligands in the trications than for the analogous monohydride dications; however, the M-P distances are longer, reflecting weaker M-L backbonding for these ligands. The selected bond distances and angles are shown below in Table 5 and 6. It is worth noting that in all of the metal(III) complexes, where the ideal P1-M-P4 and P2-M-P3 angles would be 180°, and the P1-M-P2 and P1-M-P3 angles would be 90° in an ideal octahedral geometry, these angles are bent so that the P1-M-P4 angles are between 173° and 175°, with two outliers at 171° and 178°. The P2-M-P3 angles are typically around 165°, although for the PMe_3 monohydride complexes they are lower, at around 155°. The P1-M-P2 and P1-M-P3 angles, corresponding to the ligand bite angles of the triphosphine backbone, are typically around 82°-84°, and none are higher than 85.4° in these complexes. Because these angles are smaller than the electronically and VSEPR-preferred angles of 90°, they appear to be conformationally-imposed restraints inherent in the triphosphine ligand, i.e. the natural bite angle of the ligand.

Table 5: *Selected bond distances and sum of electronic and thermal free energies for group 9 metal(III) tricications*

Distances (Å)	$[Co(PP_2)(PMe_3)(MeCN)_2]^{3+}$	$[Co(PP_2)(PPh_3)(MeCN)_2]^{3+}$	$[Rh(PP_2)(PMe_3)(MeCN)_2]^{3+}$	$[Rh(PP_2)(L^{PhenH})(MeCN)_2]^{3+}$	$[Rh(PP_2)(PPh_3)(MeCN)_2]^{3+}$
M–P1	2.36	2.36	2.44	2.43	2.42
M–P2	2.44	2.49	2.50	2.54	2.54
M–P3	2.42	2.48	2.49	2.52	2.53
M–P4	2.39	2.53	2.49	2.54	2.59
M–N1	1.88	1.87	2.00	2.01	2.00
M–N2	1.86	1.87	1.98	1.98	1.99
Energy (Hartree)	-1876.82994	-2453.48207	-1841.31286	-2822.18263	-2417.97350

Table 6: *Selected bond angles for group 9 metal(III) trications (Degrees)*

		$[Co(PP_2)(PMe_3)(MeCN)_2]^{3+}$			
P1–Co–P2	83.0	P3–Co–P4	98.4	N1–Co–N2	179.0
P1–Co–P3	82.7	N1–Co–P1	90.4	N2–Co–P1	90.6
P1–Co–P4	178.6	N1–Co–P2	86.2	N2–Co–P2	93.7
P2–Co–P3	164.3	N1–Co–P3	87.4	N2–Co–P3	92.9
P2–Co–P4	95.8	N1–Co–P4	88.9	N2–Co–P4	90.1
		$[Co(PP_2)(PPh_3)(MeCN)_2]^{3+}$			
P1–Co–P2	83.3	P3–Co–P4	97.0	N1–Co–N2	176.0
P1–Co–P3	81.9	N1–Co–P1	87.4	N2–Co–P1	90.4
P1–Co–P4	176.6	N1–Co–P2	84.3	N2–Co–P2	92.2
P2–Co–P3	163.0	N1–Co–P3	86.6	N2–Co–P3	96.3
P2–Co–P4	98.3	N1–Co–P4	95.8	N2–Co–P4	86.5
		$[Rh(PP_2)(PMe_3)(MeCN)_2]^{3+}$			
P1–Rh–P2	80.5	P3–Rh–P4	97.5	N1–Rh–N2	178.8
P1–Rh–P3	81.9	N1–Rh–P1	91.4	N2–Rh–P1	89.8
P1–Rh–P4	178.9	N1–Rh–P2	88.2	N2–Rh–P2	92.0
P2–Rh–P3	161.4	N1–Rh–P3	86.1	N2–Rh–P3	94.0
P2–Rh–P4	100.0	N1–Rh–P4	87.7	N2–Rh–P4	91.0
		$[Rh(PP_2)(L^{PhenH})(MeCN)_2]^{3+}$			
P1–Rh–P2	81.8	P3–Rh–P4	98.3	N1–Rh–N2	178.9
P1–Rh–P3	81.3	N1–Rh–P1	90.4	N2–Rh–P1	90.3
P1–Rh–P4	178.7	N1–Rh–P2	93.7	N2–Rh–P2	87.2
P2–Rh–P3	163.2	N1–Rh–P3	86.3	N2–Rh–P3	93.0
P2–Rh–P4	98.5	N1–Rh–P4	88.4	N2–Rh–P4	90.9
		$[Rh(PP_2)(PPh_3)(MeCN)_2]^{3+}$			
P1–Rh–P2	82.6	P3–Rh–P4	97.9	N1–Rh–N2	176.5
P1–Rh–P3	81.3	N1–Rh–P1	87.0	N2–Rh–P1	90.8
P1–Rh–P4	177.0	N1–Rh–P2	83.8	N2–Rh–P2	93.2
P2–Rh–P3	161.9	N1–Rh–P3	87.0	N2–Rh–P3	95.4
P2–Rh–P4	98.6	N1–Rh–P4	95.8	N2–Rh–P4	86.4

The geometries of the group 9 metal(I) monohydride complexes, shown in Figure 13 were intermediate between square pyramidal and trigonal bipyramidal, but favoring the latter, with τ_5 values ranging from 0.624 to 0.781. The largest τ_5 values were

for the more sterically congested [HM(PP_2)(PPh_3)] complexes, and, interestingly, the smallest value was for the [HM(PP_2)(L^{PhenH})] complex rather than the presumably less hindered PMe_3 complexes. The axial positions within the distorted trigonal bipyramid were the central phosphorus atom of the triphosphine ligand (P1) and the hydride, making the monophosphine (P4) and the terminal phosphorus donors (P2 and P3) the equatorial positions. The preferred structures for these group 9 complexes were therefore the "apical–P" isomers, placing the monophosphine (P4) *cis* to the central phosphine atom (P1) and the hydride *trans* to P_1. This arrangement maximizes the angles between the bulkier phosphine groups; a square pyramidal geometry with an apical–H arrangement, for instance, would have one large *trans* (P1-M-P4) angle of approximately 180° but two *cis* (P2/P3-M-P4) angles of approximately 90°. Similarly, an "apical–H" arrangement within a trigonal bipyramidal geometry would make the monophosphine in an axial position, with two close (~90°) P-M-P angles with respect to P2 and P3. Instead, the distorted trigonal bipyramidal geometry with an apical–P arrangement appears to consistently give smaller P1-M-P4 angles, ranging from 102.8° in [HCo(PP_2)(PMe_3)] to 107.3° in [HRh(PP_2)(L^{PhenH})], and larger P2/P3-M-P4 angles of approximately 110° to approximately 130°, which are approximately equal to that of the P2-M-P3 angle between the terminal phosphorus atoms of the triphosphine ligand. The M-H distances are longer, but the M-P distances are all considerably shorter than in the corresponding metal(III) ions. For instance, each M-P distance is approximately 0.05 Å shorter in the metal(I) monohydrides than in the corresponding metal(III) monohydride dications and 0.1 Å shorter than in the metal(III) trication disolvate complexes. This is again

attributable to greater metal-phosphorus backbonding in the more electron-rich complexes. The selected bond distances and angles are given below in Table 7 and 8.

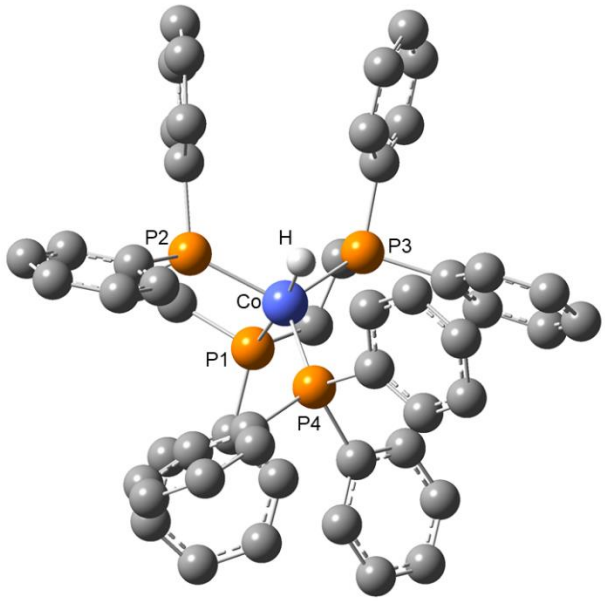

Figure 13. *Optimized structure of [HCo(PP$_2$)(PPh$_3$)]. Hydrogen atoms, other than the metal hydrides have been omitted.*

Table 7: *Selected bond distances and sum of electronic and thermal free energies along with τ_5 for group 9 metal(I) monohydride complexes*

Distances (Å)	[HCo(PP$_2$)(PMe$_3$)]	[HCo(PP$_2$)(PPh$_3$)]	[HRh(PP$_2$)(PMe$_3$)]	[HRh(PP$_2$)(L^{PhenH})]	[HRh(PP$_2$)(PPh$_3$)]
M–P1	2.25	2.26	2.38	2.39	2.40
M–P2	2.22	2.22	2.37	2.37	2.38
M–P3	2.21	2.23	2.41	2.42	2.38
M–P4	2.25	2.24	2.40	2.42	2.42
M–H	1.51	1.49	1.60	1.60	1.59
Energy (Hartree)	-1611.74950	-2188.43125	-1576.24891	-2557.13366	-2152.93401
τ_5	0.694	0.755	0.676	0.624	0.781

Table 8: *Selected bond angles for group 9 metal(I) monohydride complexes (Degrees)*

	[HCo(PP_2)(PMe_3)]		
P1–Co–P2	88.3	P3–Co–P4	117.8
P1–Co–P3	88.1	H–Co–P1	171.4
P1–Co–P4	102.8	H–Co–P2	87.4
P2–Co–P3	129.8	H–Co–P3	88.9
P2–Co–P4	111.8	H–Co–P4	85.7
	[HCo(PP_2)(PPh_3)]		
P1–Co–P2	88.6	P3–Co–P4	117.9
P1–Co–P3	87.7	H–Co–P1	169.4
P1–Co–P4	105.1	H–Co–P2	83.8
P2–Co–P3	116.5	H–Co–P3	89.1
P2–Co–P4	124.1	H–Co–P4	85.3
	[HRh(PP_2)(PMe_3)]		
P1–Rh–P2	85.8	P3–Rh–P4	110.3
P1–Rh–P3	84.4	H–Rh–P1	172.1
P1–Rh–P4	104.5	H–Rh–P2	89.5
P2–Rh–P3	117.8	H–Rh–P3	92.2
P2–Rh–P4	131.6	H–Rh–P4	83.4
	[HRh(PP_2)(L^{PhenH})]		
P1–Rh–P2	85.2	P3–Rh–P4	102.8
P1–Rh–P3	83.1	H–Rh–P1	169.0
P1–Rh–P4	107.3	H–Rh–P2	88.8
P2–Rh–P3	125.4	H–Rh–P3	92.9
P2–Rh–P4	131.6	H–Rh–P4	83.6
	[HRh(PP_2)(PPh_3)]		
P1–Rh–P2	85.7	P3–Rh–P4	120.5
P1–Rh–P3	84.9	H–Rh–P1	167.4
P1–Rh–P4	105.6	H–Rh–P2	88.1
P2–Rh–P3	118.6	H–Rh–P3	88.5
P2–Rh–P4	120.5	H–Rh–P4	87.0

The structures of the d^8 group 9 metal(I) cations are, as expected, essentially square planar structures, with τ_4 values that ranged from 0.163 to 0.195. The main deviation from ideal square planar geometry is due to the chelate bite angle within the triphosphine ligand, which limits the P1-M-P2/P3 angles to between 82-85°, rather than

the angles of 90° expected for an ideal square planar geometry. Interestingly, the Co-P distances in the Co(I) hydride complexes are shorter, on average, than those in the Co(I) cations: for the Co(I) PMe_3 complexes, the Co-P distances are 0.041 Å shorter, on average, in the hydride, and for the PPh_3 complexes the Co-P distances are 0.073 Å shorter, on average, in the hydride. However, for the Rh complexes the trend is the opposite: the Rh-P differences are slightly longer, on average, in the cations than in the hydride, with the average differences being +0.019 Å, +0.022 Å, and +0.0011 Å, for the PMe_3, L^{PhenH}, and PPh_3 complexes, respectively. It is not entirely clear why, but since the M-P distances seem to depend strongly on the backbonding character and hence the electron density of the metal, these differences may reflect a fundamental difference in character between the first- and second-row metal hydrides; in the Co complexes, the d^8 hydrides appear to be more electron-rich than the d^8 cations, whereas in the Rh complexes, the cations are more electron-rich. The tables below give the selected bond distances and angles.

Table 9: *Selected bond distances and sum of electronic and thermal free energies along with τ_4 for group 9 metal(I) cations*

Distances (Å)	$[Co(PP_2)(PMe_3)]^+$	$[Co(PP_2)(PPh_3)]^+$	$[Rh(PP_2)(PMe_3)]^+$	$[Rh(PP_2)(L^{PhenH})]^+$	$[Rh(PP_2)(PPh_3)]^+$
M–P1	2.25	2.25	2.34	2.32	2.34
M–P2	2.27	2.34	2.37	2.39	2.40
M–P3	2.27	2.32	2.37	2.39	2.41
M–P4	2.29	2.33	2.39	2.40	2.43
Energy (Hartree)	-1611.00655	-2187.67596	-1575.51414	-2556.39582	-2152.18753
τ_4	0.195	0.176	0.167	0.213	0.163

Table 10: *Selected bond angles for group 9 metal(I) cations (Degrees)*

	$[Co(PP_2)(PMe_3)]^+$		
P1–Co–P2	85.0	P2–Co–P3	155.8
P1–Co–P3	84.2	P2–Co–P4	96.3
P1–Co–P4	176.7	P3–Co–P4	95.7
	$[Co(PP_2)(PPh_3)]^+$		
P1–Co–P2	83.2	P2–Co–P3	166.7
P1–Co–P3	83.5	P2–Co–P4	96.6
P1–Co–P4	168.5	P3–Co–P4	96.4
	$[Rh(PP_2)(PMe_3)]^+$		
P1–Rh–P2	83.3	P2–Rh–P3	158.4
P1–Rh–P3	82.9	P2–Rh–P4	96.1
P1–Rh–P4	177.7	P3–Rh–P4	97.0
	$[Rh(PP_2)(L^{PhenH})]^+$		
P1–Rh–P2	82.5	P2–Rh–P3	160.3
P1–Rh–P3	82.7	P2–Rh–P4	99.4
P1–Rh–P4	169.6	P3–Rh–P4	97.5
	$[Rh(PP_2)(PPh_3)]^+$		
P1–Rh–P2	82.6	P2–Rh–P3	164.1
P1–Rh–P3	82.3	P2–Rh–P4	96.9
P1–Rh–P4	172.9	P3–Rh–P4	97.4

The optimized structures for the Ni(II) hydrides were very similar to those of the group 9 metal(I) monohydrides (distances in Table 11, angles in Table 12), especially the isoelectronic Co(I) hydride complexes. The most notable difference is in the bond distances: the Ni-H distances are approximately 0.05 Å shorter and the Ni-P distances are approximately 0.05 Å longer than the corresponding distances in the cobalt complexes. This difference is similar to that between the M(I) and M(III) monohydride species described above: the Ni complexes, with a more electronegative metal center and additional positive charge, are less electron-rich and therefore possess weaker M-P interactions due to decreased backbonding.

Table 11: *Selected bond distances and sum of electronic and thermal free energies along with τ_5 for nickel(II) hydride complexes*

Distances (Å)	$[HNi(PP_2)(PMe_3)]^+$	$[HNi(PP_2)(PPh_3)]^+$
M–P1	2.28	2.29
M–P2	2.27	2.28
M–P3	2.29	2.32
M–P4	2.31	2.31
M–H	1.46	1.46
Energy (Hartree)	-1635.88407	-2212.56397
τ_5	0.672	0.732

Table 12: *Selected bond angles for nickel(II) hydride complexes (Degrees)*

	$[HNi(PP_2)(PMe_3)]^+$		
P1–Ni–P2	88.9	P3–Ni–P4	111.3
P1–Ni–P3	88.7	H–Ni–P1	170.9
P1–Ni–P4	104.0	H–Ni–P2	86.6
P2–Ni–P3	130.5	H–Ni–P3	88.2
P2–Ni–P4	117.2	H–Ni–P4	85.1
	$[HNi(PP_2)(PPh_3)]^+$		
P1–Pd–P2	89.4	P3–Pd–P4	117.1
P1–Pd–P3	87.9	H–Pd–P1	169.5
P1–Pd–P4	106.1	H–Pd–P2	82.8
P2–Pd–P3	115.3	H–Pd–P3	89.1
P2–Pd–P4	125.6	H–Pd–P4	84.2

The Pd(II) and Pt(II) hydride cations surprisingly adopt a different geometry altogether than those described above. In these complexes, the structures calculated with an “apical-H” input geometry were found to have a lower energy than those with an “apical-P” input. Although the latter structures were similar to those described above for the Ni, Co, and Rh hydrides, the “apical-H” structures rearranged to essentially lower-energy, essentially four-coordinate geometries, in which one of the terminal phosphorus

atoms from the triphosphine ligand virtually dissociated from the metal center, shown in Figures 14, 15, and 16. The square planar arrangement of the remaining four donor atoms (τ_4 values of approximately 0.1-0.2) place the hydride *trans* to the remaining terminal phosphorus donor and the monophosphine *trans* to the central phosphorus donor atom of the triphosphine ligand. The orientations of the dissociated phosphorus atoms do not suggest any significant M-P bonding, and the M-P distances for these groups range from 3.73 to 4.46 Å. The reason for these unusual geometries is not entirely clear, but it appears that these ions prefer a 16-electron, four-coordinate structure, which is common for d^8 metal ions, over the expected 18-electron, five-coordinate structure. This preference may be related to the weak M-P bonding resulting from reduced backbonding in these complexes, which are charged species with comparatively small, electronegative metal centers. Because of the additional positive charge and the higher effective nuclear charge in the $[HPd]^+$ ions, for example, relative to the [HRh] complexes, the d_π orbitals used for metal-phosphine backbonding are at lower energy and therefore less capable of metal-ligand π-donation. It is also likely that the optimized geometries for these structures are not the species that would actually exist in solution. Assuming that these DFT-calculated geometries reflect a tendency of the complexes to dissociate one of its phosphine donors and form a square planar ion, it seems more likely that in a real complex, due to the chelate effect, the monophosphine would dissociate rather than one of the terminal phosphines. Thus, these geometries are interpreted as suggesting that the actual species observed in solution should be $[HM(PP_2)]^+$ and free PR_3. Table 13 shows the selected bond distances and Table 14 shows the selected bond angles.

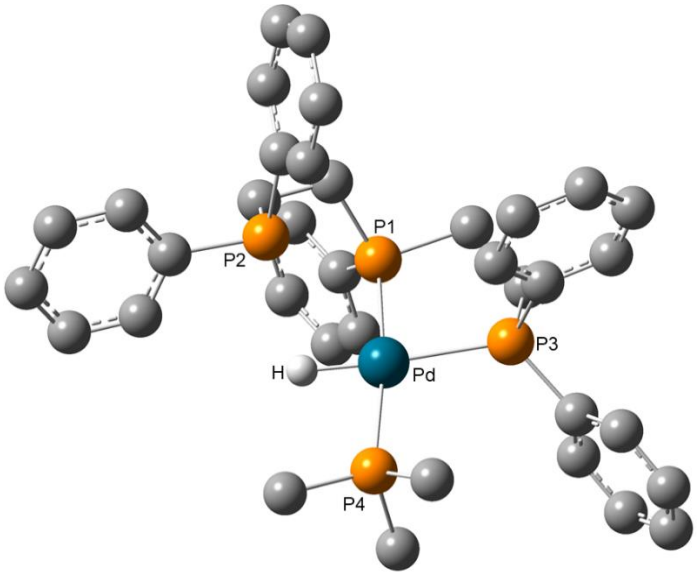

Figure 14. *Optimized structure of [HPd(PP$_2$)(PMe$_3$)]$^+$. Hydrogen atoms, other than the metal hydrides have been omitted.*

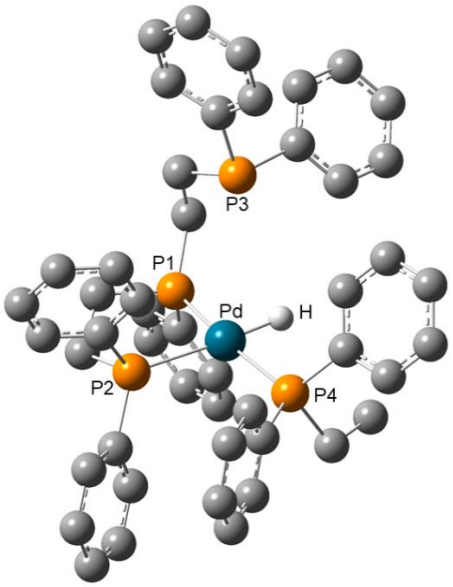

Figure 15. *Optimized structure of [HPd(PP$_2$)(PPh$_2$C$_2$H$_5$)]$^+$. Hydrogen atoms, other than the metal hydrides have been omitted.*

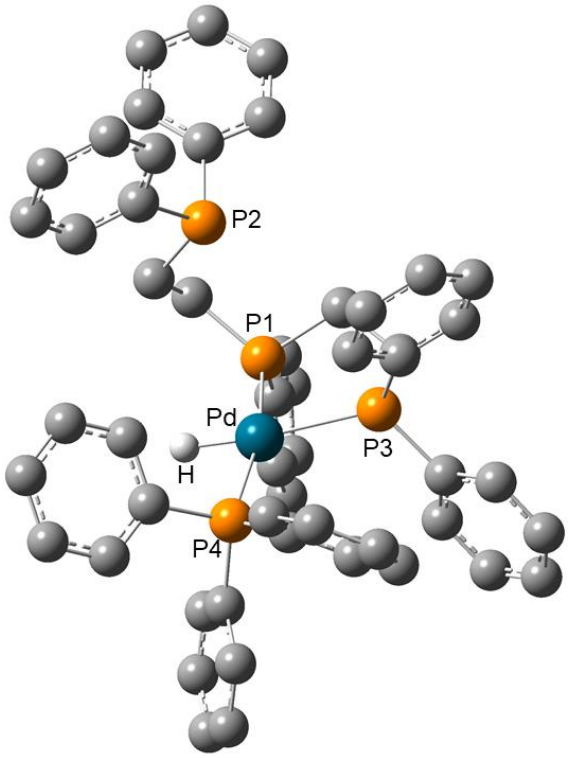

Figure 16. *Optimized structure of $[HPd(PP_2)(PPh_3)]^+$. Hydrogen atoms, other than the metal hydrides have been omitted.*

Table 13: *Selected bond distances and sum of electronic and thermal free energies along with τ_5 for palladium hydride and platinum hydride complexes*

Distances (Å)	$[HPd(PP_2)(PMe_3)]^+$	$[HPd(PP_2)(PPh_2C_2H_5)]^+$	$[HPd(PP_2)(PPh_3)]^+$	$[HPt(PP_2)(PMe_3)]^+$	$[HPt(PP_2)(PPh_3)]^+$
M–P1	2.37	2.37	2.37	2.37	2.36
M–P2	3.73	2.46	4.47	3.72	4.45
M–P3	2.45	3.94	2.48	2.44	2.45
M–P4	2.38	2.39	2.40	2.37	2.38
M–H	1.57	1.57	1.57	1.60	1.60
Energy (Hartree)	-1593.34730	-2017.22831	-2170.02852	-1585.79367	-2162.47201
τ_4	0.112	0.144	0.152	0.092	0.116
τ_5	0.009	0.069	0.050	0.005	0.026

Table 14: *Selected bond angles for palladium hydride and platinum hydride complexes (Degrees)*

	$[HPd(PP_2)(PMe_3)]^+$		
P1–Pd–P2	73.5	P3–Pd–P4	102.1
P1–Pd–P3	85.3	H–Pd–P1	87.9
P1–Pd–P4	171.8	H–Pd–P2	62.1
P2–Pd–P3	118.8	H–Pd–P3	172.4
P2–Pd–P4	105.4	H–Pd–P4	84.6
	$[HPd(PP_2)(PPh_2C_2H_5)]^+$		
P1–Pd–P2	85.4	P3–Pd–P4	115.0
P1–Pd–P3	66.8	H–Pd–P1	86.8
P1–Pd–P4	167.8	H–Pd–P2	171.9
P2–Pd–P3	109.9	H–Pd–P3	68.9
P2–Pd–P4	104.5	H–Pd–P4	82.9
	$[HPd(PP_2)(PPh_3)]^+$		
P1–Pd–P2	55.7	P3–Pd–P4	106.9
P1–Pd–P3	85.3	H–Pd–P1	85.5
P1–Pd–P4	167.7	H–Pd–P2	84.9
P2–Pd–P3	90.6	H–Pd–P3	170.8
P2–Pd–P4	122.6	H–Pd–P4	82.3
	$[HPt(PP_2)(PMe_3)]^+$		
P1–Pt–P2	70.9	P3–Pt–P4	101.1
P1–Pt–P3	85.1	H–Pt–P1	89.3
P1–Pt–P4	173.4	H–Pt–P2	67.1
P2–Pt–P3	113.7	H–Pt–P3	173.6
P2–Pt–P4	108.1	H–Pt–P4	84.3
	$[HPt(PP_2)(PPh_3)]^+$		
P1–Pt–P2	56.1	P3–Pt–P4	103.8
P1–Pt–P3	85.2	H–Pt–P1	87.6
P1–Pt–P4	171.0	H–Pt–P2	89.5
P2–Pt–P3	87.7	H–Pt–P3	172.6
P2–Pt–P4	123.5	H–Pt–P4	83.5

Unlike the group 10 metal(II) hydrides, the structures of the four-coordinate group 10 metal(II) dications, shown in Figure 17 are straightforward and similar to those of the isoelectronic group 9 metal(I) cations, although the τ_4 values are consistently higher,

indicating greater deviations from ideal square planar structures. The bond distances and angles for the Ni(II) structures are in Table 15 and Table 16. For the Pd(II) and Pt(II) structures, the data is in Table 17 and Table 18.

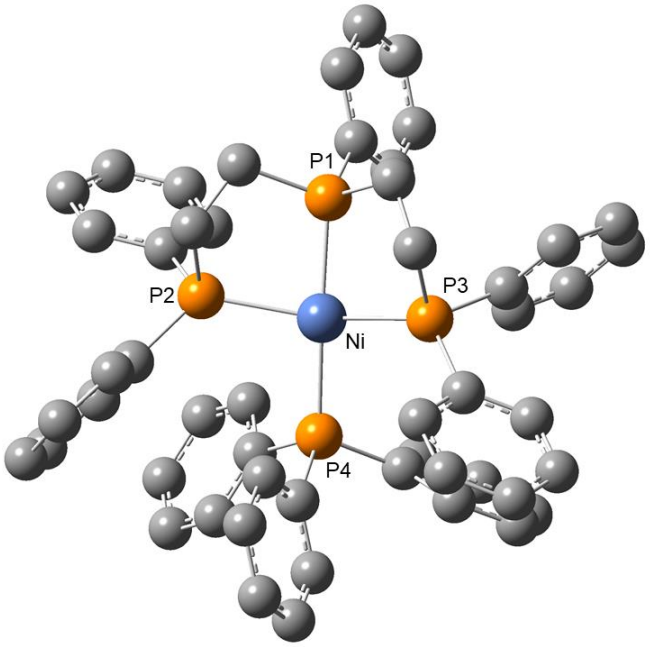

Figure 17. *Optimized structure of* $[Ni(PP_2)(PPh_3)]^{2+}$. *Hydrogen atoms, other than the metal hydrides have been omitted.*

Table 15: *Selected bond distances and sum of electronic and thermal free energies along with* τ_4 *for nickel(II) dication complexes*

Distances (Å)	$[Ni(PP_2)(PMe_3)]^{2+}$	$[Ni(PP_2)(PPh_3)]^{2+}$
M–P1	2.30	2.32
M–P2	2.30	2.34
M–P3	2.30	2.34
M–P4	2.30	2.33
Energy (Hartree)	-1635.11017	-2211.77765
τ_4	0.258	0.241

Table 16: *Selected bond angles for nickel(II) dication complexes (Degrees)*

	$[Ni(PP_2)(PMe_3)]^{2+}$		
P1–Ni–P2	84.7	P2–Ni–P3	150.9
P1–Ni–P3	84.8	P2–Ni–P4	97.2
P1–Ni–P4	172.6	P3–Ni–P4	96.7
	$[Ni(PP_2)(PPh_3)]^{2+}$		
P1–Ni–P2	83.2	P2–Ni–P3	153.0
P1–Ni–P3	83.4	P2–Ni–P4	98.0
P1–Ni–P4	173.0	P3–Ni–P4	98.1

Table 17: *Selected bond distances and sum of electronic and thermal free energies along with τ_4 for palladium and platinum dication complexes*

Distances (Å)	$[Pd(PP_2)(PMe_3)]^{2+}$	$[Pd(PP_2)(PPh_2C_2H_5)]^{2+}$	$[Pd(PP_2)(PPh_3)]^{2+}$	$[Pt(PP_2)(PMe_3)]^{2+}$	$[Pt(PP_2)(PPh_3)]^{2+}$
M–P1	2.40	2.38	2.38	2.39	2.40
M–P2	2.41	2.43	2.46	2.40	2.42
M–P3	2.41	2.43	2.45	2.40	2.42
M–P4	2.41	2.43	2.47	2.41	2.43
Energy (Hartree)	-1592.57640	-2016.45101	-2169.24739	-1585.01798	-2161.68815
τ_4	0.178	0.247	0.162	0.171	0.199

Table 18: *Selected bond angles for palladium and platinum dication complexes (Degrees)*

	$[Pd(PP_2)(PMe_3)]^{2+}$		
P1–Pd–P2	82.4	P2–Pd–P3	156.0
P1–Pd–P3	82.8	P2–Pd–P4	97.6
P1–Pd–P4	178.9	P3–Pd–P4	97.6
	$[Pd(PP_2)(PPh_2C_2H_5)]^{2+}$		
P1–Pd–P2	83.2	P2–Pd–P3	151.9
P1–Pd–P3	82.2	P2–Pd–P4	96.9
P1–Pd–P4	173.2	P3–Pd–P4	100.4
	$[Pd(PP_2)(PPh_3)]^{2+}$		
P1–Pd–P2	82.0	P2–Pd–P3	163.5
P1–Pd–P3	82.3	P2–Pd–P4	97.8
P1–Pd–P4	173.6	P3–Pd–P4	97.2

(continued)

	$[Pt(PP_2)(PMe_3)]^{2+}$		
P1–Pt–P2	82.8	P2–Pt–P3	157.9
P1–Pt–P3	82.9	P2–Pt–P4	97.5
P1–Pt–P4	178.0	P3–Pt–P4	97.3
	$[Pt(PP_2)(PPh_3)]^{2+}$		
P1–Pt–P2	82.1	P2–Pt–P3	156.4
P1–Pt–P3	82.4	P2–Pt–P4	98.1
P1–Pt–P4	175.6	P3–Pt–P4	98.7

Finally, the structures for the group 10 metal(0) complexes, as anticipated, optimized to distorted tetrahedral geometries, shown in Figure 18, with τ_4 values of approximately 0.8. The ligand bite angles within the triphosphine increase by approximately 5° relative to the square planar metal(II) species but are still constrained to be only approximately 90°, which is less than the angles of 109.5° expected for an ideal tetrahedron. In the structures of group 10 metal bis(diphosphine) complexes in the literature, a contraction of the M-P bond distances of approximately 0.04-0.06 Å is consistently observed upon reduction from the metal(II) to metal(0) structures.[5,28,29] No such consistent trend is observed in these (triphosphine)(monophosphine) complexes. For the Ni complexes, a contraction of -0.04 to -0.06 Å is indeed observed. However, for the Pd complexes, an increase of 0.03 to 0.10 Å is observed upon reduction. In the Pt complexes, the bond distances in the Pt^{II} and Pt^0 species are essentially identical. The selected bond distances and angles for Ni^0 complexes are in Table 19 and 20. For the Pd^0 and Pt^0 complexes the distances and angles are in Table 21 and 22.

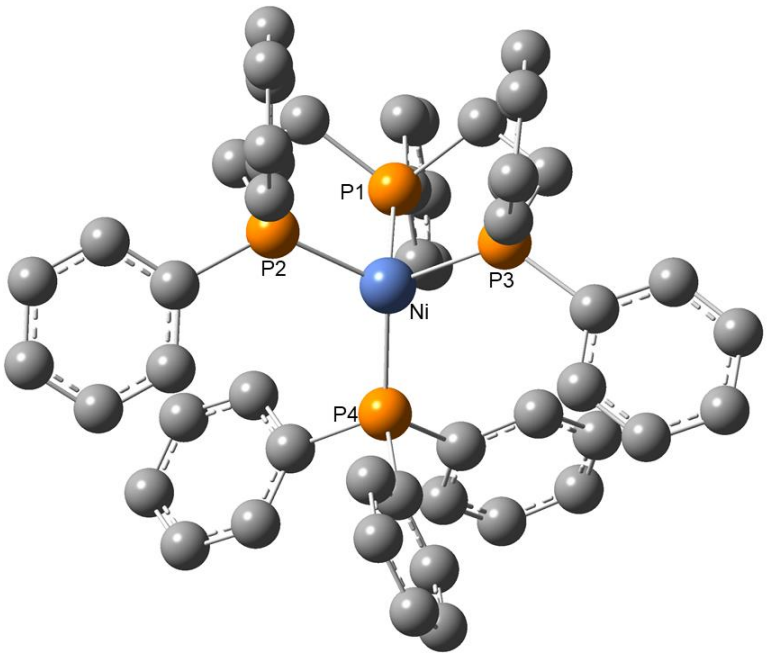

Figure 18. *Optimized structure of [Ni^0(PP$_2$)(PPh$_3$)]. Hydrogen atoms, other than the metal hydrides have been omitted.*

Table 19: *Selected bond distances and sum of electronic and thermal free energies along with τ_4 for nickel(0) complexes*

Distances (Å)	[Ni^0(PP$_2$)(PMe$_3$)]	[Ni^0(P5P$_2$)(PPh$_3$)]
M–P1	2.26	2.27
M–P2	2.26	2.27
M–P3	2.26	2.27
M–P4	2.26	2.25
Energy (Hartree)	-1635.42389	-2212.11307
τ_4	0.843	0.879

Table 20: *Selected bond angles for nickel(0) complexes (Degrees)*

[Ni^0(PP$_2$)(PMe$_3$)]			
P1–Ni–P2	90.1	P2–Ni–P3	120.3
P1–Ni–P3	90.7	P2–Ni–P4	113.1
P1–Ni–P4	120.8	P3–Ni–P4	116.9

(continued)

	$[Ni^0(PP_2)(PPh_3)]$		
P1–Ni–P2	90.3	P2–Ni–P3	117.8
P1–Ni–P3	90.7	P2–Ni–P4	117.6
P1–Ni–P4	118.3	P3–Ni–P4	116.0

Table 21: *Selected bond distances and sum of electronic and thermal free energies along with τ_4 for palladium(0) and platinum(0) complexes*

Distances (Å)	$[Pd^0(PP_2)(PMe_3)]$	$[Pd^0(PP_2)(PPh_2C_2H_5)]$	$[Pd^0(PP_2)(PPh_3)]$	$[Pt^0(PP_2)(PMe_3)]$	$[Pt^0(PP_2)(PPh_3)]$
M–P1	2.50	2.48	2.47	2.42	2.43
M–P2	2.51	2.49	2.48	2.42	2.43
M–P3	2.53	2.46	2.48	2.43	2.43
M–P4	2.49	2.44	2.44	2.39	2.38
Energy (Hartree)	-1592.89354	-2016.77893	-2169.58006	-1585.31335	-2161.99685
τ_4	0.798	0.811	0.825	0.702	0.827

Table 22: *Selected bond angles for palladium(0) and platinum(0) complexes (Degrees)*

	$[Pd^0(PP_2)(PMe_3)]$		
P1–Pd–P2	86.1	P2–Pd–P3	121.4
P1–Pd–P3	86.3	P2–Pd–P4	109.0
P1–Pd–P4	125.1	P3–Pd–P4	122.4
	$[Pd^0(PP_2)(PPh_2C_2H_5)]$		
P1–Pd–P2	85.8	P2–Pd–P3	118.4
P1–Pd–P3	84.9	P2–Pd–P4	117.8
P1–Pd–P4	127.3	P3–Pd–P4	115.8
	$[Pd^0(PP_2)(PPh_3)]$		
P1–Pd–P2	85.2	P2–Pd–P3	116.4
P1–Pd–P3	86.6	P2–Pd–P4	119.4
P1–Pd–P4	124.2	P3–Pd–P4	116.9
	$[Pt^0(PP_2)(PMe_3)]$		
P1–Pt–P2	85.8	P2–Pt–P3	125.2
P1–Pt–P3	86.3	P2–Pt–P4	112.6
P1–Pt–P4	135.8	P3–Pt–P4	110.4
	$[Pt^0(PP_2)(PPh_3)]$		
P1–Pt–P2	85.7	P2–Pt–P3	115.9

(continued)

P1–Pt–P3	86.5	P2–Pt–P4	118.2
P1–Pt–P4	125.2	P3–Pt–P4	117.8

2.3 Acidity and hydricity analysis

Using the energies of the geometry-optimized structures, the thermodynamic acidity (pK_a) and hydricity (ΔG^o_H-) values were calculated based on a strategy developed by Qi *et al*.[24] In this scheme, the pK_a or ΔG^o_H- value of each species was determined relative to that of a structurally related metal hydride with a known acidity or hydricity, rather than calculating the energy of the acidity or hydricity half-reaction directly. The acidity values were calculated using the thermodynamic cycle shown in Figure 19, in which the free energy of H^+ dissociation from the target metal hydride ($[HM_{target}]^{n+1}$, eq. 30) is equal to the sum of the energy for proton transfer from the target hydride to a reference metal complex (M_{ref}^{n+1}, eq. 31) and the energy for proton dissociation from the reference metal hydride ($[HM_{ref}]^{n+1}$, eq. 32). The pK_a of the target hydride is therefore calculated as shown in eq. 33.

$$[HM]^{n+1}_{target} \rightleftharpoons M^{n+}_{target} + H^+ \quad 1.364pK_{a\ target} \qquad \text{eq. 30}$$

$$[HM]^{n+1}_{target} + M^{n+}_{ref} \rightleftharpoons M^{n+}_{target} + [HM]^{n+1}_{ref} \quad \Delta G_{exchange} \qquad \text{eq. 31}$$

$$[HM]^{n+1}_{ref} \rightleftharpoons M^{n+}_{ref} + H^+ \quad 1.364pK_a\ (ref) \qquad \text{eq. 32}$$

$$pK_{a\ target} = \frac{1.364pK_a\ (ref) + \Delta G_{exchange}}{1.364} \qquad \text{eq. 33}$$

Figure 19. *Relationship between acidity of target M–H species and proton transfer with a reference M–H species of known acidity*

For example, to determine the pK_a of $[HPt(PP_2)(PPh_3)]^+$, the reference hydride was $[HPt(dmpp)_2]^+$, whose pK_a in MeCN has been determined experimentally to be 30.4.[5] The free energy of H^+ transfer from $[HPt(PP_2)(PPh_3)]^+$ to $[Pt^0(dmpp)_2]$, forming $[Pt^0(PP_2)(PPh_3)]$, and $[HPt(dmpp)_2]^+$, was calculated from the energies of the

geometry-optimized structures of each of these species, giving the value for $\Delta G°_{exchange}$ in eq. 31. The purpose of modeling a proton-transfer reaction and using a reference metal hydride, rather than calculating the energy of eq. 30 directly, is to minimize the errors in the calculations by containing similar metals, charges, and structures on both sides of the reaction.

An analogous scheme was used for the hydricity calculations, modeling hydride transfer between the target hydride donor and a reference hydride acceptor of known hydricity. From these calculations, and the hydricity of the reference complex, the hydricity of the target complex was calculated using the thermodynamic cycle shown in Figure 20.

$$[HM]^{n-1}_{target} \rightleftharpoons M^{n+}_{target} + H^- \quad \Delta G°_{H^-\ target} \quad \text{eq. 34}$$

$$[HM]^{n-1}_{target} + M^{n+}_{ref} \rightleftharpoons M^{n+}_{target} + [HM]^{n-1}_{ref} \quad \Delta G_{exchange} \quad \text{eq. 35}$$

$$[HM]^{n-1}_{ref} \rightleftharpoons M^{n+}_{ref} + H^- \quad \Delta G°_{H^-}\ (ref) \quad \text{eq. 36}$$

$$\Delta G°_{H^-\ target} = \Delta G_{exchange} + \Delta G°_{H^-}\ (ref) \quad \text{eq. 37}$$

Figure 20. *Relationship between hydricity of target M-H species and hydride transfer with a reference M-H species of known hydricity*

To confirm that the thermodynamic data obtained from these DFT calculations were reliable, a series of validation calculations were performed, using metal bis(diphosphine) complexes whose pK_a and $\Delta G°_{H^-}$ values have been established experimentally. For example, the pK_a value of $[HNi(dmpe)_2]^+$, known experimentally to be 24.4 in MeCN,[20] was calculated using $[HPt(dmpp)_2]^+$ (pK_a 30.4)[5] as a reference hydride, as shown in Figure 21.

$$[HNi^{II}(dmpe)_2]^+ \rightleftharpoons [Ni^0(dmpe)_2] + H^+ \qquad 1.364pK_a\ (HNi) \qquad \text{eq. 38}$$

$$[HNi^{II}(dmpe)_2]^+ + [Pt^0(dmpp)_2] \rightleftharpoons [Ni^0(dmpe)_2] + [HPt^{II}(dmpp)_2]^+ \qquad \Delta G_{exchange} = -9.16 \qquad \text{eq. 39}$$

$$[HPt^{II}(dmpp)_2]^+ \rightleftharpoons [Pt^0(dmpp)_2] + H^+ \qquad 1.364\ (30.4)\ (ref) \qquad \text{eq. 40}$$

$$pK_{a\ HNi} = \frac{(-9.16) + 1.364(30.4)}{1.364} = 23.7 \qquad \text{eq. 41}$$

Figure 21. *Example calculation for the acidity determination of* $[HNi(dmpe)_2]^+$

From the difference between the product and reactant free energies for the species in eq. 39, the free energy for proton transfer was calculated to be -9.16 kcal/mol, corresponding to a pK_a value of 23.7 for $[HNi(dmpe)_2]^+$. This is within 1 unit of the experimentally measured value. The values for other metal hydride and dihydride species used for validation are shown in Table 23. Both group 9 metal dihydride and group 10 metal hydrides were calculated, covering each transition metal used in the subsequent studies of triphosphine complexes. Each calculated value is in excellent agreement with the experimental values, demonstrating that this method can reliably determine the pK_a values for the metal hydride and dihydride complexes of interest in this study.

Table 23: *DFT-Calculated and experimental* pK_a *values of known bis(diphosphine) complexes*

Transition-Metal Hydrides	pK_a (calc.)	pK_a (exp.)	Reference Complex	ref
$[H_2Co(dmpe)_2]^+$	34.2	33.7	$[H_2Rh(dmpe)_2]^+$	24
$[H_2Rh(dmpe)_2]^+$	36.2	36.7	$[H_2Co(dmpe)_2]^+$	23
$[HCo(dppe)_2(MeCN)]^{2+}$	10.2	11.3	$[HRh(dmpe)_2(MeCN)]^{2+}$	27
$[HNi(dmpe)_2]^+$	23.7	24.4 ± 0.2	$[HPt(dmpp)_2]^+$	20
$[HPd(depe)_2]^+$	23.3	23.2 ± 0.2	$[HPt(dmpp)_2]^+$	28
$[HPt(dmpp)_2]^+$	31.1	30.4	$[HNi(dmpe)_2]^+$	5

A similar series of hydricity calculations were carried out to validate the method for this parameter, as shown in Figure 22 using the calculation of ΔG_{H^-} for $[HNi(dmpe)_2]^+$ as an example.

$$[HNi^{II}(dmpe)_2]^+ \rightleftharpoons [Ni^{II}(dmpe)_2]^{2+} + H^- \qquad \Delta G^\circ_{H^-}\text{ (HNi)} \qquad \text{eq. 42}$$

$$[HNi^{II}(dmpe)_2]^+ + [Pt^{II}(dmpp)_2]^{2+} \rightleftharpoons [Ni^{II}(dmpe)_2]^{2+} + [HPt^{II}(dmpp)_2]^+ \quad \Delta G_{exchange} = -1.14 \qquad \text{eq. 43}$$

$$[HPt^{II}(dmpp)_2]^+ \rightleftharpoons [Pt^{II}(dmpp)_2]^{2+} + H^- \qquad \Delta G^\circ_{H^-}\text{ (ref)} = 50.7 \qquad \text{eq. 44}$$

$$\Delta G^\circ_{H^-\ HNi} = (-1.14) + 50.7 = 49.6 \qquad \text{eq. 45}$$

Figure 22. *Example calculation for the hydricity determination for* $[HNi(dmpe)_2]^+$

The DFT-calculated value using this method was 49.6 kcal/mol, which is in good agreement with the experimental value of 50.7 kcal/mol.[5] The results for a series of other metal hydrides are shown in Table 24. The calculated and experimental values roughly match to within 1 kcal/mol, indicating that the method to calculate hydricity values is accurate and can be used for further calculations on new metal-hydrides.

Table 24: *DFT-Calculated and experimental hydricity values of known bis(diphosphine) complexes*

Transition-Metal Hydrides	Calc. $\Delta G°_{H^-}$ (kcal/mol)	Exp. $\Delta G°_{H^-}$ (kcal/mol)	Reference Complex	ref
$[HRh(dmpe)_2]$	26.0	26.6	$[HRh(dppbz)_2]$	23
$[HRh(dppbz)_2]$	34.6	34.0	$[HRh(dmpe)_2]$	19
$[HNi(dmpe)_2]^+$	49.6	50.7	$[HPt(dmpp)_2]^+$	27
$[HPt(dmpp)_2]^+$	51.8	50.7	$[HPt(dmpp)_2]^+$	20

Having demonstrated the accuracy of these methods, the DFT calculations were used to determine the pK_a and $\Delta G°_{H^-}$ values for the series of novel

metal(triphosphine)(monophosphine) complexes that are the focus of this work. The pK_a values calculated for these complexes are summarized in Table 25.

Table 25: *DFT-Calculated pK_a values for metal triphosphine complexes*

Transition-Metal Hydrides	pK_a (calc.)	Reference Complex
$[HCo(PP_2)(PMe_3)(MeCN)]^{2+}$	16.9	$[HRh(dmpe)_2(MeCN)]^{2+}$
$[HCo(PP_2)(PPh_3)(MeCN)]^{2+}$	12.2	$[HRh(dmpe)_2(MeCN)]^{2+}$
$[H_2Co(PP_2)(PMe_3)]^{+}$	26.8	$[H_2Co(dmpe)_2]^{+}$
$[H_2Co(PP_2)(PPh_3)]^{+}$	19.5	$[H_2Co(dmpe)_2]^{+}$
$[HRh(PP_2)(PMe_3)(MeCN)]^{2+}$	12.2	$[HRh(dmpe)_2(MeCN)]^{2+}$
$[HRh(PP_2)(L^{PhenH})(MeCN)]^{2+}$	4.7	$[HRh(dmpe)_2(MeCN)]^{2+}$
$[HRh(PP_2)(PCy_3)(MeCN)]^{2+}$	5.6	$[HRh(dmpe)_2(MeCN)]^{2+}$
$[HRh(PP_2)(PPh_3)(MeCN)]^{2+}$	5.7	$[HRh(dmpe)_2(MeCN)]^{2+}$
$[HRh(PP_2)(PF_3)(MeCN)]^{2+}$	-2.6	$[HRh(dmpe)_2(MeCN)]^{2+}$
$[H_2Rh(PP_2)(PMe_3)]^{+}$	27.3	$[H_2Rh(dmpe)_2]^{+}$
$[H_2Rh(PP_2)(L^{PhenH})]^{+}$	21.3	$[H_2Rh(dmpe)_2]^{+}$
$[H_2Rh(PP_2)(PCy_3)]^{+}$	21.4	$[H_2Rh(dmpe)_2]^{+}$
$[H_2Rh(PP_2)(PPh_3)]^{+}$	16.2	$[H_2Rh(dmpe)_2]^{+}$
$[H_2Rh(PP_2)(PF_3)]^{+}$	1.0	$[H_2Rh(dmpe)_2]^{+}$
$[HNi(PP_2)(PMe_3)]^{+}$	23.7	$[HNi(dmpe)_2]^{+}$
$[HNi(PP_2)(PPh_3)]^{+}$	19.5	$[HNi(dmpe)_2]^{+}$
$[HPd(PP_2)(PMe_3)]^{+}$	20.1	$[HPt(dmpp)_2]^{+}$

(continued)

$[HPd(PP_2)(PPh_2C_2H_5)]^+$	18.1	$[HPt(dmpp)_2]^+$
$[HPd(PP_2)(PPh_3)]^+$	17.6	$[HPt(dmpp)_2]^+$
$[HPt(PP_2)(PMe_3)]^+$	32.3	$[HPt(dmpp)_2]^+$
$[HPt(PP_2)(PPh_3)]^+$	31.5	$[HPt(dmpp)_2]^+$

The pK_a values calculated for the group 9 monohydrides range from approximately 5 to 17, with the Rh hydrides being more acidic by approximately 4.5-6.5 pK_a units than the Co complexes, and the PPh_3 complexes similarly being more acidic by approximately 4.5-6.5 pK_a units than the PMe_3 complexes. The values and trends for the PPh_3 complexes are similar to those of the analogous $[HM(dppe)_2(CH_3CN)]^{2+}$ analogues.[6,27] However, an interesting difference is that the $[HCo(PP_2)(PPh_3)(MeCN)]^{2+}$ complex is more basic than the analogue $[HCo(dppe)_2(MeCN)]^{2+}$ that has an experimental value of 11.3,[27] but the $[HRh(PP_2)(PPh_3)(MeCN)]^{2+}$ complex is significantly more acidic than the analogue $[HRh(dppe)_2(MeCN)]^{2+}$ that has an experimental value of 9.0.[6] On the other hand, the pK_a values of the Co dihydrides are similar to those of the corresponding Rh dihydrides, but without a consistent trend: for the PPh_3^+ complexes, the Rh dihydride is more acidic, but for the PMe_3 complexes, the Co dihydride is more acidic. For each metal, the PPh_3 complex is more acidic than the PMe_3 complex by approximately 7-10 pK_a units. Experimental values for the corresponding bis(diphosphine) complexes are not complete enough to allow a clear trend for comparison of the metals, but the difference between PPh_3 and PMe_3 complexes is in line with the differences between $[H_2M(dppe)_2]^+$ and $[H_2M(dmpe)_2]^+$ analogues. The $[H_2M(PP_2)(PPh_3)]$ complexes were more acidic than the known analogues, such as

$[H_2Co(dppe)_2]^+$ with an experimental value of 22.8.[27] All of the metal(III) dihydride complexes in this study are dramatically more acidic than the $[H_2Co(dmpe)_2]^+$ and $[H_2Rh(dmpe)_2]^+$ complexes that have been used as CO_2 hydrogenation catalysts (33.7 and 36.7, respectively).[16] The overall differences between the mixed (triphosphine)(monophosphine) complexes and the analogous bis(diphosphine) complexes are likely to be based in steric factors, considering the similar electronic donor properties in the ligand sets. The differences between the metal(III) dihydrides and the metal(III) monohydrides, on the other hand, are likely due to electronic factors. The dihydrides are more electron-rich, containing a strongly σ-donating hydride ligand instead of a weakly bound acetonitrile ligand and one fewer positive charge.

Both electronic and steric factors contribute to the acidities of these complexes. In studies of the bis(diphosphine) complexes, both steric and electronic factors were found to influence the acidities of the metal(III) monohydrides, but steric factors had much larger effects.[6] The hydrides became more acidic with increasing steric bulk on the substituents on the phosphine ligands or increasing the bite angle of the diphosphine. In this study, similar effects are seen, with the highest pK_a values in complexes that have smaller and more electron-donating substituents. Comparing these trends, steric factors appear to play the largest role. Strikingly, $[HRh(PP_2)(PCy_3)(MeCN)]^{2+}$, with a bulky, electron-donating trialkylphosphine, has a pK_a of 5.65, nearly identical to that of $[HRh(PP_2)(PPh_3)(MeCN)]^{2+}$, which has a similarly bulky but much less donating triarylphosphine. $[HRh(PP_2)(PMe_3)(MeCN)]^{2+}$ (pK_a 12.20) on the other hand, which has a much smaller trialkylphosphine, is much less acidic. Of course, electronic factors still play a role, and the strongly π-acidic PF_3 complex, which has a steric profile similar to

that of PMe_3, is a strong acid (pK_a -2.53). Similar trends exist for the dihydride complexes, but here sterics appear to play a smaller role; the PCy_3 complex, for instance, is significantly less acidic than the PPh_3 complex. For the monohydride complexes, such as $[HRh(PP_2)(PPh_3)(MeCN)]^{2+}$, H^+ dissociation is associated with the loss of MeCN, forming, e.g. $[Rh(PP_2)(PPh_3)]^+$ and free MeCN; therefore, the change is from a six-coordinate to a four-coordinate structure. For the dihydride complexes, e.g. $[H_2Rh(PP_2)(PPh_3)]^+$, H^+ dissociation yields only the five-coordinate hydride, e.g. $[HRh(PP_2)(PPh_3)]$. Therefore, a larger structural change is associated with the pK_a values of the monohydrides, and steric factors, such as the interactions of the phosphine substituents with the bound MeCN ligand, are thus more important for the dihydrides.

The pK_a values calculated for group 10 metal hydrides range from ca. 18 to 33 and are consistently higher than the $[HM(dppe)_2]^+$ analogues, such as $[HNi(dppe)_2]^+$ and $[HPt(dppe)_2]^+$ with experimental values of 14.7 ± 0.3 and 22.2, respectively.[5] The differences should be largely attributable to structural differences between the complexes, since the PPh_3 complexes are electronically similar to the bis(dppe) analogues. The observed trend of increasing pK_a in the order Pd < Ni < Pt matches that of the $[HM(diphosphine)_2]^+$ complexes,[18, 35] although the pK_a values of the Ni and Pd complexes are close to one another, while the Pt complexes are considerably higher in value. Interestingly, for a given metal, there was only a small (1-3) difference between the pK_a values for the PMe_3 and PPh_3 complexes. The Ligand Acidity Constants developed by Morris, based on correlations between acidities of metal hydrides with various ligands, predict that exchanging a triarylphosphine (LAC 2.7) for a trialkylphosphine (LAC 4.9) will result in an increase in pK_a of 2.2, on average, based on

electronic factors.[18] Since this difference roughly matches the differences between PMe_3 and PPh_3 complexes in this study, the electronic differences between these ligands are sufficient to explain the trend. This is in line with previous studies of acidities for group 10 metal hydrides, in which structural differences between the ligands were found to have minimal effect.[28,29]

Table 26 displays the calculated hydricity value for new metal-hydrides and the reference complex used.

Table 26: *DFT-Calculated hydricity values for metal triphosphine complexes*

Transition-Metal Hydride	Calc. $\Delta G°_{H}$- (kcal/mol)	Reference Complex
$[HCo(PP_2)(PMe_3)]$	42.8	$[HCo(dmpe)_2]$
$[HCo(PP_2)(PPh_3)]$	50.5	$[HCo(dmpe)_2]$
$[H_2Co(PP_2)(PMe_3)]^+$	55.9	$[H_2Rh(dmpe)_2]^+$
$[H_2Co(PP_2)(PPh_3)]^+$	60.1	$[H_2Rh(dmpe)_2]^+$
$[HRh(PP_2)(PMe_3)]$	35.7	$[HRh(dmpe)_2]$
$[HRh(PP_2)(L^{PhenH})]$	37.7	$[HRh(dmpe)_2]$
$[HRh(PP_2)(PCy_3)]$	40.0	$[HRh(dmpe)_2]$
$[HRh(PP_2)(PPh_3)]$	43.1	$[HRh(dmpe)_2]$
$[HRh(PP_2)(PF_3)]$	65.8	$[HRh(dmpe)_2]$
$[H_2Rh(PP_2)(PMe_3)]^+$	55.5	$[H_2Rh(dmpe)_2]^+$
$[H_2Rh(PP_2)(L^{PhenH})]^+$	59.4	$[H_2Rh(dmpe)_2]^+$
$[H_2Rh(PP_2)(PCy_3)]^+$	60.6	$[H_2Rh(dmpe)_2]^+$
$[H_2Rh(PP_2)(PPh_3)]^+$	56.5	$[H_2Rh(dmpe)_2]^+$

(continued)

$[H_2Rh(PP_2)(PF_3)]^+$	69.7	$[H_2Rh(dmpe)_2]^+$
$[HNi(PP_2)(PMe_3)]^+$	57.9	$[HPt(dmpp)_2]^+$
$[HNi(PP_2)(PPh_3)]^+$	65.7	$[HPt(dmpp)_2]^+$
$[HPd(PP_2)(PMe_3)]^+$	56.0	$[HPt(dmpp)_2]^+$
$[HPd(PP_2)(PPh_2C_2H_5)]^+$	60.0	$[HPt(dmpp)_2]^+$
$[HPd(PP_2)(PPh_3)]^+$	62.4	$[HPt(dmpp)_2]^+$
$[HPt(PP_2)(PMe_3)]^+$	59.0	$[HPt(dmpp)_2]^+$
$[HPt(PP_2)(PPh_3)]^+$	66.3	$[HPt(dmpp)_2]^+$

The $\Delta G°_H$- values for group 9 metal(I) monohydrides range from 35 to 51 kcal/mol. The metal(III) monohydrides range from 55 to 60 kcal/mol. Both group 9 monohydrides and dihydrides are in agreement with the trend observed for bis(diphosphine) complexes that ΔG_H- values for metal hydrides in the same group increase in the order second row < third row ≪ first row.[19] For the Co(I) and Rh(I) hydrides, the PMe_3 complexes are approximately 8 kcal/mol stronger hydride donors than the corresponding PPh_3 complexes. For the metal(III) dihydrides, the trend is less clear, with $[H_2Co(PP_2)(PMe_3)]^+$ being approximately 4 kcal/mol stronger than the PPh_3 complex, but a difference of only 1 kcal/mol for the rhodium dihydrides. The cobalt(I) monohydride species $[HCo(PP_2)(PPh_3)]$ is roughly equivalent in hydricity to its $[HCo(dppe)_2]$ analogue ($\Delta G°_H$- = 49.9 kcal/mol),[27] but the hydricities for the other metal(I) monohydrides reflect generally weaker hydride donors (higher ΔG_H-) than the bis(diphosphine) analogues. However, the $[H_2M(PP_2)(PPh_3)]^+$ species are more hydridic (lower $\Delta G°_H$-) in comparison to $[H_2M(dppe)_2]^+$ analogues, such as $[H_2Co(dppe)_2]^+$

(65.1 kcal/mol).[27] Since hydricity values are strongly influenced by both steric and electronic factors, the PCy_3 complex was studied and found to have a hydricity (40.0 kcal/mol) between the electronically similar PMe_3 complex (35.7 kcal/mol) and the sterically similar PPh_3 complex (43.1 kcal/mol), confirming that both factors contribute significantly to the hydricity.

The $\Delta G°_{H^-}$ values for the group 10 species range from 55 to 67 kcal/mol, significantly higher than the group 9 species, which is in line with previously observed trends and is expected based on the greater positive charges. As expected, the PMe_3 complexes were stronger donors than the PPh_3 complexes, by 6-8 kcal/mol. The nickel hydride species appear to be similar, but less hydridic (higher $\Delta G°_{H^-}$) than the $[HNi(diphosphine)_2]^{n+}$ analogues, based on the comparison between $[HNi(PP_2)(PPh_3)]^+$ (65.7 kcal/mol) vs. $[HNi(dppe)_2]^+$ (62.8 kcal/mol).[5] However, the Pd and Pt hydrides appear to be dramatically weaker hydride donors than the bis(diphosphine) analogues. For instance, the hydricity of $[HPt(PP_2)(PPh_3)]^+$ is 66.3 kcal/mol, compared to 52.8 kcal/mol[5] for $[HPt(dppe)_2]^+$. As a result, the observed trend for these metals is that ΔG_{H^-} increases in the order Pd < Ni < Pt, which is significantly different from the trend observed for the bis(diphosphines). The differences are almost certainly due to the unusual structures observed for the Pd and Pt $[HM(PP_2)(PR_3)]^+$ complexes, which resulted from dissociation of one of the terminal phosphine donors. Since this distortion apparently gave a lower energy structure than that of the expected five-coordinate hydride, the resulting metal hydride is more stable and therefore a weaker hydride donor than originally expected.

2.4 Conclusion

Using DFT calculations, the structures of a series of metal(triphosphine)(monophosphine) complexes have been determined for group 9 and 10 metals. The structures examined in this study include metal(I) hydrides, metal(I) cations, metal(III) monohydride dications, and metal(III) dihydride cations for Co and Rh, and metal(II) dications, metal(II) hydride cations, and metal(0) complexes for Ni, Pd, and Pt. The structures are largely similar to those of the bis(diphosphine) analogues, with the notable exception of the Pd(II) and Pt(II) hydride cations. In these latter complexes, a virtually four-coordinate, square planar structure is observed, resulting from dissociation of one of the terminal phosphines of the triphosphine ligand. Group 9 metal(I) cations of the form $[M(PP_2)(PR_3)]^+$ and group 10 metal(II) cations of the form $[M(PP_2)(PR_3)]^{2+}$ showed the approximately square planar structures expected for four-coordinate d^8 metal ions, and group 10 metal(0) complexes of the formula $[M(PP_2)(PR_3)]$ showed distorted tetrahedral structures as expected for four-coordinate d^{10} complexes. Group 9 metal(III) dihydrides, monohydrides, and disolvate complexes of the formulas $[H_2M(PP_2)(PR_3)]^+$, $[HM(PP_2)(PR_3)(MeCN)]^{2+}$, and $[M(PP_2)(PR_3)(MeCN)_2]^{3+}$ showed the octahedral geometries expected for six-coordinate, d^6 ions. Group 9 metal(I) monohydrides and the nickel(II) monohydrides showed five-coordinate geometries intermediate between trigonal bipyramidal and square pyramidal but were closer to the former. These monohydrides adopted an “apical-P” conformation which placed the central atom of the triphosphine and the hydride ligand in the axial positions of the trigonal bipyramid and placed the terminal phosphines of the triphosphine and the monophosphine in the equatorial positions. The M-P bond distances were similar to those of analogous metal

bis(diphosphine) complexes and showed significant contractions for more electron-rich complexes, in lower oxidation states or with more donating ligands, consistent with significant M-P backbonding interactions.

The structures were used to calculate acidity (pK_a) and ($\Delta G°_{H}$-) values for the various hydrides. This methodology and its accuracy were validated by calculating these parameters for metal bis(diphosphine) complexes from the literature whose pK_a and ΔG_{H}- values are known. Because the values for these complexes match the calculated values to within 1 pK_a units or kcal/mol, respectively, the method appears to be reliable and accurate. The values for the new, mixed-ligand complexes are useful in guiding the discovery of new catalysts for CO_2 hydrogenation, as discussed below in Chapter 3.

2.5 Experimental

General. Geometric structure calculations were performed using Gaussian09W software.[36] In all cases, the geometry optimizations and frequency calculations were performed using density functional theory, the B3P86 functional, and an effective core potential (LANL2DZp) with acetonitrile solvent corrections modeled using C-PCM (polarized conductor calculation model), since this functional and basis set have been used effectively in similar studies.[17,24] The free energies were calculated at 298 K. Each optimized structure was confirmed by the frequency calculation at the same level to be the real minimum. Efforts were made to find the lowest energy conformations for the $[HM(PP_2)(PR_3)]^+$, and $[HM(PP_2)(PR_3)]$ complexes by performing geometry optimizations with both “apical-P” and “apical-H” input geometries as described above.

CHAPTER III

Synthesis and Characterization of Rhodium Metal Hydrides

3.1 Introduction

After estimating the pK_a and ΔG_H- values of the metal hydride species described in Ch 2, the remaining goals of this project were to:

1) use this data to identify the metal hydrides with the greatest potential to act as catalytic intermediates in CO_2 hydrogenation and related reactions, and
2) synthesize the complexes that showed the greatest potential for catalysis and conduct experimental studies of their reactivity.

The potential of the various metal hydrides to act as effective catalysts depends on the thermodynamic favorability of the various steps in the expected catalytic cycles described in Ch 1. Briefly, for the group 9 metals, Co and Rh, H_2 activation at the metal(I) cation, i.e. $[M(PP_2)(PR_3)]^+$ is expected to form a metal(III) dihydride, $[H_2M(PP_2)(PR_3)]^+$. This is deprotonated by an external base to form a metal(I) monohydride, $[HM(PP_2)(PR_3)]$, which reacts with CO_2 to form HCO_2^- and regenerate the original metal (I) cation. For the group 10 metals, Ni, Pd, and Pt, heterolytic H_2 activation involving the reaction between H_2, the metal(II) dication, $[M(PP_2)(PR_3)]^{2+}$, and an external base, forming a metal(II) monohydride, $[HM(PP_2)(PR_3)]^+$, which reacts directly with CO_2. The favorability of hydride transfer to CO_2 depends only on the hydricity of the metal hydride and the hydride acceptor ability of CO_2, and Figure 23 shows the proposed catalytic cycle.

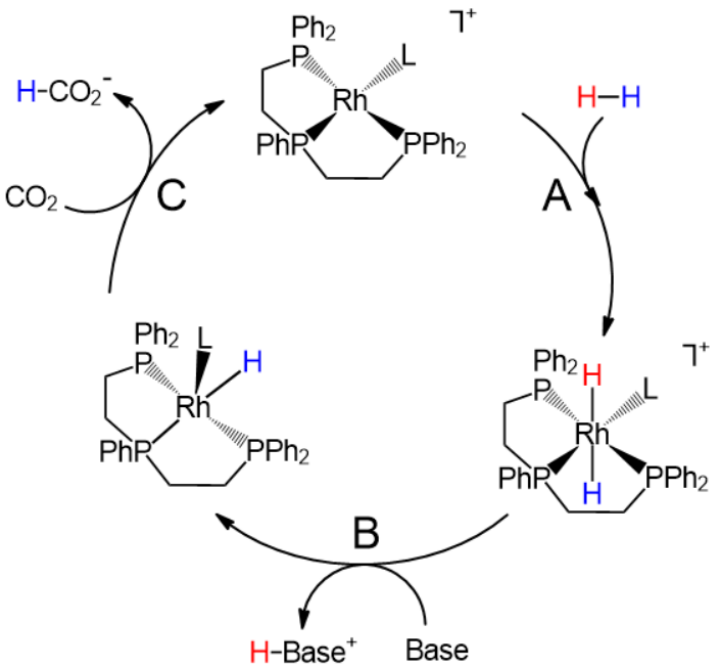

Figure 23. *Proposed catalytic cycle for CO_2 hydrogenation using the novel rhodium(triphosphine)(monophosphine) complexes*

Metal hydrides with ΔG_{H^-} values > 44 kcal/mol will not react favorably with CO_2, while those with lower values will react favorably. Of the complexes in this study, none of the group 10 metal hydrides and none of the Rh(III) or Co(III) monohydride or dihydride complexes had hydricities ≤ 44 kcal/mol, but all Rh(I) and Co(I) monohydrides, other than [HCo(PP_2)(PPh_3)], had hydricities < 44 kcal/mol. These results are largely in line with studies of the analogous bis(diphosphine) complexes. In all cases, there are no Ni, Co(III), or Rh(III) hydrides that have ΔG_{H^-} < 50 kcal/mol, whereas all Rh(I) monohydrides have ΔG_{H^-} < 44 kcal/mol, with the exception of [HRh($depx)_2$], which has a xanthene backbone with a very large bite angle.[37] The metals that are on the borderline are Co(I) hydrides, for which complexes with all aryl substituents have hydricities that are too weak (ΔG_{H^-} = 50.5 kcal/mol and 49.9 kcal/mol for [HCo(PP_2)(PPh_3)] and [HCo($dppe)_2$], respectively),[27] but dialkyl or trialkyl phosphines

give ΔG_H- values < 44 kcal/mol. The Pd and Pt bis(diphosphine) complexes show a similar range, based on the use of aryl or alkyl substituents (ΔG_H- = 41.4 and 44.0 kcal/mol for $[HPt(dmpe)_2]^+$ and $[HPt(depe)_2]^+$, respectively,[5] and 43.0 for $[HPd(depe)_2]^+$ but ΔG_H- = 52.8 kcal/mol for $[HPt(dppe)_2]^+$ and ΔG_H- = 55.6 kcal/mol for $[HPd(dppe)_2]^+$),[5,19,28] and are weaker hydride donors if ligands with larger bite angles are used.[19] However, the Pd and Pt triphosphine complexes in this study are all on the weaker side.

On the basis of these DFT-calculated hydricities, Rh and Co complexes were identified as potential catalysts. In addition to the thermodynamics of hydride transfer, the thermodynamics of H_2 activation must also be made favorable so that the reactive hydrides can be regenerated over the course of a catalytic cycle. ΔG_{H2}, or the free energy for the reaction of a metal(I) cation with H_2 to form a metal(III) dihydride, can be calculated using one of two schemes. Method A uses the pK_a of the metal(III) monohydride and the ΔG_H- for the metal(III) dihydride, in addition to the free energy for H_2 heterolysis (Figure 24). Method B instead uses the pK_a of the metal(III) dihydride and the ΔG_H- of the metal(I) hydride (Figure 25).[6]

Method A				**$\Delta G°$ (kcal/mol)**
$[ML_n]^+$ + H_2	⇌	$[H_2ML_n]^+$		$\Delta G°_{H2}$
H_2	⇌	H^+ + H^-		76
$[ML_n]^+$ + MeCN + H^+	⇌	$[HM(MeCN)L_n]^{2+}$		-1.364pK_a
$[HM(MeCN)L_n]^{2+}$ + H^-	⇌	$[H_2ML_n]^+$ + MeCN		$\Delta G°_H$-

$$\Delta G°_{H2} = 76 - 1.364pK_a([HM(MeCN)L_n]^{2+}) - \Delta G°_H\text{-}([H_2ML_n]^+)$$

Figure 24. *Thermodynamic cycle to calculate the free energy of H_2 activation by Method A*

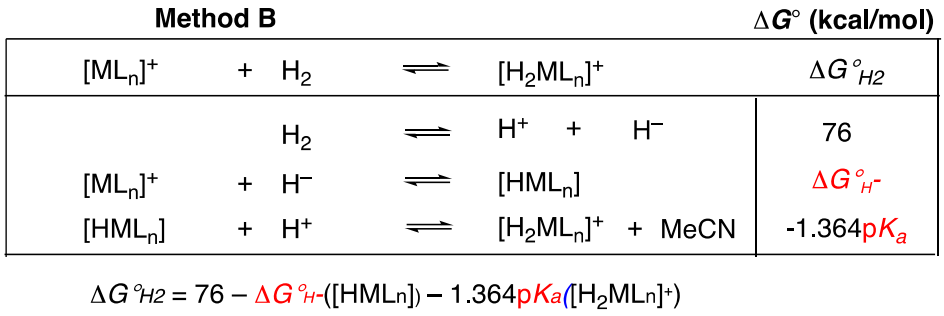

Figure 25. *Thermodynamic cycle to calculate the free energy of H_2 activation by Method B*

Since these two schemes are based on different parameters, comparing the results provides a useful check for the self-consistency of the DFT-calculated thermodynamic parameters. The results for the Co and Rh species that have been determined are given in Table 27.

Table 27: *Free energy of the reaction of a metal(I) cation with H_2 to form a metal(III) dihydride*

Transition-Metal Hydrides	ΔG_{H2} (kcal/mol, Method A)	ΔG_{H2} (kcal/mol, Method B)
[Rh(PP$_2$)(PMe$_3$)]$^+$	2.89	3.87
[Rh(PP$_2$)(PPh$_3$)]$^+$	10.7	11.7
[Co(PP$_2$)(PMe$_3$)]$^+$	-3.36	-2.93
[Co(PP$_2$)(PPh$_3$)]$^+$	-1.20	-0.75

For each complex, the values calculated for the two methods match within 1 kcal/mol, although interestingly the values calculated using Method B are consistently higher (more positive) than those in Method A. This may be due to a difference in the treatment of charges within the DFT calculations, as the species involved in Method B have smaller charges than those in Method A. It may also reflect differences in the accuracy of the

reference compounds used to calculate the hydricities or acidity values. However, the difference of ≤ 1 kcal/mol is well within the usual error for DFT-calculated energies. These results indicate that H_2 activation at both Co(I) ions is thermodynamically favorable, whereas for the Rh ions, formation of $[H_2Rh(PP_2)(PMe_3)]^+$ is slightly unfavorable but still accessible, but formation of $[H_2Rh(PP_2)(PPh_3)]^+$ is considerably more unfavorable. The difference between Co and Rh complexes is in line with the literature for the Co bis(diphosphine) complexes, which all have favorable values for ΔG_{H2}, and Rh bis(diphosphine) complexes, which are all unfavorable except for $[Rh(dmpe)_2]^+$.[6] Still, the unusually large value of ΔG_{H2} for $[Rh(PP_2)(PPh_3)]^+$ is somewhat unexpected, as the analogous bis(diphospine) complex, $[Rh(dppe)_2]^+$, has a value of only 3.8 kcal/mol.[6] The predominant factor determining the values of ΔG_{H2} for $[Rh(diphosphine)_2]^+$ complexes in the literature appears to be the steric bulk of the substituents on the diphosphine ligand, with the bulkiest diphosphines, dcpe and dppe, giving unfavorable ΔG_{H2} values, 4.2 and 3.8 kcal/mol, respectively,[6] despite having very different electronic properties. The least hindered rhodium bis(diphosphine) complexes, those of dmpbz and dmpe, have the lowest ΔG_{H2} values, 0.2 and -0.4 kcal/mol, respectively,[30] even though their methyl substituents have similar electronic properties to the cyclohexyl groups in $[Rh(dcpe)_2]^+$. In the present study, the large ΔG_{H2} for $[Rh(PP_2)(PPh_3)]^+$ suggests that there are strong steric interactions in the structure of $[H_2Rh(PP_2)(PPh_3)]^+$ that make H_2 addition unusually unfavorable. In the proposed mechanism for hydrogenation of CO_2, the addition of H_2 is followed by deprotonation of the metal(III) dihydride to form the metal(I) hydride. The favorability of this step requires a base whose conjugate acid has a higher pK_a than that of the metal(III)

dihydride. For $[H_2Rh(PP_2)(PPh_3)]^+$, triethylamine (NEt_3, pK_{aH} 18.5)[38] is strong enough to drive the formation of $[HRh(PP_2)(PPh_3)]$; for $[H_2Co(PP_2)(PPh_3)]^+$, NEt_3 would give an essentially thermoneutral deprotonation to form $[HCo(PP_2)(PPh_3)]$, and a stronger base, such as 1,1,3,3-tetramethylguanidine (TMG, pK_{aH} 23.4)[39] or 1,8-diazabicyclo[5.4.0]undec-7-ene (DBU, pK_{aH} 24.3)[39] would provide a greater driving force. For the more basic metal(III) PMe_3 complexes, even stronger organic superbases, such as the phosphazene tert-butylimino-tris(pyrrolidino)phosphorane ($P_1{}^tBu$, pK_{aH} 28.5),[39] or Verkade's superbase 2,8,9-triisopropyl-2,5,8,9-tetraaza-1-phosphabicyclo[3,3,3]undecane (Vkd, pK_{aH} 33.6),[25] will be required to drive the deprotonation. The results for the cobalt complexes are in line with those of the analogous bis(diphosphine) complexes: for instance, $[HCo(dmpe)_2]$ is an extremely active catalyst for CO_2 hydrogenation but requires a very strong base like Vkd to achieve efficient catalysis.[16,38] The results for the Rh complexes show a much greater difference from the bis(diphosphine) complexes: the pK_a values for $[H_2Rh(diphosphine)_2]^+$ complexes in the literature range from 24.0 for $[H_2Rh(dcpe)_2]^+$ to 36.5 for $[H_2Rh(dmpe)_2]^+$.[6] These very high values limit the effectiveness of the rhodium bis(diphosphines) as catalysts, because even with strong bases like Vkd, the deprotonation step is extremely slow. Conversely the lower pK_a values for the cobalt bis(diphosphines) allow them to serve as highly active catalysts. The rhodium bis(diphosphines) are excessively strong hydride donors, which comes at the cost of being difficult species to regenerate. Therefore, while the Rh(triphosphine)(monophosphine) complexes are more modest hydride donors, they are still thermodynamically capable of reducing CO_2, and the less excessive hydricity allows a lower pK_a, which should allow them to be regenerated more efficiently during catalysis.

The analysis of thermodynamic parameters described above allows us to identify species that have the potential to be effective catalysts. Species with mismatched thermodynamic parameters are inherently ill-suited for catalysis. However, thermodynamic parameters alone do not guarantee that a complex will be an effective catalyst, because kinetic factors, such as sterics and conformational issues, may cause the reaction steps to be slow, regardless of their thermodynamic favorability. To assess the actual reactivity of these complexes, Rh complexes of this type were synthesized, and stoichiometric studies of the key steps, namely H_2 activation, H^+ transfer, and H^- transfer, were conducted. Preliminary studies of catalytic CO_2 hydrogenation were also conducted using $[Rh(PP_2)(PPh_3)]^+$, showing that it is a competent but slow catalyst even at ambient temperature and near-ambient pressures of H_2 and CO_2.

3.2 Synthesis of mixed triphosphine-, monophosphine-ligated Rh(I) complexes

The $[Rh(PP_2)(PPh_3)]^+$ cation was previously prepared by Long *et al.* as a salt containing a carborane anion, through the reaction of a corresponding $[Rh(PPh_3)_3]$[carborane] salt with the triphos (PP_2) ligand.[40] This complex was not characterized beyond its ^{31}P NMR spectrum. In this study, the $[Rh(PP_2)(PPh_3)]^+$ cation, paired with more conventional SbF_6^- and BF_4^- anions, was first synthesized as a precursor for the further reactivity studies. Its hydride form, $[HRh(PP_2)(PPh_3)]$, was also prepared and characterized by ^1H and ^{31}P NMR spectroscopy. In addition, the related Rh^I cation $[Rh(PP_2)(L^{Phen+})]^{2+}$, containing an alkyldiphenylphosphine ligand tethered to a redox-active *N*-alkyl-phenanthridinium group, was prepared, along with its reduced dihydrophenanthridinium form, $[Rh(PP_2)(L^{PhenH})]^+$, bearing an organic hydride. The Rh^I hydride species $[HRh(PP_2)(L^{PhenH})]$ was also synthesized. $[Rh(PP_2)(PPh_3)][SbF_6]$ was

synthesized from the known Rh(I) norbornadiene (NBD) complex $[Rh(PP_2)(NBD)][SbF_6]$ shown in Figure 26.[41]

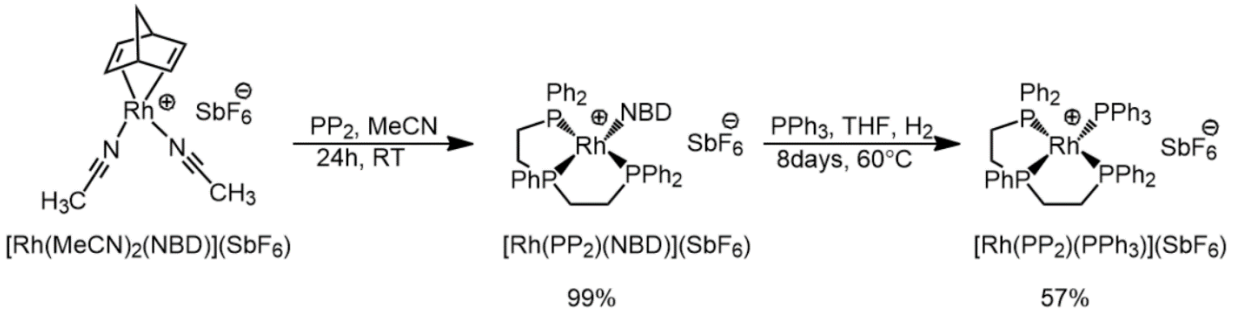

Figure 26. *Synthesis of $[Rh(PP_2)(PPh_3)][SbF_6]$*

Addition of excess PPh_3 to this precursor at room temperature showed no conversion to the desired PPh_3 adduct, but after extended heating, product formation was observed by ^{31}P NMR spectroscopy. This result was consistent with previous reports that the NBD ligand in this complex could be substituted, upon heating in THF, by halide ions. However, because the formation of $[Rh(PP_2)(PPh_3)][SbF_6]$ under these conditions also showed some unidentified species, H_2 was added to increase the lability of the NBD ligand by hydrogenating its alkene groups. These conditions did allow for clean and essentially quantitative conversion to $[Rh(PP_2)(PPh_3)][SbF_6]$, as observed by ^{31}P NMR spectroscopy, although the reaction still required prolonged heating (8 days) to reach full conversion and gave a lower yield upon isolating the product. The ^{31}P NMR spectrum of $[Rh(PP_2)(PPh_3)][SbF_6]$ appears very similar to that of $[Rh(PP_2)(PPh_3)]$[carborane] reported by Long *et al*, but with slightly different chemical shifts, possibly due to the different solvents (CD_3CN or DMSO-d_6 vs. 10% C_6D_6/90% THF).[40] Three ^{31}P signals are observed in a 1:2:1 ratio, consistent with a structure possessing mirror symmetry and making the two terminal phosphines (P_2 and P_3 in the labeling scheme of Figure 13, equivalent on the NMR timescale. The coupling constants are also consistent with the

expected square planar structure, with two similar, small coupling constants for the mutually *cis* phosphines ($J_{P1\text{-}P2/P3}$ = 29.6 Hz, $J_{P4\text{-}P2/P3}$ = 33.6 Hz), and a very large value for the mutually *trans* phosphines ($J_{P1\text{-}P4}$ = 259 Hz), identical to that previously observed in the carborane complex and similar to those observed in the Zall group for structurally similar square planar palladium(II) analogues, i.e. $[Pd(PP_2)(PR_3)]^{2+}$. The Rh-P coupling constants (123.9, 141.1, 133.7 Hz) are similar to those in other square planar triphosphine complexes, such as $Rh(PP_2)Cl$ and $[Rh(PP_2)(MeCN)]^+$, and other square planar Rh(I) tetraphosphine ions, such as $Rh(dmpe)_2^+$.[23,42] Notably, Rh-P coupling constants are typically between 125-135 Hz, but the corresponding Rh(III) dihydrides or monohydrides are typically 80-100 Hz. No evidence for Rh-H coupling was observed in the ^{31}P NMR data, and no signal for a Rh-H resonance was observed in the ^{1}H NMR spectrum, despite the use of H_2 in synthesizing $[Rh(PP_2)(PPh_3)][SbF_6]$. The lack of any signs of a rhodium hydride is consistent with the DFT-calculated ΔG_{H2} value, that H_2 addition to $[Rh(PP_2)(PPh_3)]^+$ is thermodynamically unfavorable by >10 kcal/mol. The analogue containing a phenanthridnium group, $[Rh(PP_2)(L^{PhenH})][SbF_6]$, could be prepared cleanly in a similar fashion. However, due to the long reaction times needed to prepare these complexes from $[Rh(PP_2)(NBD)][SbF_6]$, an alternative route was developed, starting from the known MeCN complex $[Rh(PP_2)(MeCN)][BF_4]$, whose more labile MeCN ligand could easily be replaced by a monophosphine (PPh_3, L^{PhenH}, or L^{Phen+}), shown in Figure 27 and Figure 28.

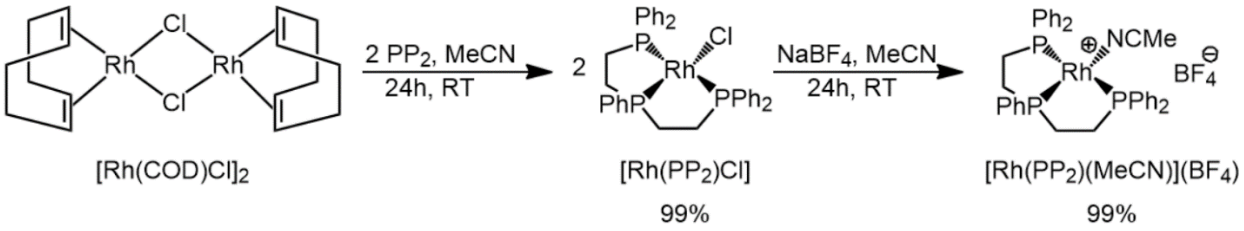

Figure 27. *Synthesis of [Rh(PP₂)(MeCN)][BF₄]*

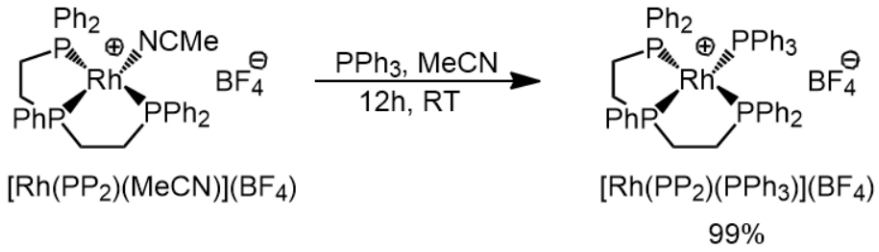

Figure 28. *Synthesis of [Rh(PP₂)(PPh₃)][BF₄]*

These reactions yielded the BF_4 salts $[Rh(PP_2)(PPh_3)][BF_4]$, $[Rh(PP_2)(L^{PhenH})][BF_4]$, and the analogue with an oxidized phenanthridinium group, $[Rh(PP_2)(L^{Phen+})][BF_4]_2$, cleanly and essentially quantitatively, with full conversion observed by ^{31}P NMR spectroscopy of the crude reaction mixtures, within minutes. The spectra of the BF_4 salts were essentially identical to those of the SbF_6 salts. The Rh(I) monohydride species, $[HRh(PP_2)(PPh_3)]$, and $[HRh(PP_2)(L^{PhenH})]$ could be prepared by reacting the corresponding Rh(I) cation with $LiBEt_3H$ (ΔG_H- = 26 kcal/mol), as shown in Figure 29, but not with $NaBH_4$, which is a weaker hydride donor.

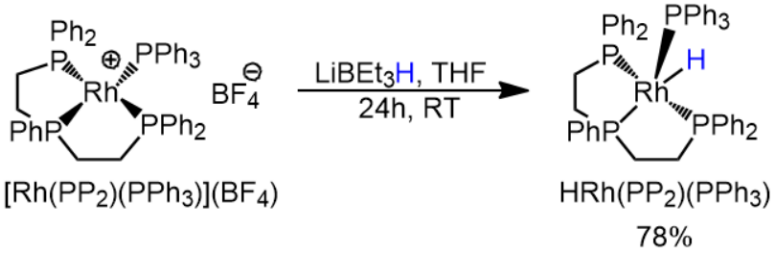

Figure 29. *Reaction to synthesize the [HRh(PP₂)(PPh₃)] complex*

The Rh(I) hydride with an oxidized phenanthridinium group, $[HRh(PP_2)(L^{Phen+})]^+$, could not be synthesized by this route, consistent with the expectation that the phenanthridinium group is a better hydride acceptor than the Rh(I) center. Addition of 1 equivalent of $LiBEt_3H$ to a solution of $[Rh(PP_2)(L^{Phen+})]^{2+}$ gave the complex with a reduced ligand, $[Rh(PP_2)(L^{PhenH})]^+$, and no evidence for a Rh-H species was observed. In the ^{31}P NMR spectra for the Rh-H species, the structures appear to retain mirror symmetry but not necessarily a *trans* arrangement of P1 and P4. The shifts for the monophosphine (PPh_3 and L^{PhenH}) ligands do not change substantially from the cation to the hydride, but the terminal phosphorus resonance shifts upfield by 13-14 ppm in both $[HRh(PP_2)(PR_3)]$ structures, consistent with the DFT-optimized geometries that have roughly *trans* arrangements between this group and the hydride atom (P_1-Rh-H angles of approximately 170° in both structures), which has a powerful *trans* influence, and much smaller P_1-Rh-P_4 angles 105.6 and 107.6°. The Rh-H signal is observed at -8 to -9 ppm.

3.3 Stoichiometric reactivity studies of rhodium(I) triphosphine complexes

The Rh(I) cations and Rh(I) hydrides were used as starting materials in subsequent reactivity studies, to experimentally evaluate the accuracy of the DFT-calculated thermodynamic values and to demonstrate the hydride transfer and H_2 activation reactions proposed to occur during catalysis. Direct H_2 addition (up to 1.8 atm) to solutions of the Rh(I) cations showed no conversion to the corresponding dihydrides. For the L^{PhenH} complex, broadening of the peaks for $[Rh(PP_2)(L^{PhenH})]^+$ as well as broadening of the H_2 peak itself were observed in the ^1H and ^{31}P NMR spectra, but no new peaks were observed. Neither the reaction with the PPh_3 or the L^{PhenH} complex showed any ^1H NMR signal for a Rh–H peak. For Rh bis(diphosphine) complexes, these

peaks appear in a consistent range of -9.0 to -12.0 ppm.[6] These results support the DFT-calculated result that H_2 addition to the PPh_3 complex is strongly unfavorable but suggest that H_2 addition to the slightly less bulky and more electron-rich L^{PhenH} complex may be closer to thermoneutral, resulting in a rapid but unfavorable H_2-binding equilibrium. To confirm that H_2 addition to the L^{PhenH} complex is thermodynamically unfavorable, the reverse reaction was studied. $[HRh(PP_2)(L^{PhenH})]$ reacted cleanly with 1 equivalent of H(DMF)OTf (pK_a 6.1 in MeCN, DMF = dimethylformamide, OTf = trifluoromethylsulfonate, $CF_3SO_3^-$)to give $[Rh(PP_2)(L^{PhenH})][OTf]$ and H_2, as shown in Figure 30.[43] This reaction demonstrates that H_2 elimination from the rhodium(I) hydride is favorable, and this reaction presumably occurs through the reductive elimination of H_2 from a rhodium(III) dihydride intermediate formed upon protonation, although no evidence for the dihydride intermediate was observed.

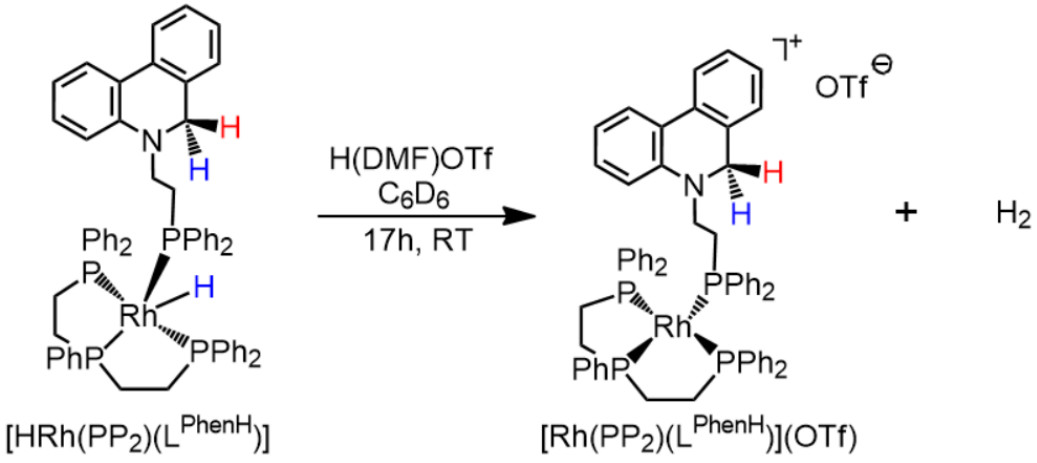

Figure 30. *Protonation and H_2 elimination from $[HRh(PP_2)(L^{PhenH})]$*

Because this demonstrates that the Rh(III) dihydride intermediate, if it forms, loses H_2 to form the Rh(I) cation, the addition of H_2 to the Rh(I) cation must therefore be thermodynamically unfavorable. Although direct H_2 addition to form a dihydride was found to be unfavorable, heterolytic activation of H_2 in the presence of a base resulted in

conversion to the Rh(I) hydride in an equilibrium that depends on the hydricity of the resulting Rh(I) hydride and the pK_a of the base, shown in Figure 31 and the structures of the bases and protonated forms is shown in Figure 32. When H_2 was added (1 atm) to a solution of $[Rh(PP_2)(PPh_3)]^+$ in the presence of 1 equiv. NEt_3 (pK_{a}H 18.5 in MeCN), no hydride formation was observed. However, in the presence of much stronger bases, namely the phosphazene P_1-*t*Bu (pK_{a}H 28.5), and Verkade's superbase (pK_{a}H 33.6), full conversion to the Rh(I) hydride was observed.

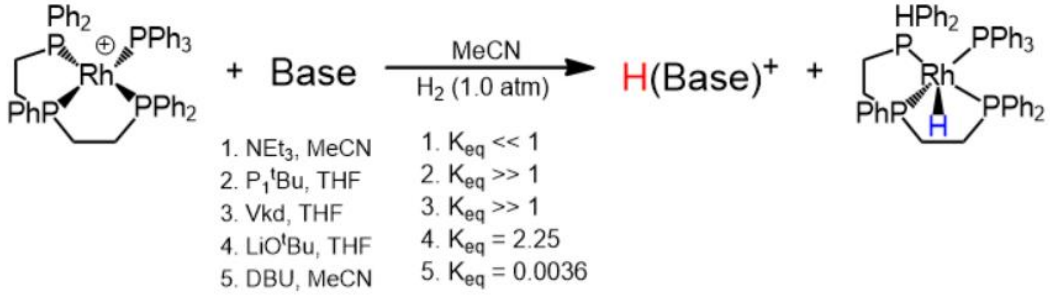

Figure 31. *H_2 heterolysis reactions and K_{eq} values using various bases*

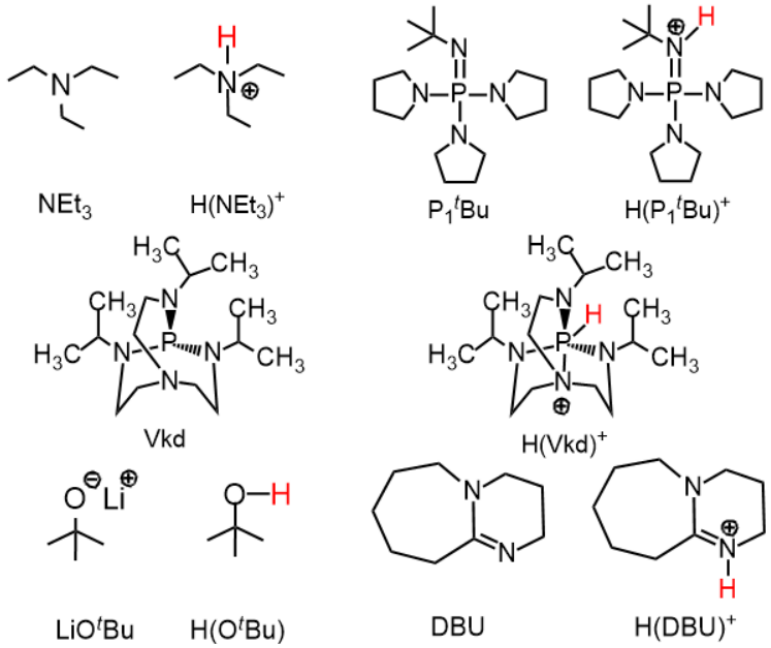

Figure 32. *Bases used for H_2 heterolysis and their conjugate acids*

Using the thermodynamic cycle described in Ch 1, these experiments allowed the hydricity of $[HRh(PP_2)(PPh_3)]$ to be bracketed to between 37 and 50 kcal/mol. When

using LiO^{t}Bu as the base in THF, the reaction gave a measurable equilibrium. The value of K_{eq} was determined based on the ratio of the rhodium hydride to the rhodium(I) cation as measured by ^{31}P NMR spectroscopy, which was 1.5:1 after the reaction reached equilibrium. Assuming an identical ratio of HO^{t}Bu to O^{t}Bu$^-$ based on reaction stoichiometry, this gave K_{eq} = 2.25 atm^{-1} and a $\Delta G°$ for H_2 heterolysis of -0.48 kcal/mol. However, because the pK_a of HO^{t}Bu is not well defined in THF or MeCN, this value cannot be converted to a hydricity. Instead, a reaction using DBU as a base was able to provide a quantitative measurement for the hydricity of [HRh(PP$_2$)(PPh$_3$)], by providing a measurable equilibrium for H_2 heterolysis with a base of well-defined p$K_{a\mathrm{H}}$. In the presence of approximately 1 equiv. DBU in MeCN, [Rh(PP$_2$)(PPh$_3$)]$^+$ reacted with H_2 to form a small amount of [HRh(PP$_2$)(PPh$_3$)] and HDBU$^+$, with a ratio of HRh:Rh$^+$ of approximately 1:20, corresponding to an equilibrium constant of 0.0036 atm^{-1}, determined analogously to the previous reaction. Using the pK_a of 24.3 for HDBU$^+$, this corresponds to ΔG_{H}- = 39.5 kcal/mol for [HRh(PP$_2$)(PPh$_3$)]. This value is in reasonable agreement, although notably lower, than the DFT-calculated value of 43.1 kcal/mol. It is closer to the value of 36.2 for the analogous bis(diphosphine), [HRh(dppe)$_2$], suggesting that the DFT-calculated value may slightly overestimate the stability of [HRh(PP$_2$)(PPh$_3$)] or underestimate the stability of [Rh(PP$_2$)(PPh$_3$)]$^+$. Nevertheless, both the experimentally measured value and the DFT-calculated value are in agreement that the reaction of [HRh(PP$_2$)(PPh$_3$)] with CO_2 should be modestly favorable. The experimental and computational studies are also in agreement that, while direct H_2 activation at [Rh(PP$_2$)(PPh$_3$)]$^+$ is unfavorable, heterolytic H_2 activation to form [HRh(PP$_2$)(PPh$_3$)] is favorable in the presence of bases stronger than NEt$_3$. Other

stoichiometric studies were carried out to determine the reactivity of the novel Rh(I) complex, $[Rh(PP_2)(L^{PhenH})]^+$, particularly its redox-active phenanthridinium group, which is an organic hydride donor of moderate strength. The oxidized form of this complex can be synthesized through direct addition of L^{Phen+} to $[Rh(PP_2)(MeCN)]^+$ or by hydride abstraction from $[Rh(PP_2)(L^{PhenH})]^+$: the reaction of the latter complex with CPh_3BF_4, a strong hydride acceptor, cleanly gave $[Rh(PP_2)(L^{Phen+})]^{2+}$ and $HCPh_3$, shown in Figure 33. Whereas no rhodium-hydride formation is observed in the presence of H_2 and triethylamine, $[Rh(PP_2)(L^{Phen+})]^{2+}$ reacted with H_2 (1 atm) in the presence of NEt_3 to form $[Rh(PP_2)(L^{PhenH})]^+$, demonstrating that the metal and ligand can work cooperatively to activate H_2 to generate a ligand-based hydride equivalent.

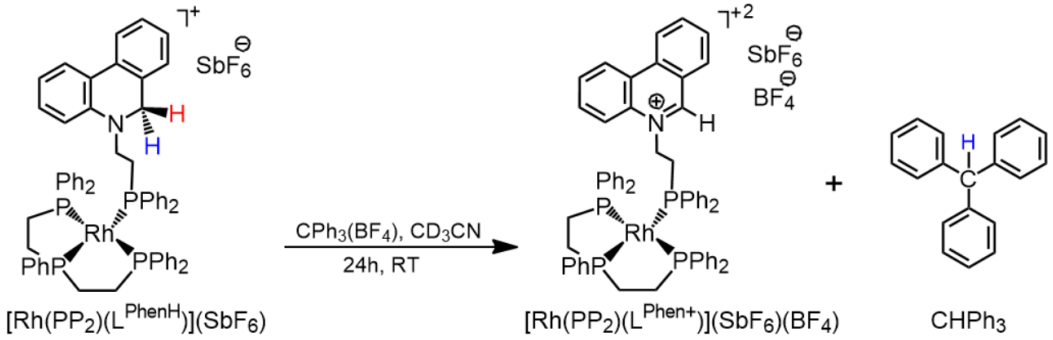

Figure 33. *Oxidation of the L^{PhenH} ligand by a tritylium salt*

3.4 Preliminary studies of catalytic CO_2 hydrogenation using $Rh(PP_2)(L^{PhenH})]^+$

Having demonstrated that heterolytic H_2 activation to form the Rh(I) hydride is feasible using bases like DBU and Vkd, and that the Rh(I) hydride is thermodynamically capable of reducing CO_2 to formate, studies of catalytic CO_2 hydrogenation were conducted. NMR-scale reactions of $[Rh(PP_2)(L^{PhenH})]^+$ with a 1:1 mixture of H_2 and CO_2 (1.8 atm) in the presence of NEt_3, DBU or Vkd were conducted in gas-tight J-Young NMR tubes, as summarized in Figure 34. The reactions using NEt_3 and DBU were

conducted in CD_3CN using 20 equivalents of base per equivalent of $[Rh(PP_2)(L^{PhenH})]^+$, or 5 mol % catalyst, implying a maximum turnover number (TON) of 20, assuming a 1:1 ratio of HCO_2^- to $H(Base)^+$. The reactions were followed by ^1H NMR spectroscopy to observe the formation of formate, which typically has a characteristic ^1H resonance of 8.8 ppm, although hydrogen bonding can shift and broaden this resonance. As expected, when using NEt_3 as a base, no formate was created with the $[Rh(PP_2)(L^{PhenH})]^+$ catalyst , since its basicity was not sufficient to drive the formation of the rhodium hydride. This reaction instead demonstrated that the ligand-based hydride donor in $[Rh(PP_2)(L^{PhenH})]^+$ was inert towards the hydrogenation of CO_2, since it can be regenerated under these conditions but has a weak estimated ΔG_H- value of approximately 60 kcal/mol.[44] Instead, a stronger base was needed to drive the formation of the more reactive rhodium hydride. As expected, with DBU as the base, formate was observed immediately after addition of the H_2/CO_2 gas. Through the first 50 hours of reaction time, the formate concentration grew at a slow but relatively constant rate corresponding to a TOF of 0.16 h^{-1}; after this time, even with further addition of gas, the rate plateaued, giving a final TON of 12.5, corresponding to 62.5% conversion, as shown in Figure 35.

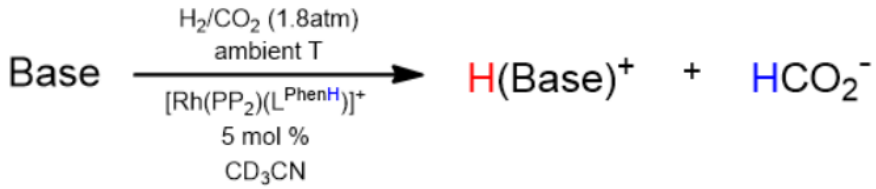

Figure 34. *Catalytic reaction and conditions for CO_2 hydrogenation*

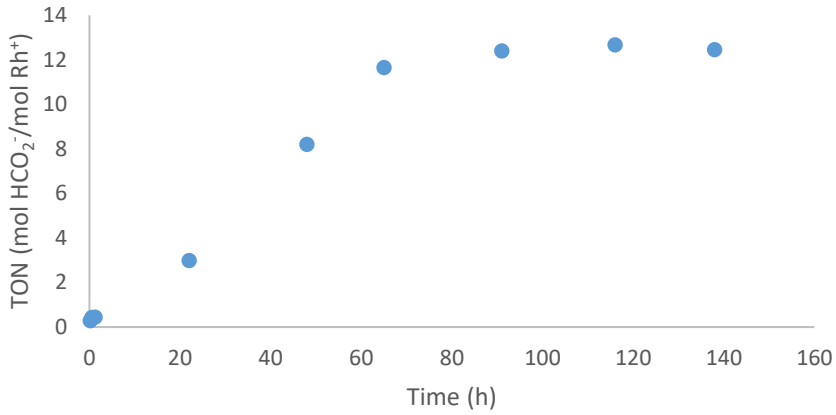

Figure 35. *Reaction progress for the catalytic hydrogenation of CO_2 using 5 mol % $[Rh(PP_2)(L^{PhenH})]^+$ relative to DBU under 1.8 atm H_2/CO_2 (1:1, ambient temperature, CD_3CN solvent), as measured by ^1H NMR spectroscopy*

These values are modest but demonstrate that $[Rh(PP_2)(L^{PhenH})]^+$ is capable of catalyzing the hydrogenation of CO_2 even under extremely mild conditions. The only intermediate observed in the ^{31}P NMR spectra was $[Rh(PP_2)(L^{PhenH})]^+$, and no Rh–H signal was observed in the ^1H NMR spectra. Evidently, CO_2 reduction is comparatively rapid, and the bottleneck in catalysis is H_2 activation. Because the stoichiometric H_2 activation studies showed weak equilibria for Rh hydride formation with DBU but complete conversion to the rhodium hydride when using Vkd, a follow-up study of catalysis was conducted with this much stronger base. Because Verkade's base is not stable in MeCN or CD_3CN, this reaction was conducted in THF, which prevented the reaction from being monitored by ^1H NMR spectroscopy. Instead, the reaction progress was monitored by ^{31}P NMR, comparing the signals for Vkd (approximately 118 ppm) and $HVkd^+$ (approximately -13 ppm). The reaction showed rapid initial conversion: within the first timepoint, at 20 minutes, 25% of the base was converted, corresponding to a TON of 25

and an initial TOF of 75 h^{-1}, assuming a 1:1 ratio of $HVkd^+$ to formate. Despite this rapid initial rate, the reaction reached completion only after 250 h, as shown in Figure 36.

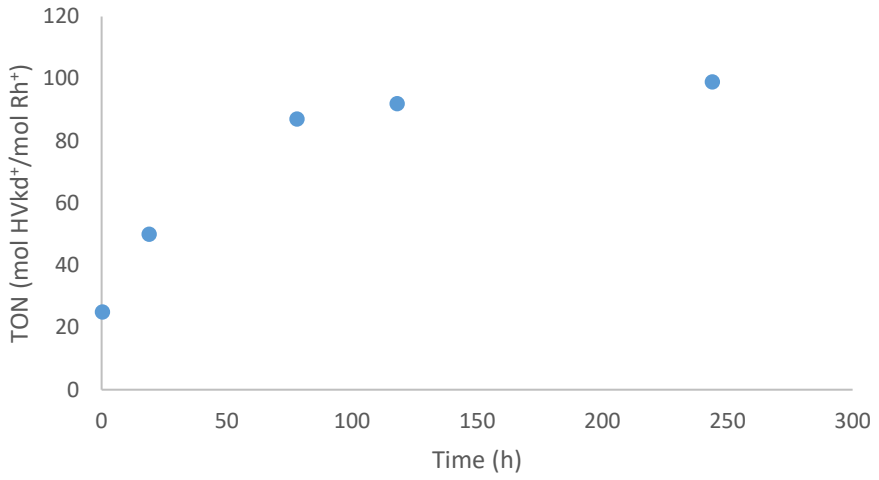

Figure 36. *Reaction progress for the catalytic hydrogenation of CO_2 using 1 mol % $[Rh(PP2)(L^{PhenH})]^+$ relative to Verkade's base under 1.8 atm H_2/CO_2 (1:1, ambient temperature, THF solvent), as measured by ^{31}P NMR spectroscopy*

This is a preliminary study of catalysis, and subsequent studies of the analogous reaction using cobalt(triphosphine)(monophosphine) catalysts in the Zall group have found that, under these conditions, the rate of catalysis is limited by the availability and mass-transfer rate of H_2 and CO_2: good mixing and frequent gas additions are required to ensure that a sufficient concentration of dissolved gas is present in the reaction mixture. Because the formate concentration in this reaction was not measured directly, the final reaction mixture was dried under vacuum to remove THF and redissolved in DMSO-d_6 (pK_a 5.8 in MeCN).[43] The ^1H NMR spectrum showed the presence of formate, although only in a 1:5 ratio with $HVkd^+$, suggesting that only 20% of the reaction conversion may have productively yielded formate. If this percentage of conversion was constant throughout the reaction, the TON would be as low as 20 and the initial TOF would be

15 h^{-1}. It is likely that the initial TOF is higher and close to the value of 90 h^{-1} determined by the ^{31}P NMR spectra, as the unproductive side-reactions that consume Vkd without producing formate become competitive with CO_2 hydrogenation only after the catalytic reaction slows. The TON of 20 suggested by the ^{1}H NMR spectra may also be an underestimate of the yield, due to decomposition reactions, such as catalytic dehydrogenation of formate under vacuum, during the transfer of the solution to the deuterated solvent. Regardless of the precise values, this preliminary data indicates that $[Rh(PP_2)(L^{PhenH})]^+$ is a competent catalyst for CO_2 hydrogenation even under extremely mild conditions of temperature and pressure. The activity of this catalyst is comparable to that of $[Rh(dmpe)_2]^+$, which gave a TON of 55 and TOF of 90 h^{-1} under essentially identical conditions (400 mM Vkd, 2.7 mM catalyst, 1.8 atm H_2/CO_2). Notably, the more electronically analogous complex, $[Rh(dppe)_2]^+$, showed comparable activity (TOF = 130 h^{-1}, TON = 70) only at a gas pressure of 20 atm and a slightly higher catalyst loading of 7.1 mM; at 1.8 atm, it gave essentially no catalytic activity.[30] The ^{31}P NMR spectra observed during catalysis using Vkd as a base and $[Rh(PP_2)(L^{PhenH})]^+$ as a catalyst precursor showed $[HRh(PP_2)(L^{PhenH})]$ as the only observable catalytic intermediate. This is different from the reaction using DBU, in which $[Rh(PP_2)(L^{PhenH})]^+$ was the observed resting state. Therefore, the stronger base significantly increases the rate of H_2 activation and changes the rate determining step to CO_2 reduction, creating a buildup of the rhodium hydride. This is slightly different from catalysis using the better-studied bis(diphosphine) complex, $[Rh(dmpe)_2]^+$, in which the dihydride, $[H_2Rh(dmpe)_2]^+$ was found to be the catalyst resting state.[30] For $[Rh(dmpe)_2]^+$, CO_2 reduction is strongly favored and H_2 addition is slightly favorable, but the pK_a of the dihydride is extremely

high (36.5 in MeCN), making the deprotonation step disfavored and rate-determining even with an extremely strong base like Vkd. With DBU as a base, both direct H_2 addition to form $[H_2Rh(PP_2)(L^{PhenH})]^+$ and deprotonation to form $[HRh(PP_2)(L^{PhenH})]$ are unfavorable equilibria, making $[Rh(PP_2)(L^{PhenH})]^+$ the catalyst resting state.

3.5 Conclusion

The suitability of a variety of Group 9 and 10 metal(triphosphine)(monophosphine) complexes as catalysts for the hydrogenation of CO_2 was assessed based on the energies for these species that were determined by DFT. On this basis, the Rh and Co complexes bearing PMe_3 and L^{PhenH} ligands were identified as promising candidates, because their metal(I) monohydrides have sufficient hydricity to reduce CO_2, their free energy for H_2 oxidative addition is thermally accessible, and the pK_a values for their dihydrides allows them to be deprotonated by reasonably strong bases. By contrast, the hydricity of $[HCo(PP_2)(PPh_3)]$ is insufficient to reduce CO_2, and the free energy of H_2 activation for $[Rh(PP_2)(PPh_3)]^+$ is too great to make these species ideal catalysts. To test these DFT-based predictions, Rh complexes containing PPh_3, L^{PhenH}, and L^{Phen+} ligands, in both the cationic metal(I) and metal(I) hydride forms, were synthesized. Using these complexes, a variety of stoichiometric reactivity studies were conducted. These demonstrated the predicted unfavorability of direct H_2 addition for $[Rh(PP_2)(PPh_3)]^+$, and the favorability of heterolytic activation to form $[HRh(PP_2)(PPh_3)]$ in the presence of strong bases. For the Rh complex containing an L^{Phen+} ligand, H_2 activation in the presence of NEt_3 generated a ligand-based hydride, L^{PhenH}. In the presence of stronger bases, the Rh hydride was formed for both PPh_3 and L^{PhenH} complexes. In the case of DBU, an equilibrium constant corresponding to a hydricity of

39.5 kcal/mol for [HRh(PP_2)(PPh_3)] was measured. Catalytic studies were conducted, which demonstrated that the L^{PhenH} complex is an active catalyst for CO_2 hydrogenation using the very strong base Vkd, and a much less active catalyst using DBU. The resting states of the catalyst are different for these two reactions, indicating different rate determining steps. Using Vkd, the resting state was the Rh hydride, indicating that H_2 activation was rapid and CO_2 reduction was slow. Using DBU, the Rh cation was the resting state, indicating that H_2 activation was much slower using this base. These very preliminary results support the broader DFT-based data discussed in Ch 2 and have allowed the identification of a promising new catalyst for CO_2 hydrogenation.

3.6 Experimental

General. All starting materials and reagents were purchased from commercial sources (Sigma Aldrich and Alfa Aesar) and used without further purification, unless noted below. Most of the air sensitive reactions were performed inside a glove box (Vigor Sci-Lab) under a nitrogen atmosphere. Solvents were degassed under argon and dried by passage through columns of activated alumina and molecular sieves using a Glass Contour GC-SPS-7 solvent purification system, then stored inside the glove box. Molecular sieves were activated by heating to 300 °C under vacuum for three days and were stored in the glove box. Triethylamine and DMSO-d_6 were degassed by freeze-pump-thaw cycles and dried over 3 Å molecular sieves. DBU was dried over P_2O_5 and distilled under reduced pressure, then stored over 3 Å molecular sieves. C_6D_6 and CD_3CN were dried over CaH_2, distilled under N_2, and stored over 3 Å molecular sieves. All the air sensitive reagents were stored inside the glove box under nitrogen atmosphere. Glassware was dried in an oven at 140 °C for at least 4 h before use. H_2 and a 1:1 mixture

of H_2/CO_2 were purchased from Airgas as the highest available purity and used as received. All acidity, catalytic, equilibrium and hydricity studies were conducted in a J-Young valved NMR tube. ^{1}H NMR and ^{31}P NMR spectra were recorded on a JEOL Eclipse 300+ spectrometer. Chemical shifts are reported in δ (ppm) relative to tetramethylsilane (^{1}H) and 85 % H_3PO_4 (^{31}P). The ^{1}H NMR spectra were referenced based on the residual protons in deuterated solvents (CD_3CN: 1.94 ppm, C_6D_6: 7.16 ppm, DMSO- d_6: 2.50 ppm) while 1% $P(OMe)_3$ in acetone-d_6 (140.68 ppm) was used as the external reference for ^{31}P NMR spectra. The synthesis of $[Rh(PP_2)(NBD)](SbF_6)$ was prepared according to that of Beck *et al*.[41] The synthesis of $[Rh(PP_2Cl]$ was prepared according to a procedure reported by Marder and co-workers.[42] The ligands L^{PhenH} and L^{Phen+} were prepared within the Zall group.[26]

Synthesis of compounds

Synthesis of $[Rh(PP_2)(CH_3CN)][BF_4]$. $[Rh(PP_2)Cl]$ (18.0 mg, 0.0267 mmol) was dissolved in 6 mL MeCN and added to a solution of sodium tetrafluoroborate ($NaBF_4$) (3.0 mg, 0.027 mmol) in 3 mL MeCN. The light-yellow mixture turned dark green and cloudy and was stirred at ambient temperatures overnight. The mixture was filtered, and the golden-yellow filtrate was dried under vacuum to give a yellow powder (20.3 mg, 99.0%). ^{1}H NMR (CD_3CN, 300 MHz, Figure A40): δ 8.03 – 7.83 (m, 2H), 7.74 – 7.23 (m, 23H), 3.14 – 2.48 (m, 4H), 2.05 (m, 2H), 1.83 (s, 3H), 1.80 (m, 2H). ^{31}P $\{^{1}H\}$ NMR (CD_3CN, 121 MHz, Figure A41): δ 113.01 (dt, 1P, J = 156.0, 30.2 Hz), 49.23 (dd, 2P, J = 139.8, 30.2 Hz).

Synthesis of $[Rh(PP_2)(PPh_3)][BF_4]$. $[Rh(PP_2)(MeCN)][BF_4]$ (24.0 mg, 0.0314 mmol) was dissolved in 3 mL MeCN and added to a solution containing

triphenylphosphine (8.2 mg, 0.031 mmol) in 5 mL MeCN. The golden-yellow solution was stirred at ambient temperature overnight. After stirring, the solution was dried under vacuum, giving a golden-yellow solid (30 mg, 99%). ^{1}H NMR (DMSO-d_6, 300 MHz, Figure A42): δ 8.19 – 7.95 (m, 2H), 7.71 – 6.80 (m, 38H), 3.06 – 2.66 (m, 4H), 2.07 (m, 4H). ^{31}P {^{1}H} NMR (DMSO-d_6, 121 MHz, Figure A43): δ 109.58 (ddt, 1P, J = 258.6, 123.9, 29.6 Hz), 53.12 (ddd, 2P, J = 141.1, 33.6, 29.6 Hz), 27.69 (ddt, 1P, J = 258.7, 133.7, 33.6 Hz).

Synthesis of [Rh(PP$_2$)(PPh$_3$)][SbF$_6$]. [Rh(PP$_2$)(NBD)][SbF$_6$] (50.0 mg, 0.0518 mmol) was dissolved in 5 mL THF and added to a solution containing PPh$_3$ (13.6 mg, 0.0518 mmol) in 5 mL THF in a vial. The golden-yellow solution was transferred to a Schlenk flask under N_2 and heated for 8 days at 70°C. The solution was filtered, and the filtrate was dried under vacuum, giving a golden-yellow solid (62.5 mg, 57.1%). The NMR spectra are identical to [Rh(PP$_2$)(PPh$_3$)][BF$_4$].

Synthesis of [Rh(PP$_2$)(L^{PhenH})][BF$_4$]. [Rh(PP$_2$)(MeCN)][BF$_4$] (21.0 mg, 0.0274 mmol) was dissolved in 3 mL MeCN and added to a solution containing the L^{PhenH} (10.8 mg, 0.0274 mmol) ligand in 5 mL MeCN. The golden-yellow solution was stirred at ambient temperatures overnight, then dried under vacuum, giving a golden-yellow solid (32.6 mg, 99.4%). ^{1}H NMR (DMSO-d_6, 300 MHz, Figure A44): δ 8.11 – 6.52 (m, 43H), 5.45 (d, J = 8.2 Hz, 1H), 3.52 (s, 2H) 3.12 – 2.64 (m, 4H), 2.00-1.80 (m, 4H). ^{31}P {^{1}H} NMR (DMSO-d_6, 121 MHz, Figure A45): δ 111.34 (ddt, 1P, J = 258.2, 122.3, 29.9 Hz), 53.25 (ddd, 2P, J = 141.7, 33.7, 30.4 Hz), 17.27 (ddt, 1P, J = 258.8, 130.0, 34.2 Hz).

Synthesis of [Rh(PP$_2$)(L^{PhenH})][SbF$_6$]. [Rh(PP$_2$)(NBD)][SbF$_6$] (60.3 mg, 0.0625 mmol) was dissolved in 5 mL THF and added to a solution containing L^{PhenH} (24.6 mg, 0.0625 mmol) in 5 mL THF in a vial. The yellow reaction mixture was stirred for 30 minutes before transferring to a Teflon-stoppered reaction flask under N_2. The flask was frozen in liquid nitrogen, evacuated, and H_2 gas (1 atm) was added. After stirring for 2 days the solution was dried under vacuum and a hexane wash was conducted and filtered. The yellow solid powder was collected and yielded 86.0 mg (72.7%). The NMR spectra are identical to [Rh(PP$_2$)(L^{PhenH})][BF$_4$].

Synthesis of [Rh(PP$_2$)(L^{Phen+})][BF$_4$]$_2$. [Rh(PP$_2$)(MeCN)][BF$_4$] (30.0 mg, 0.0392 mmol) was dissolved in 3 mL MeCN and added to a solution containing L^{Phen+} (15.4 mg, 0.0392 mmol) in 5 mL MeCN and displayed a golden-yellow color and was stirred overnight. The golden-yellow solution was dried under vacuum, yielding the product as a golden-yellow powder (44.9 mg, 95.2%). ^{1}H NMR (DMSO-d_6, 300 MHz, Figure A46): δ 9.67 (s, 1H), 9.16 (t, 2H), 8.69 – 8.28 (m, 2H), 8.28 – 7.83 (m, 4H), 7.83 – 7.09 (m, 35 H), 6.89 (m, 12H), 6.64 (d, J = 9.4 Hz, 1H), 4.49 (s, 2H), 3.49 – 2.64 (m, 4H), 2.18 (s, 2H), 1.99 – 1.56 (m, 4H). ^{31}P {^{1}H} NMR (DMSO-d_6, 121 MHz, Figure A47): δ 110.73 (ddt, 1P, J = 261.7, 124.4, 30.0 Hz), 53.08 (ddd, 2P), 18.31 (ddt, 1P, J = 261.0, 132.5, 34.3 Hz).

Synthesis of [HRh(PP$_2$)(PPh$_3$)]. [Rh(PP$_2$)(PPh$_3$)][BF$_4$] (10.0 mg, 0.0101 mmol) was dissolved in 4 mL THF in a vial. LiEt$_3$BH (15.2µL, 1 M in THF, 0.0152 mmol) was injected into the vial. After the addition, the golden-yellow solution was left to stir overnight. The solution was dried under vacuum and was crystallized by vapor diffusion of hexane into a toluene solution for 21 days. The crystalline material was separated from

the supernatant and dried to yield 7.2 mg (79%). ^{1}H NMR (C_6D_6, 300 MHz, Figure A48): δ 7.80 – 6.33 (m, 40H), 2.36 (m, 2H), 1.66-0.86 (m, 8H), -8.53 (dd, *J* = 124.0, 21.8 Hz, 1H). ^{31}P {^{1}H} NMR (C_6D_6, 121 MHz, Figure A49): δ 95.44 – 92.10 (m, 1P), 65.91 (ddd, 2P, *J* = 161.3, 102.8, 21.6 Hz), 44.25 (dtd, 1P, *J* = 154.7, 102.9, 22.3 Hz).

Synthesis of [HRh(PP$_2$)(L^{PhenH})]. [Rh(PP$_2$)(L^{PhenH})][SbF$_6$] (5.0 mg, 0.0039 mmol) was dissolved in 3 mL THF in a vial. LiEt$_3$BH (4.0 μL, 0.0039 mmol) was injected into the vial with a 25 μL syringe. After the addition, the golden-yellow solution was left to stir overnight. The solution was dried under vacuum and purified through hexane extraction, ether extraction, and THF extraction. The solid was dried under vacuum and yielded 3.3 mg (80%). ^{1}H NMR (C_6D_6, 300 MHz, Figure A50): δ 8.32 – 5.94 (m, 43H), 3.68 (s, 2H), 3.38 (m, 2H), 2.27 (m, 4H), 1.89 (m, 4H), -8.90 (dd, *J* = 123.5, 16.7 Hz, 1H). ^{31}P {^{1}H} NMR (C_6D_6, 121 MHz, Figure A51): δ 93.71 (dd, 1P, *J* = 106.7, 23.0 Hz), 66.16 (ddd, 2P, *J* = 159.8, 108.1, 22.7 Hz), 24.55 (dtd, 1P, *J* = 154.9, 108.0, 107.6, 23.6 Hz).

Reaction of [Rh(PP$_2$)(L^{PhenH})][SbF$_6$] and CPh$_3$(BF$_4$).). [Rh(PP$_2$)(L^{PhenH})][SbF$_6$] (12 mg, 0.0095 mmol) was dissolved in 2 mL MeCN and added to a solution of triphenylcarbenium tetrafluoroborate (3.1 mg, 0.0095 mmol) in 3 mL MeCN. A yellow color solution was observed immediately and was stirred overnight. The solution was dried under vacuum and washed with hexane and ether. The solution was dried once more and dissolved in approximately 0.6 mL of CD$_3$CN and transferred to an NMR tube. For the NMR spectrum, refer to Figure A52.

Reaction of [Rh(PP$_2$)(L^{Phen+})](SbF$_6$)[BF$_4$] and NEt$_3$ with H$_2$ Gas. Triethylamine (1.0 μL, 0.0096 mmol) and [Rh(PP$_2$)(L^{Phen+})][SbF$_6$] (13 mg, 0.0096 mmol)

in approximately 0.6 mL of CD_3CN was added to a J Young tube. This tube was then charged with 1.0 atm of H_2 gas (0 psig) and inverted several times to induce mixing. Spectral data were obtained immediately after mixing and followed by ^1H NMR for 3 days. The ^1H NMR spectrum is shown in Figure A53, showing $[Rh(PP_2)(L^{PhenH})]^+$ as the only Rh-containing species.

Reaction of $HRh(PP_2)(L^{PhenH})$ and H(DMF)OTf. A yellow solution of $[HRh(PP_2)(L^{PhenH})]$ in C_6D_6 was prepared in situ by the reaction of $[Rh(PP_2)(L^{PhenH})][SbF_6]$ (5.1 mg, 0.0040 mmol) and $LiEt_3BH$ (4.0 μL, 0.0040 mmol), and this solution was used to dissolve H(DMF)OTf (0.9 mg, 0.0040 mmol), and the resulting yellow mixture was transferred to a J Young NMR tube. The tube was inverted several times to induce mixing and spectral data obtained immediately. The reaction was followed by ^1H NMR for 17 hours. Noticeable precipitate appeared in the tube after 17 hours. The precipitate was filtered from the solution and dissolved in 0.6 mL of CD_3CN and spectral data obtained immediately after mixing. The ^1H NMR spectrum is shown in Figure A54. The ^{31}P NMR spectrum is shown in Figure A55, showing $[Rh(PP_2)(L^{PhenH})]^+$ as the only Rh-containing species.

Reaction of $[Rh(PP_2)(L^{PhenH})][BF_4]$ and H(DMF)OTf. The acid (1.0 mg, 0.0045 mmol) was added to $[Rh(PP_2)(L^{PhenH})][BF_4]$ (5.0 mg, 0.0045 mmol) in approximately 0.3 mL of C_6D_6. The mixture noticeably became oily and approximately 0.3 mL of DMSO-d_6 was added. The solution was transferred to an NMR tube and spectral data was immediately obtained. The ^{31}P NMR spectrum is shown in Figure A56, showing $[Rh(PP_2)(L^{PhenH})]^+$ as the only Rh-containing species.

Equilibrium of [Rh(PP$_2$)(L^{PhenH})](SbF$_6$) and Verkade's Base under H$_2$ and CO$_2$ Gas. In a J Young NMR tube, [Rh(PP$_2$)(L^{PhenH})][SbF$_6$] (4.5 mg, 0.0035 mmol) and Verkade's base (1.1 mg, 0.0035 mmol) were added to approximately 0.6 mL of THF and produced a yellow color solution. These species were found to be stable in solution together for 24 h as observed by their ^{31}P NMR spectra. The tube was purged with 1.8 atm of H$_2$ and CO$_2$ gases (11 psig) and inverted to induce mixing. ^{31}P NMR data was immediately obtained after mixing and followed for 2 days, at which point only HVkd$^+$ and [HRh(PP$_2$)(L^{PhenH})] were observed. The mixture was dried under vacuum and dissolved with approximately 0.6 mL of DMSO-*d*$_6$ and ^{1}H NMR data obtained, showing only trace amounts of formate. The ^{31}P NMR spectrum is shown in Figure A57, showing only HVkd$^+$ and [HRh(PP$_2$)(L^{PhenH})].

Equilibrium of [Rh(PP$_2$)(L^{PhenH})][SbF$_6$] and LiO^{t}Bu under H$_2$ Gas. In a J Young NMR tube, LiO^{t}Bu (4.0 μL, 1 M, 0.0040 mmol) and [Rh(PP$_2$)(L^{PhenH})][SbF$_6$] (5.1 mg, 0.0040 mmol) were added to 0.6 mL of THF and produced a yellow color solution. ^{31}P NMR data was immediately obtained after mixing to confirm that the reactants were stable in solution together. After 24 h, the tube was purged with 1.0 atm of H$_2$ gas (0 psig) and inverted to induce mixing. Spectral data obtained after mixing. The reaction reached equilibrium after 10 days, indicated by the constant ratio of reactants and products. The final spectrum, from which the equilibrium constant was determined, is shown in Figure A58.

Equilibrium of [Rh(PP$_2$)(PPh$_3$)][BF$_4$] and Verkade's Base under H$_2$ Gas. In a J Young NMR tube, Verkade's base (1.1 mg, 0.0035 mmol) and [Rh(PP$_2$)(PPh$_3$)][BF$_4$] (3.5 mg, 0.0035 mmol) were added to approximately 0.6 mL of THF and produced a

yellow color solution. The tube was charged with 1.0 atm of H_2 gas (0 psig) and inverted to induce mixing. ^{31}P NMR data was obtained after 1 h. The reaction reached equilibrium within 2 days, showing only $HVkd^+$ and $[HRh(PP_2)(PPh_3)]$ (Figure A59).

Equilibrium of $[Rh(PP_2)(PPh_3)][BF_4]$ and $P_1{}^tBu$ under H_2 Gas. In a J Young NMR tube, $[Rh(PP_2)(PPh_3)][BF_4]$ (2.8 mg, 0.0028 mmol) and $P_1{}^tBu$ (0.9 μL, 0.0028 mmol) were added to approximately 0.6 mL of THF and produced a yellow color solution. A ^{31}P NMR was obtained after the addition. The tube was charged with 1.0 atm of H_2 gas (0 psig) and inverted to induce mixing. Spectral data were obtained after 4 hours. Another addition of gas with H_2 and CO_2 was charged to the tube at 1.0 atm (0 psig). Spectral data were obtained immediately after mixing. The reaction reached equilibrium after 74 h, showing only $HP_1{}^tBu^+$ and $[HRh(PP_2)(PPh_3)]$ (Figure A60).

Equilibrium of $[Rh(PP_2)(PPh_3)][BF_4]$ and LiO^tBu with H_2 Gas. In a J Young NMR tube, $[Rh(PP_2)(PPh_3)][BF_4]$ (5.0 mg, 0.0051 mmol) was added to LiO^tBu (5.1 μL, 0.0051 mmol) with approximately 0.6 mL of THF and produced a yellow color solution. The tube was charged with 1.0 atm of H_2 (0 psig) and inverted to induce mixing. ^{31}P NMR data was obtained immediately after mixing. The reaction was followed by NMR for 3 days. The reaction reached equilibrium after 189 h as indicated by a constant ratio of reactants and products. The final spectrum, from which the equilibrium constant was determined, is shown in Figure A61.

Equilibrium of $[Rh(PP_2)(PPh_3)][BF_4]$ and DBU with H_2 Gas. In a J Young NMR tube, DBU (1.3 μL, 0.0085 mmol) was added to $[Rh(PP_2)(PPh_3)][BF_4]$ (8.4 mg, 0.0085 mmol) in approximately 0.6 mL of acetonitrile which produced a yellow

color solution. The tube was charged with 1.0 atm of H_2 (0 psig) and inverted to induce mixing. ^{31}P NMR data was obtained immediately after mixing. The reaction was followed by NMR and reached equilibrium after 123 h as indicated by a constant ratio of reactants and products. The final spectrum, from which the equilibrium constant was determined, is shown in Figure A62.

CO_2 Hydrogenation Study with [Rh(PP_2)(L^{PhenH})][SbF_6] and DBU under H_2 and CO_2 Gas. In a J Young NMR tube, [Rh(PP_2)(L^{PhenH})][SbF_6] (1.0 mg, 0.00078 mmol) and NEt_3 (2.4 μL, 0.016 mmol) were added with approximately 0.6 mL of CD_3CN. The tube was charged with 1.8 atm of H_2 and CO_2 gas at 11 psig and inverted to induce mixing.^1H NMR data was obtained after mixing. The reaction was followed by ^1H NMR for 4 days. Afterward, DBU (2.4 μL, 0.016 mmol) was added to the mixture, and the tube was charged again with the same gas and pressure settings. Spectral data were obtained immediately after mixing. The reaction was followed by ^1H NMR for 2 days. Another gas addition by the same settings was charged into the tube and spectral data were obtained immediately after mixing. The reaction halted after a total of 138 h as indicated by a constant concentration of product. The stacked ^1H NMR data is shown in Figure A63.

CO_2 Hydrogenation Study with [Rh(PP_2)(L^{PhenH})][BF_4] and Verkade's Base under H_2 and CO_2 Gas. In a J Young NMR tube, Verkade's base (15.0 mg, 0.0500 mmol) was added to a yellow solution of [Rh(PP_2)(L^{PhenH})][BF_4] (0.05 mL, 0.01 M, 0.0050 mmol) in 0.45 mL of THF. The tube was charged with 1.8 atm of H_2 and CO_2 gas at 11 psig and inverted to induce mixing. ^{31}P NMR data was immediately obtained after mixing. The reaction was followed by ^{31}P NMR spectroscopy for 34 days, at which point all of the base had been consumed. To confirm the production of formate, the solution

was dried under vacuum and dissolved in 0.6 mL of DMSO-d_6, and ^{1}H NMR data confirmed the presence of formate, as discussed above. The stacked ^{31}P NMR data is shown in Figure A64.

REFERENCES

(1) Bose, B. K. Global Warming: Energy, Environmental Pollution, and the Impact of Power Electronics. *IEEE Industrial Electronics Magazine* **2010**, *4*, 6–17.

(2) Aresta, M.; Dibenedetto, A.; Angelini, A. Catalysis for the Valorization of Exhaust Carbon: from CO_2 to Chemicals, Materials, and Fuels. Technological Use of CO_2. *Chem. Rev.* **2014**, *114*, 1709–1742.

(3) Cokoja, M.; Bruckmeier, C.; Rieger, B.; Herrmann, W. A.; Kühn, F. E. Transformation of Carbon Dioxide with Homogeneous Transition-Metal Catalysts: A Molecular Solution to a Global Challenge?. *Angew. Chem., Int. Ed.* **2011**, *50*, 8510–8537.

(4) Leitner, W. Carbon Dioxide as a Raw Material: The Synthesis of Formic Acid and Its Derivatives from CO_2. *Angew. Chem. Int. Ed.* **1995**, *34*, 2207-2221.

(5) Berning, D. E.; Noll, B. C.; DuBois, D. L. Relative Hydride, Proton, and Hydrogen Atom Transfer Abilities of $[HM(diphosphine)_2]PF_6$ Complexes (M = Pt, Ni). *J. Am. Chem. Soc.* **1999**, *121*, 11432–11447.

(6) Wilson, A. D.; Miller, A. J. M.; Dubois, D. L.; Labinger, J. A.; Bercaw, J. E. Thermodynamic Studies of $[H_2Rh(diphosphine)_2]^+$ and $[HRh(diphosphine)_2(CH_3CN)]^{2+}$ Complexes in Acetonitrile. *Inorg. Chem.* **2010**, *49*, 3918–3926.

(7) Olah, G. A.; Prakash, G. K. S.; Goeppert, A. Anthropogenic Chemical Carbon Cycle for a Sustainable Future. *J. Am. Chem. Soc.* **2011**, *133*, 12881–12898.

(8) Bernskoetter, W. H.; Hazari, N. Reversible Hydrogenation of Carbon Dioxide to Formic Acid and Methanol: Lewis Acid Enhancement of Base Metal Catalysts. *Acc. Chem. Res.* **2017**, *50*, 1049–1058.

(9) Wesselbaum, S.; vom Stein, T.; Klankermayer, J.; Leitner, W. Hydrogenation of Carbon Dioxide to Methanol by Using a Homogeneous Ruthenium-Phosphine Catalyst. *Angew. Chem. Int. Ed.* **2012**, *51*, 7499-7502.

(10) Tanaka, R.; Yamashita, M.; Chung, L. W.; Morokuma, K.; Nozaki, K. Mechanistic Studies on the Reversible Hydrogenation of Carbon Dioxide Catalyzed by an Ir-PNP Complex. *Organometallics* **2011**, *30*, 6742–6750.

(11) Inoue, Y.; Izumida, H.; Sasaki, Y.; Hashimoto, H. CATALYTIC FIXATION OF CARBON DIOXIDE TO FORMIC ACID BY TRANSITION-METAL COMPLEXES UNDER MILD CONDITIONS. *Chem. Lett.* **1976**, 863-864.

(12) Wang, W–H.; Himeda, Y.; Muckerman, J. T.; Manbeck, G. F.; Fujita, E. CO_2 Hydrogenation to Formate and Methanol as an Alternative to Photo- and Electrochemical CO_2 Reduction. *Chem. Rev.* **2015**, *115*, 12936–12973.

(13) Tanaka, R.; Yamashita, M.; Nozaki, K. Catalytic Hydrogenation of Carbon Dioxide Using Ir(III)−Pincer Complexes. *J. Am. Chem. Soc.* **2009**, *131*, 14168–14169.

(14) Takaoka, S.; Eizawa, A.; Kusumoto, S.; Nakajima, K.; Nishibayashi, Y.; Nozaki, K. Hydrogenation of Carbon Dioxide with Organic Base by $PC^{II}P$-Ir Catalysts. *Organometallics* **2018**, *37*, 3001–3009.

(15) Filonenko, G. A.; van Putten, R.; Schulpen, E. N.; Hensen, E. J. M.; Pidko, E. A. Highly Efficient Reversible Hydrogenation of Carbon Dioxide to Formates Using a Ruthenium PNP-Pincer Catalyst. *ChemCatChem*. **2014**, *6*, 1526-1530.

(16) Jeletic, M. S.; Mock, M. T.; Appel, A. M.; Linehan, J. C. A Cobalt-Based Catalyst for the Hydrogenation of CO_2 under Ambient Conditions. *J. Am. Chem. Soc.* **2013**, *135*, 11533–11536.

(17) Qi, X.-J.; Fu, Y.; Liu, L.; Guo, Q.-X. Ab Initio Calculations of Thermodynamic Hydricities of Transition-Metal Hydrides in Acetonitrile. *Organometallics* **2007**, *26*, 4197–4203.

(18) Morris, R. H. Brønsted–Lowry Acid Strength of Metal Hydride and Dihydrogen Complexes. *Chem. Rev.* **2016**, *116*, 8588–8654.

(19) Wiedner, E. S.; Chambers, M. B.; Pitman, C. L.; Bullock, R. M.; Miller, A. J. M.; Appel, A. M. Thermodynamic Hydricity of Transition Metal Hydrides. *Chem. Rev.* **2016**, *116*, 8655–8692.

(20) Curtis, C. J.; Miedaner, A.; Ellis, W. W.; DuBois, D. L. Measurement of the Hydride Donor Abilities of $[HM(diphosphine)_2]^+$ Complexes (M = Ni, Pt) by Heterolytic Activation of Hydrogen. *J. Am. Chem. Soc.* **2002**, *124*, 1918–1925.

(21) DuBois, D. L.; Berning, D. E. Hydricity of transition-metal hydrides and its role in CO_2 reduction. *Appl. Organometal. Chem.* **2000**, *14*, 860-862.

(22) Matsubara, Y.; Fujita, E.; Doherty, M. D.; Muckerman, J. T.; Creutz, C. Thermodynamic and Kinetic Hydricity of Ruthenium(II) Hydride Complexes. *J. Am. Chem. Soc.* **2012**, *134*, 15743–15757.

(23) Mock, M. T.; Potter, R. G.; Camaioni, D. M.; Li, J.; Dougherty, W. G.; Kassel, W. S.; Twamley, B.; DuBois, D. L. Thermodynamic Studies and Hydride Transfer Reactions from a Rhodium Complex to BX_3 Compounds. *J. Am. Chem. Soc.* **2009**, *131*, 14454–14465.

(24) Qi, X.-J.; Liu, L.; Fu, Y.; Guo, Q.-X. Ab Initio Calculations of pK_a Values of Transition-Metal Hydrides in Acetonitrile. *Organometallics* **2006**, *25*, 5879–5886.

(25) Kisanga, P. B.; Verkade, J. G.; Schwesinger, R. pK_a Measurements of $P(RNCH_2CH_3)_3N$. *J. Org. Chem.* **2000**, *65*, 5431–5432.

(26) Devi, N. Development of Bifunctional Catalysts Containing Hydride-Relay Ligands for CO_2 Hydrogenation. M.S. Thesis, **2019**, Sam Houston State University, Huntsville, TX.

(27) Ciancanelli, R.; Noll, B. C.; DuBois, D. L.; DuBois, M. R. Comprehensive Thermodynamic Characterization of the Metal-Hydrogen Bond in a Series of Cobalt-Hydride Complexes. *J. Am. Chem. Soc.* **2002**, *124*, 2984–2992.

(28) Raebiger, J. W.; Miedaner, A.; Curtis, C. J.; Miller, S. M.; Anderson, O. P.; DuBois, D. L. Using Ligand Bite Angles to Control the Hydricity of Palladium Diphosphine Complexes. *J. Am. Chem. Soc.* **2004**, *126*, 5502–5514.

(29) Nimlos, M. R.; Chang, C. H.; Curtis, C. J.; Miedaner, A.; Pilath, H. M.; DuBois, D. L. Calculated Hydride Donor Abilities of Five-Coordinate Transition Metal Hydrides $[HM(diphosphine)_2]^+$ (M = Ni, Pd, Pt) as a Function of the Bite Angle and Twist Angle of Diphosphine Ligands. *Organometallics* **2008**, *27*, 2715–2722.

(30) Jeletic, M. S.; Hulley, E. B.; Helm, M. L.; Mock, M. T.; Appel, A. M.; Wiedner, E. S.; Linehan, J. C. Understanding the Relationship between Kinetics and

Thermodynamics in CO_2 Hydrogenation Catalysis. *ACS Catal* **2017**, *7*, 6008–6017.

(31) van Leeuwen, P. W. N. M.; Kamer, P. C. J.; Reek, J. N. H.; Dierkes, P. Ligand Bite Angle Effects in Metal-Catalyzed C−C Bond Formation. *Chem. Rev.* **2000**, *100*, 2741–2770.

(32) Kamer, P. C. J.; van Leeuwen, P. W. N. M.; Reek, J. N. H. Wide Bite Angle Diphosphines: Xantphos Ligands in Transition Metal Complexes and Catalysis. *Acc. Chem. Res.* **2001**, *34*, 895–904.

(33) Yang, L.; Powell, D. R.; Houser, R. P. Structural variation in copper(I) complexes with Pyridylmethylamide ligands: structural analysis with a new four-coordinate geometry index, τ4. *Dalton Trans.* **2007**, 955–964.

(34) Addison, A. W.; Rao, T. N.; Reedijk, J.; Rijn, J.; Verschoor, G. C. Synthesis, Structure, and Spectroscopic Properties of Copper(II) Compounds Containing Nitrogen-Sulphur Donor Ligands the Crystal and Molecular Structure of Aqua[1,7-bis(*N*-methylbenzimidazol-2′-yl)-2,6-dithiaheptane]copper(II) Perchlorate. *J. Chem. Soc. Dalton Trans.* **1984**, 1349–1356.

(35) Curtis, C. J.; Miedaner, A.; Raebiger, J. W.; DuBois, D. L. Periodic Trends in Metal Hydride Donor Thermodynamics: Measurement and Comparison of the Hydride Donor Abilities of the Series $HM(PNP)_2^+$ (M = Ni, Pd, Pt; PNP = $Et_2PCH_2N(Me)CH_2PEt_2$). *Organometallics* **2004**, *23*, 511–516.

(36) Gaussian 09, Revision D.01, Frisch, M. J.; Trucks, G. W.; Schlegal, H. B.; Scuseria, G. E.; Robb, M. A.; Cheeseman, J. R.; Scalmani, G.; Barone, V.; Mennucci, B.; Petersson, G. A.; Nakatsuji, H.; Caricato, M.; Li, X.; Hratchian, H.

P.; Izmaylov, A. F.; Bloino, J.; Zheng, G.; Sonnenberg, J. L.; Hada, M.; Ehara, M.; Toyota, K.; Fukuda, R.; Hasegawa, J.; Ishida, M.; Nakajima, T.; Honda, Y.; Kitao, O.; Nakai, H.; Vreven, T.; Montgometry, J. A.; Peralta, J. E.; Ogliaro, F.; Bearpark, M.; Heyd, J. J.; Brothers, E.; Kudin, K. N.; Staroverov, V. N.; Keith, T.; Kobayashi, R.; Normand, J.; Raghayachari, K.; Rendell, A.; Burant, J. C.; Ivengar, S. S.; Tomasi, J.; Cossi, M.; Rega, N.; Millam, J. M.; Klene, M.; Knox, J. E.; Cross, J. B.; Bakken, V.; Adamo, C.; Jaramillo, J.; Gomperts, R.; Stratmann, R. E.; Yazyey, O.; Austin, A. J.; Cammi, R.; Pomelli, C.; Ochterski, J. W.; Martin, R. L.; Morokuma, K.; Zakrzewski, V. G.; Voth, G. A.; Salvador, P.; Dannenberg, J. J.; Dapprich, S.; Daniels, A. D.; Farkas, O.; Foresman, J. B.; Ortiz, J. V.; Cioslowski, J.; Fox, D. J., Gaussian, Inc., Wallingford CT, 2013.

(37) Raebiger, J. W.; DuBois, D. L. Thermodynamic Studies of $HRh(depx)_2$ and $[(H)_2Rh(depx)_2](CF_3SO_3)$: Relationships between Five-Coordinate Monohydrides and Six-Coordinate Dihydrides. *Organometallics* **2005**, *24* , 110–118.

(38) Kaljurand, I.; Kütt, A.; Sooväli, L.; Rodima, T.; Mäemets, V.; Leito, I.; Koppel, I. A. Extension of the Self-Consistent Spectrophotometric Basicity Scale in Acetonitrile to a Full Span of 28 pK_a Units: Unification of Different Basicity Scales. *J. Org. Chem.* **2005**, *70*, 1019–1028.

(39) Taylor, J. E.; Bull, S. D.; Williams, J. M. J. Amidines, isothioureas, and guanidines as nucleophilic catalysts. *Chem. Soc. Rev.* **2012**, *41*, 2109–2121.

(40) Long, J. A.; Marder, T. B.; E. Behnken, P. E.; Hawthorne, M. F. Metallacarboranes in Catalysis. 3. Synthesis and Reactivity of *exo-nido*-Phosphinerhodacarboranes. *J. Am. Chem. Soc.* **1984**, *106*, 2979–2989.

(41) Beck, C. M.; Rathmill, S. E.; Park, Y. J.; Chen, J.; Crabtree, R. H.; Liable-Sands, L. M.; Rheingold, A. L. Aldehyde Decarbonylation Catalysis under Mild Conditions. *Organometallics* **1999**, *18*, 5311–5317.

(42) Westcott, S. A.; Stringer, G.; Anderson, S.; Taylor, N. J.; Marder, T. B. Synthesis, Structure, and Reactivity of RhCl(PhP{$CH_2CH_2PPh_2$}$_2$). *Inorg. Chem.* **1994**, *33*, 4589–4594.

(43) Kolthoff, I. M.; Chantooni, M. K. Jr.; Bhowmik, S. Titration of Bases in Acetonitrile. *Anal. Chem.* **1967**, *39*, 1627–1633.

(44) Ostovic, D.; Lee, I–S. H.; Roberts, R. M. G.; Kreevoy, M. M. Hydride Transfer and Oxyanion Addition Equilibria of NAD^+ Analogues. *J. Org. Chem.* **1985**, *50*, 4206-4211.

APPENDIX A

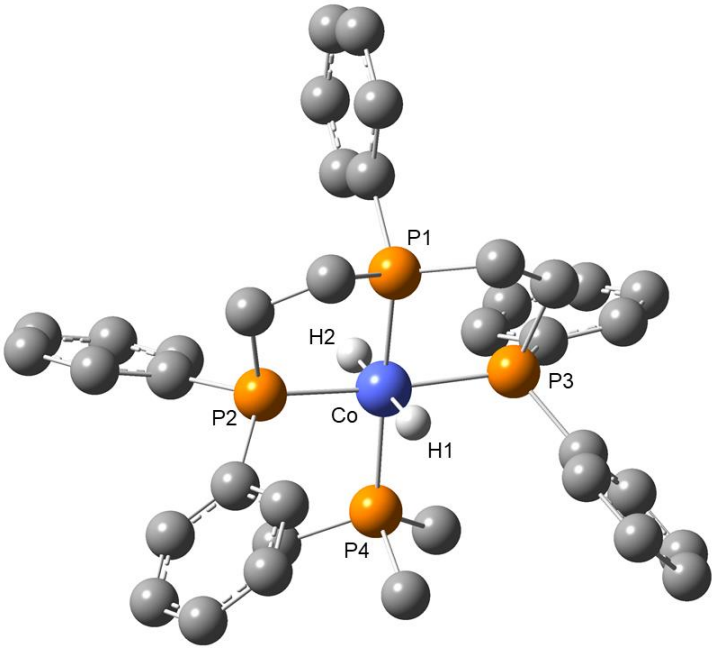

Figure A1. *Optimized structure of* $[H_2Co(PP_2)(PMe_3)]^+$. *Hydrogen atoms, other than the metal hydrides have been omitted.*

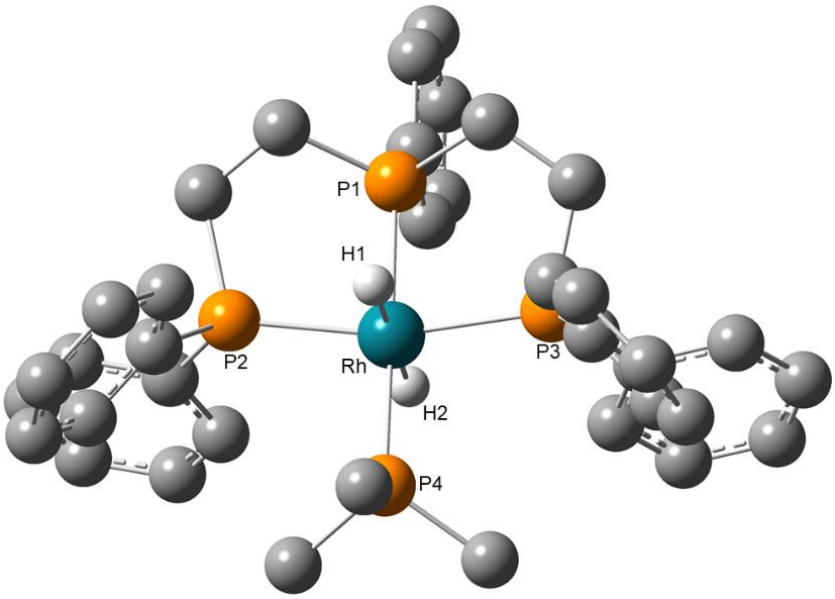

Figure A2. *Optimized structure of* $[H_2Rh(PP_2)(PMe_3)]^+$. *Hydrogen atoms, other than the metal hydrides have been omitted.*

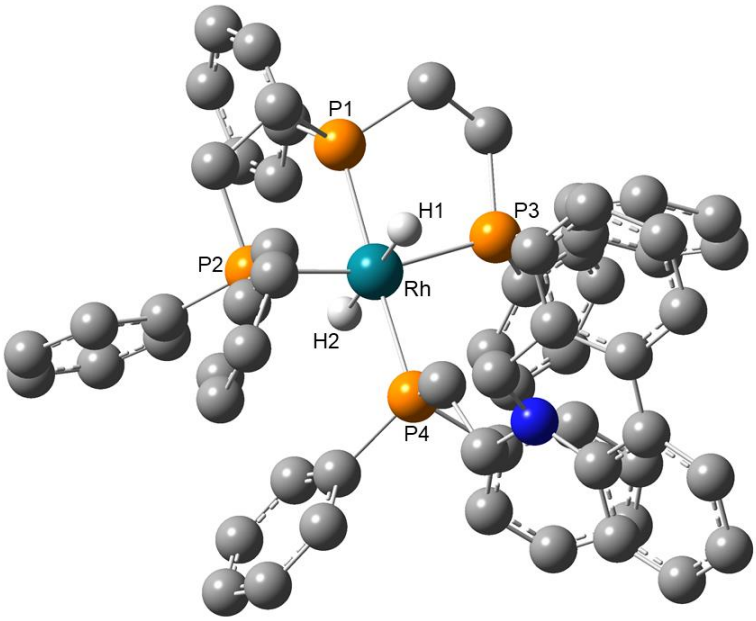

Figure A3. *Optimized structure of* $[H_2Rh(PP_2)(L^{PhenH})]^+$. *Hydrogen atoms, other than the metal hydrides have been omitted.*

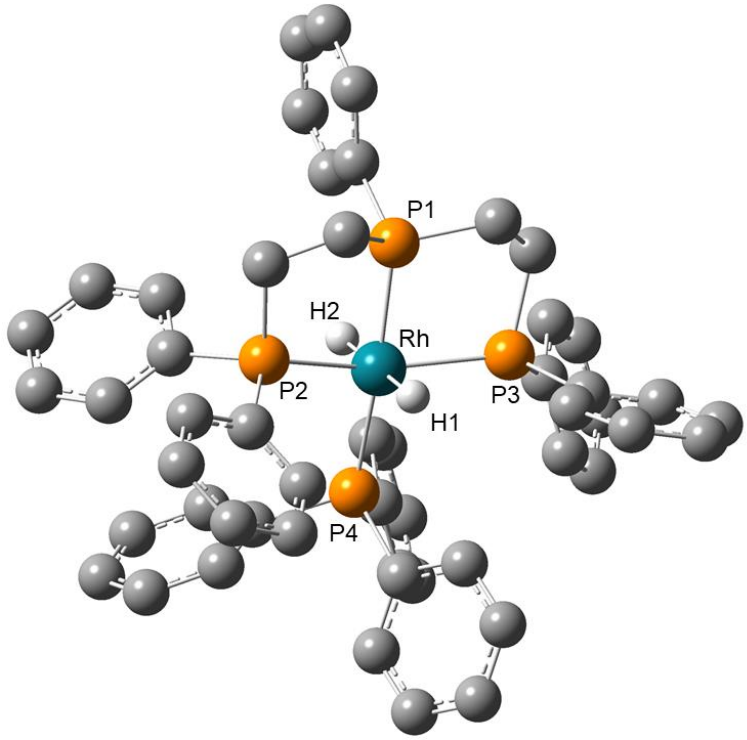

Figure A4. *Optimized structure of* $[H_2Rh(PP_2)(PPh_3)]^+$. *Hydrogen atoms, other than the metal hydrides have been omitted.*

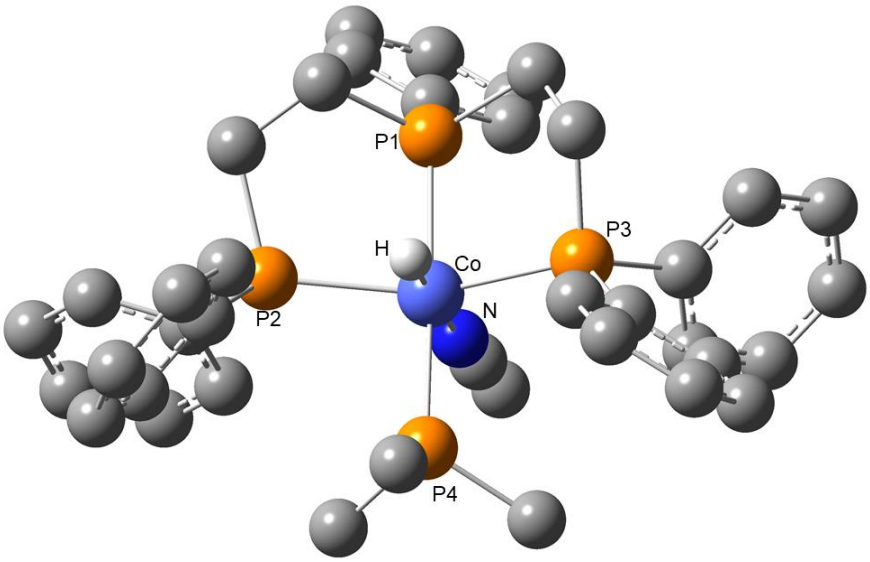

Figure A5. *Optimized structure of* $[HCo(PP_2)(PMe_3)(MeCN)]^{2+}$. *Hydrogen atoms, other than the metal hydrides have been omitted.*

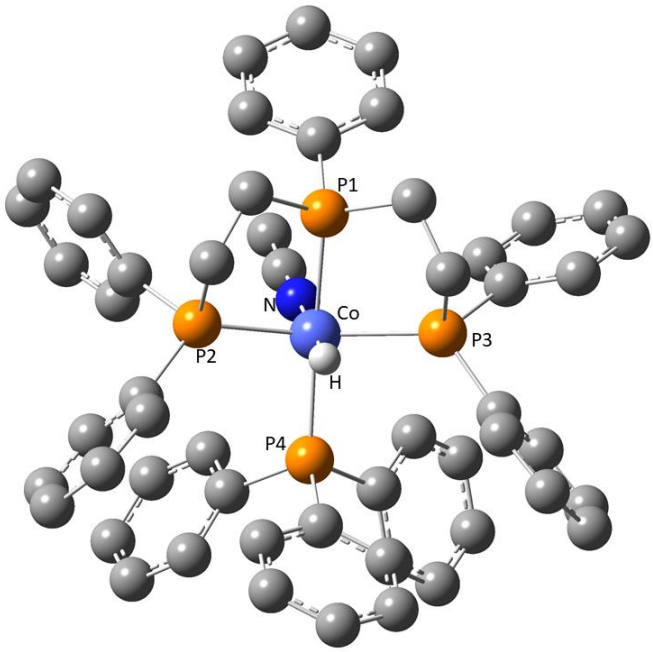

Figure A6. *Optimized structure of* $[HCo(PP_2)(PPh_3)(MeCN)]^{2+}$. *Hydrogen atoms, other than the metal hydrides have been omitted.*

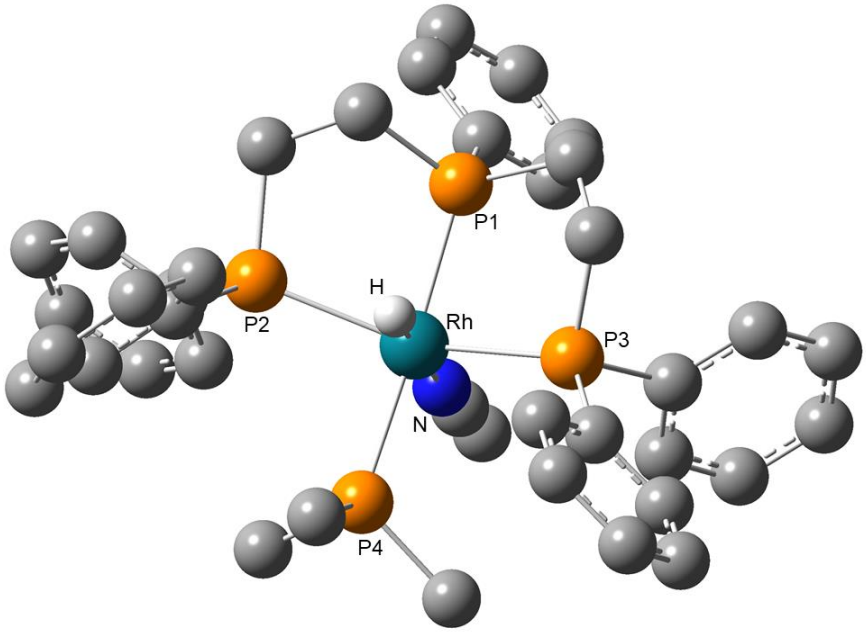

Figure A7. *Optimized structure of* $[HRh(PP_2)(PMe_3)(MeCN)]^{2+}$. *Hydrogen atoms, other than the metal hydrides have been omitted.*

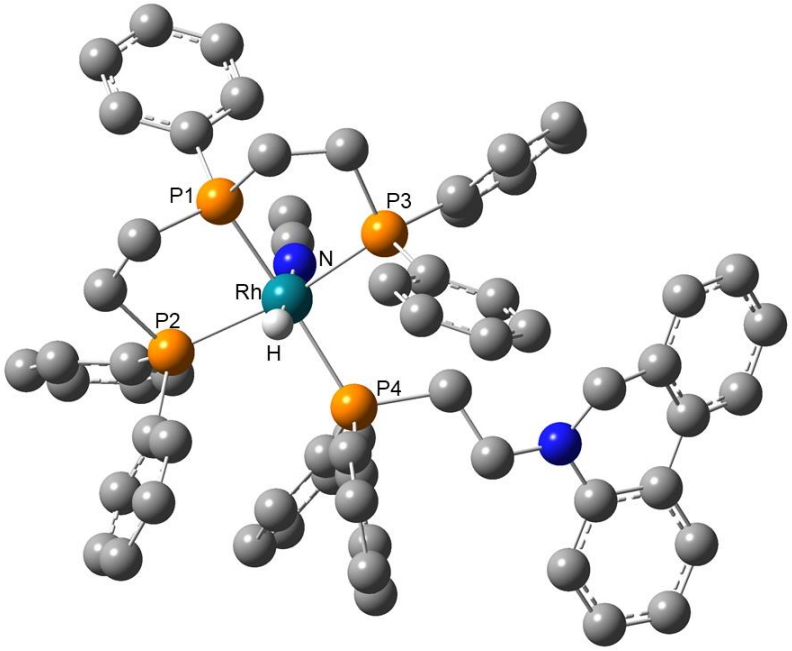

Figure A8. *Optimized structure of* $[HRh(PP_2)(L^{PhenH})(MeCN)]^{2+}$. *Hydrogen atoms, other than the metal hydrides have been omitted.*

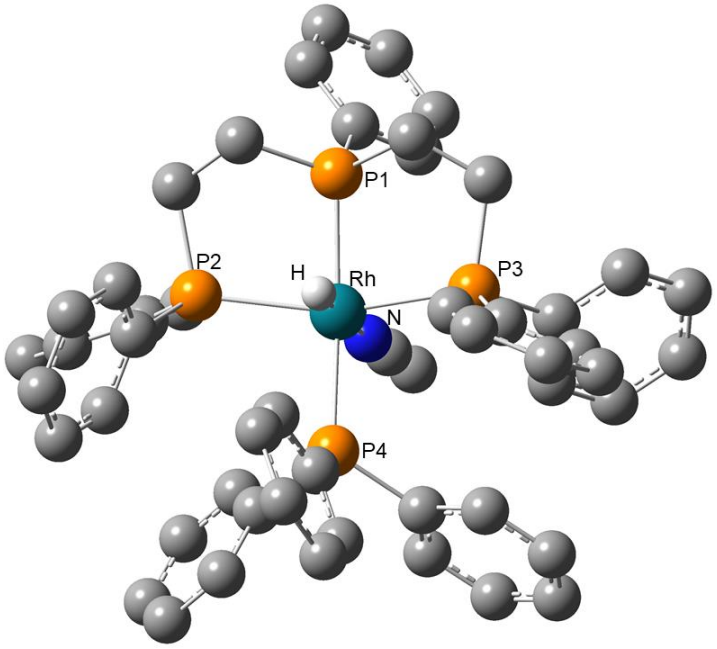

Figure A9. *Optimized structure of* $[HRh(PP_2)(PPh_3)(MeCN)]^{2+}$. *Hydrogen atoms, other than the metal hydrides have been omitted.*

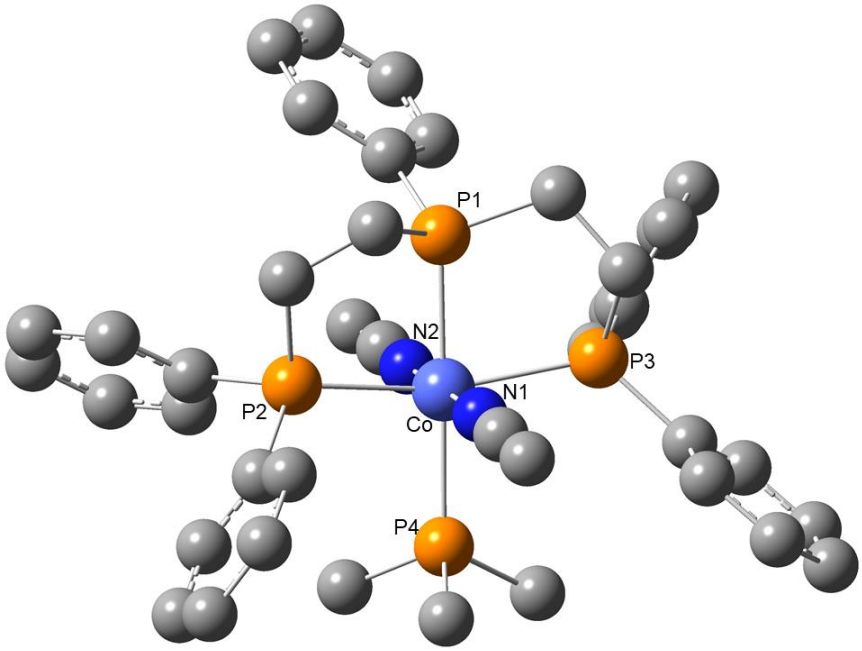

Figure A10. *Optimized structure of* $[Co(PP_2)(PMe_3)(MeCN)_2]^{3+}$. *Hydrogen atoms, other than the metal hydrides have been omitted.*

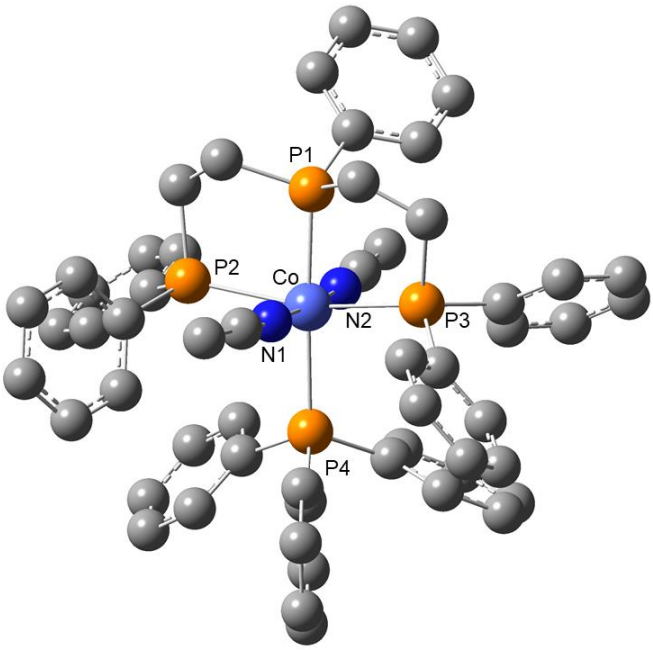

Figure A11. *Optimized structure of* $[Co(PP_2)(PPh_3)(MeCN)_2]^{3+}$. *Hydrogen atoms, other than the metal hydrides have been omitted.*

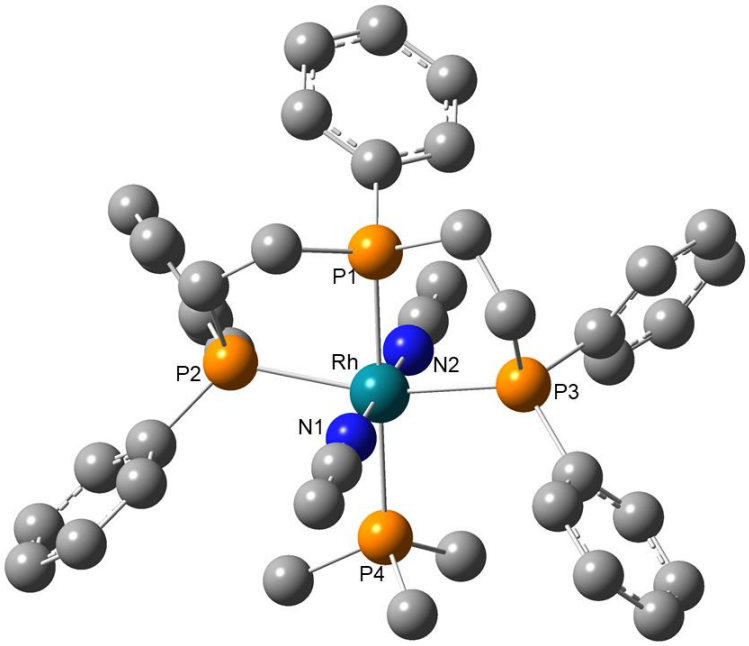

Figure A12. *Optimized structure of* $[Rh(PP_2)(PMe_3)(MeCN)_2]^{3+}$. *Hydrogen atoms, other than the metal hydrides have been omitted.*

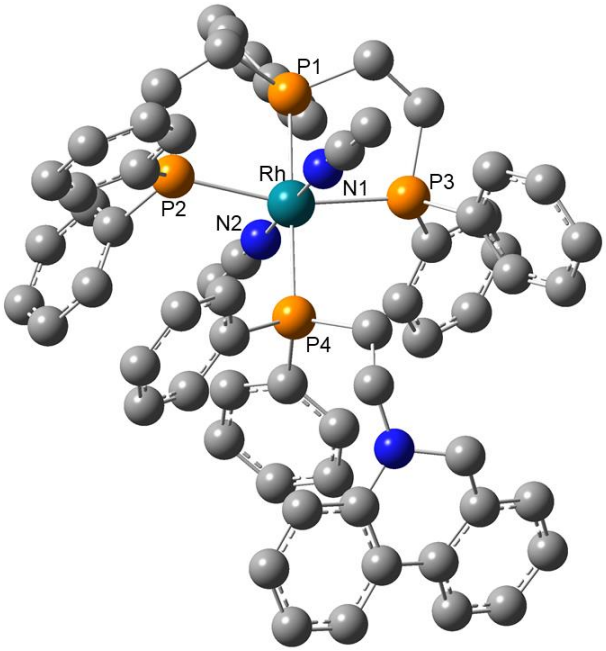

Figure A13. *Optimized structure of* $[Rh(PP_2)(L^{PhenH})(MeCN)_2]^{3+}$. *Hydrogen atoms, other than the metal hydrides have been omitted.*

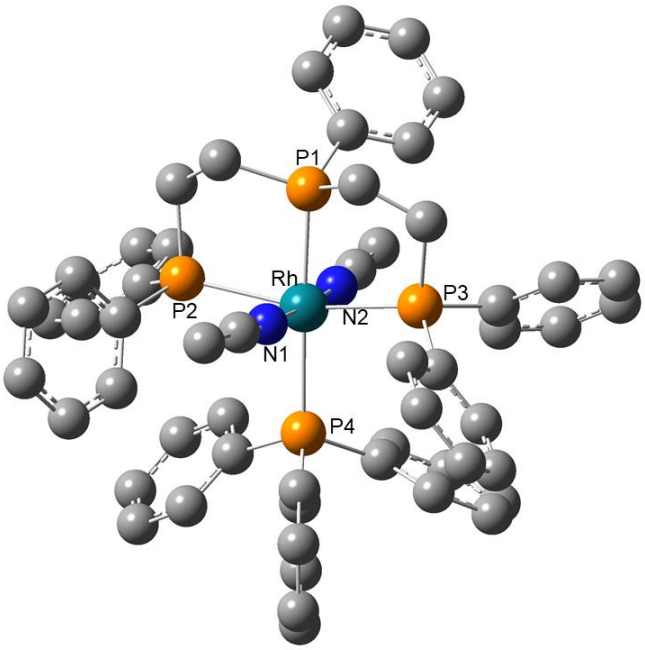

Figure A14. *Optimized structure of* $[Rh(PP_2)(PPh_3)(MeCN)_2]^{3+}$. *Hydrogen atoms, other than the metal hydrides have been omitted.*

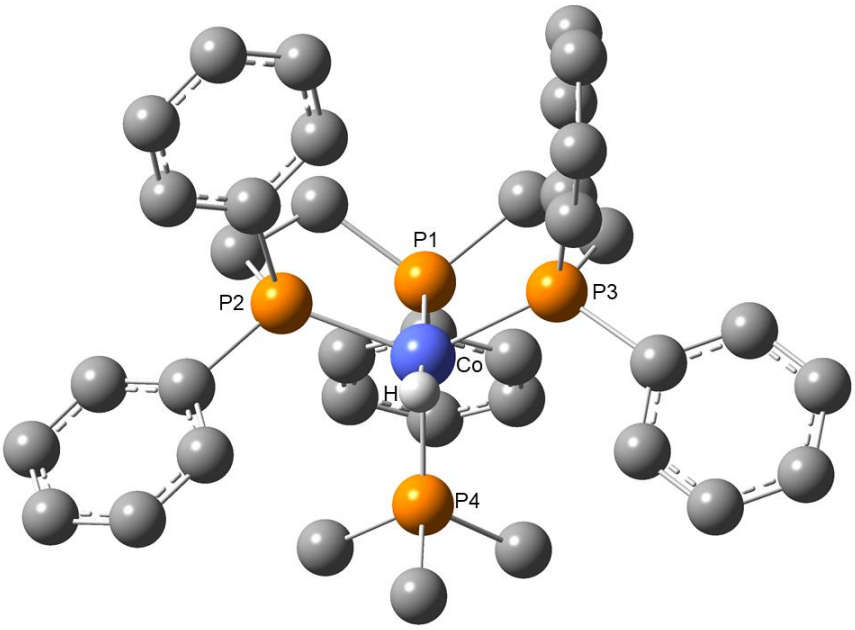

Figure A15. *Optimized structure of [HCo(PP$_2$)(PMe$_3$)]. Hydrogen atoms, other than the metal hydrides have been omitted.*

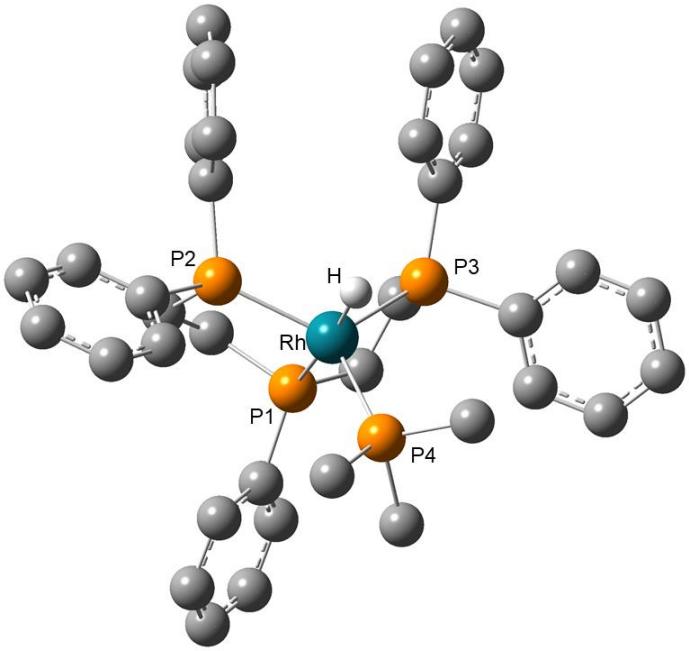

Figure A16. *Optimized structure of [HRh(PP$_2$)(PMe$_3$)]. Hydrogen atoms, other than the metal hydrides have been omitted.*

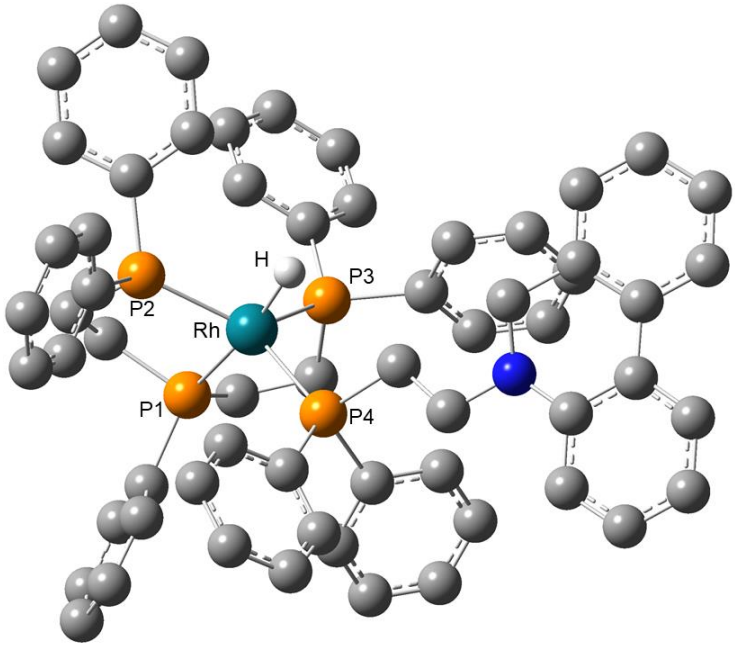

Figure A17. *Optimized structure of [HRh(PP$_2$)(L^{PhenH})]. Hydrogen atoms, other than the metal hydrides have been omitted.*

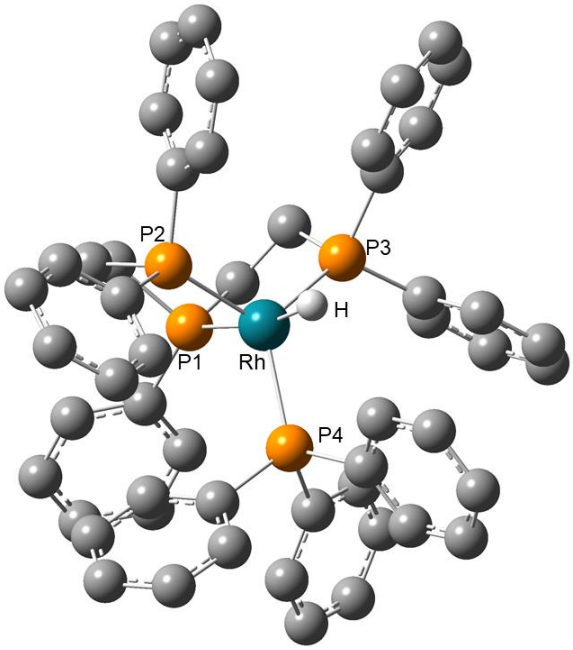

Figure A18. *Optimized structure of [HRh(PP$_2$)(PPh$_3$)]. Hydrogen atoms, other than the metal hydrides have been omitted.*

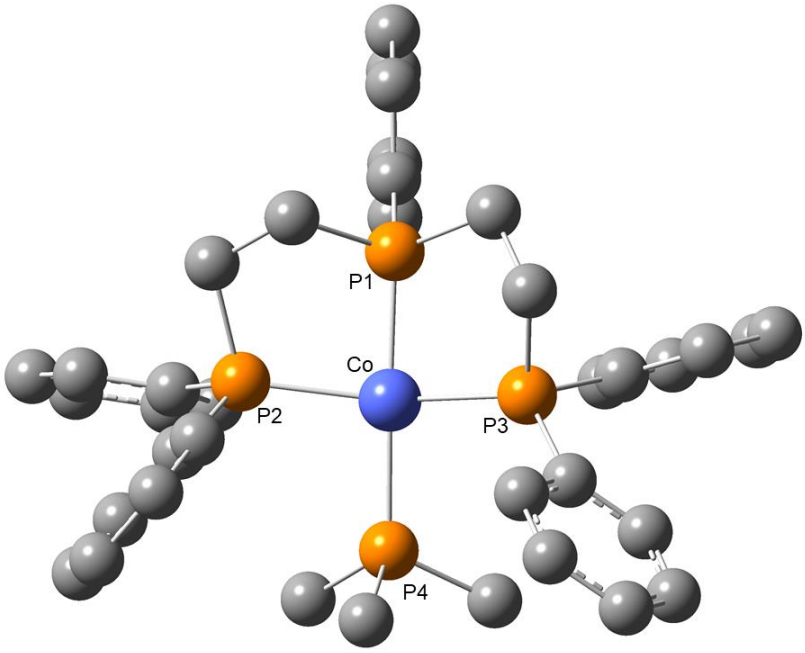

Figure A19. *Optimized structure of [Co(PP$_2$)(PMe$_3$)]$^+$. Hydrogen atoms, other than the metal hydrides have been omitted.*

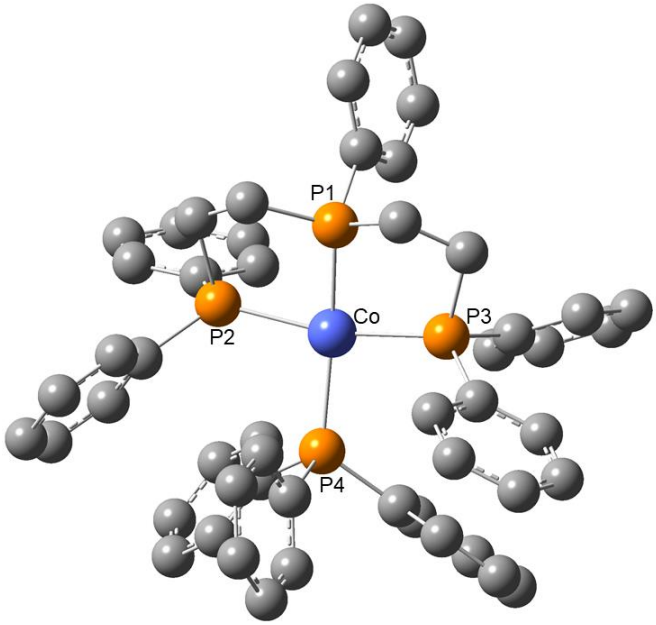

Figure A20. *Optimized structure of [Co(PP$_2$)(PPh$_3$)]$^+$. Hydrogen atoms, other than the metal hydrides have been omitted.*

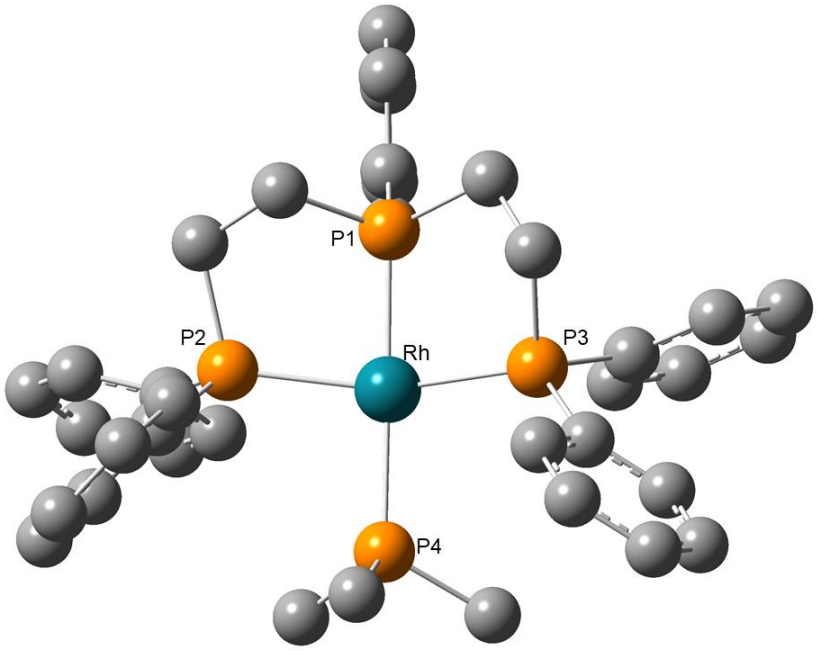

Figure A21. *Optimized structure of [Rh(PP$_2$)(PMe$_3$)]$^+$. Hydrogen atoms, other than the metal hydrides have been omitted.*

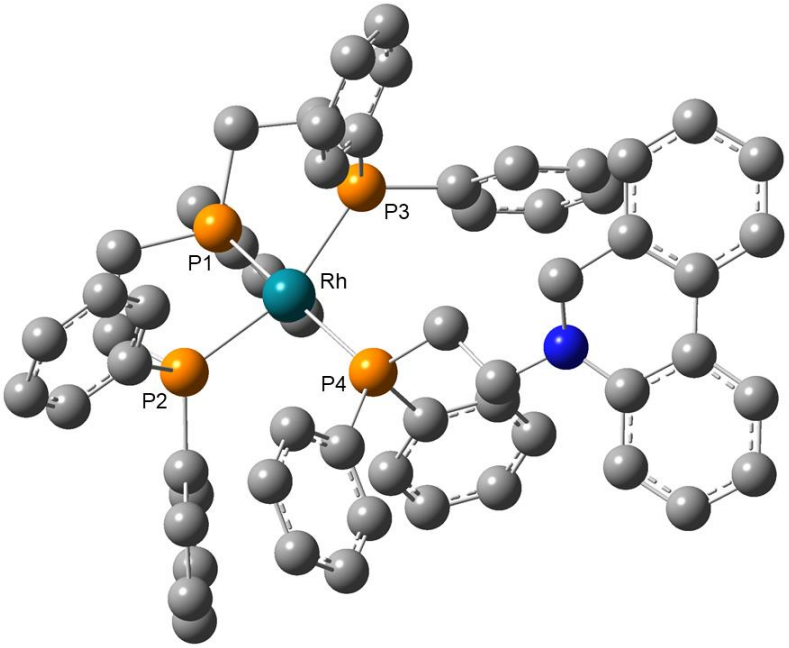

Figure A22. *Optimized structure of [Rh(PP$_2$)(L^{PhenH})]$^+$. Hydrogen atoms, other than the metal hydrides have been omitted.*

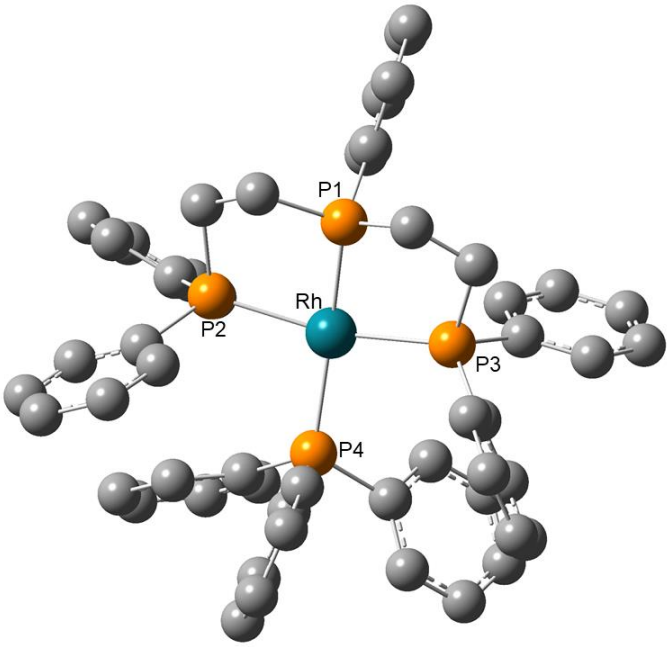

Figure A23. *Optimized structure of $[Rh(PP_2)(PPh_3)]^+$. Hydrogen atoms, other than the metal hydrides have been omitted.*

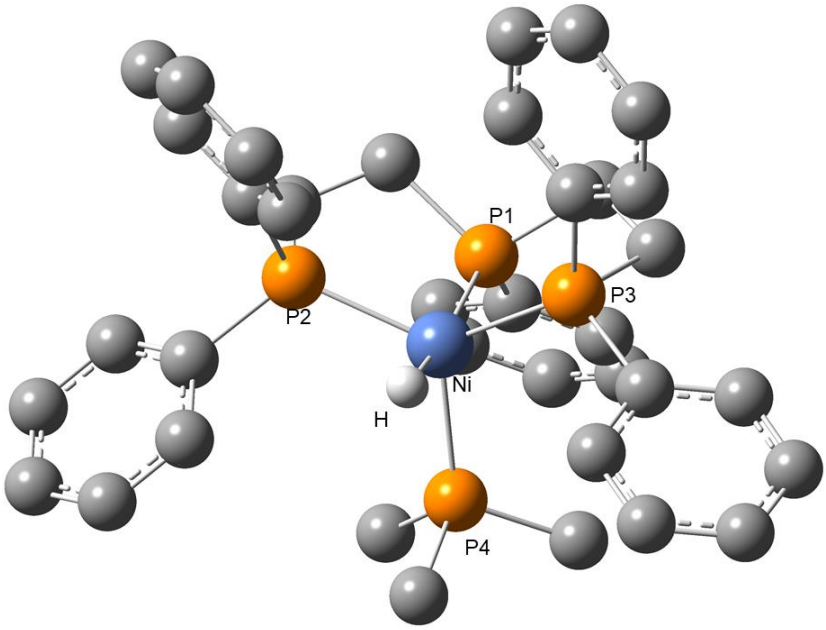

Figure A24. *Optimized structure of $[HNi(PP_2)(PMe_3)]^+$. Hydrogen atoms, other than the metal hydrides have been omitted.*

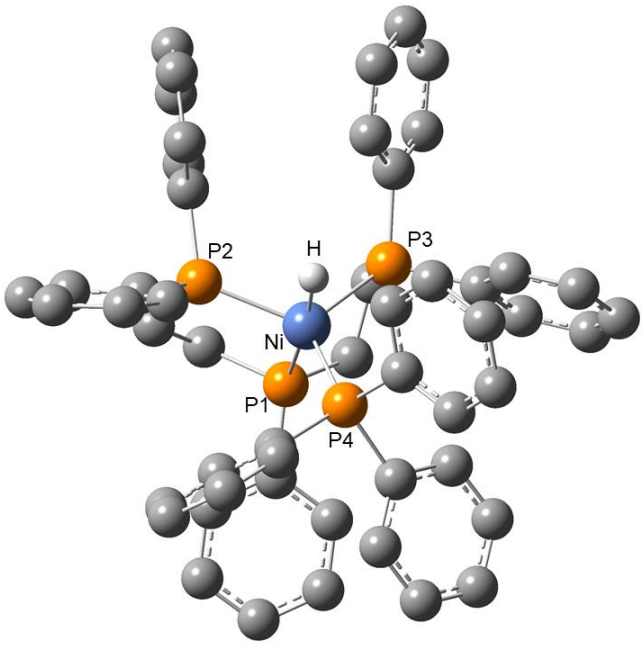

Figure A25. *Optimized structure of [HNi(PP$_2$)(PPh$_3$)]$^+$. Hydrogen atoms, other than the metal hydrides have been omitted.*

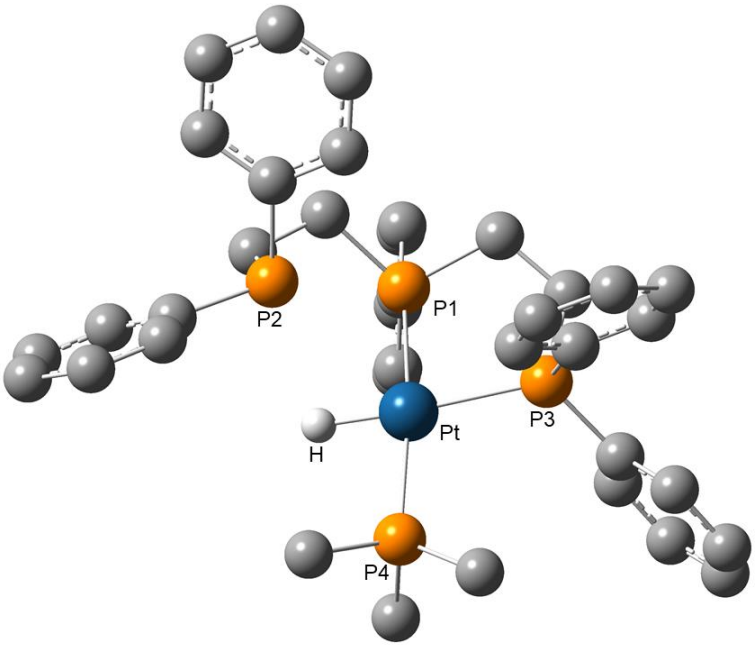

Figure A26. *Optimized structure of [HPt(PP$_2$)(PMe$_3$)]$^+$. Hydrogen atoms, other than the metal hydrides have been omitted.*

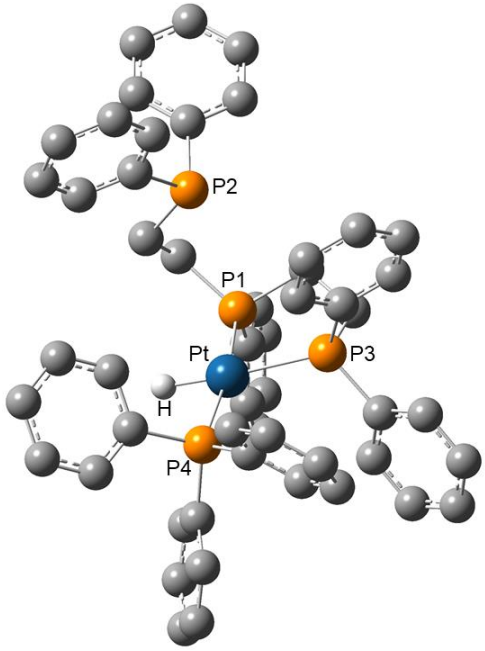

Figure A27. *Optimized structure of* $[HPt(PP_2)(PPh_3)]^+$. *Hydrogen atoms, other than the metal hydrides have been omitted.*

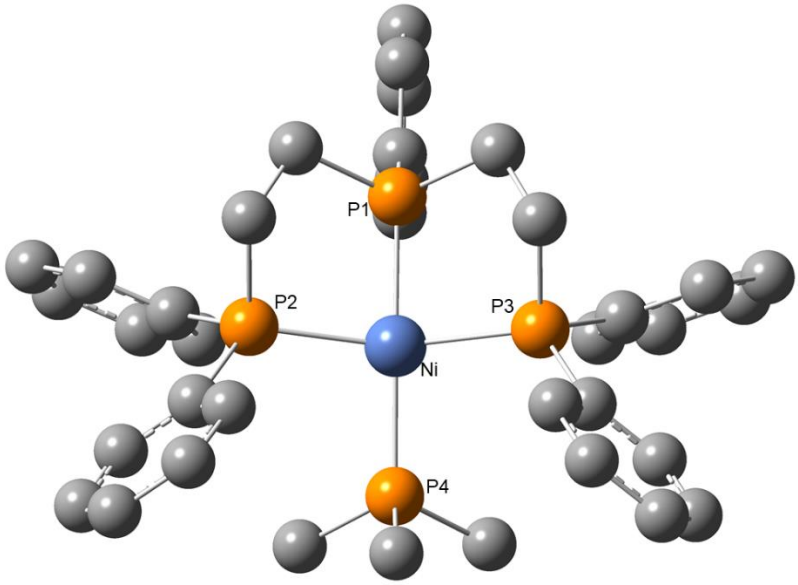

Figure A28. *Optimized structure of* $[Ni(PP_2)(PMe_3)]^{2+}$. *Hydrogen atoms, other than the metal hydrides have been omitted.*

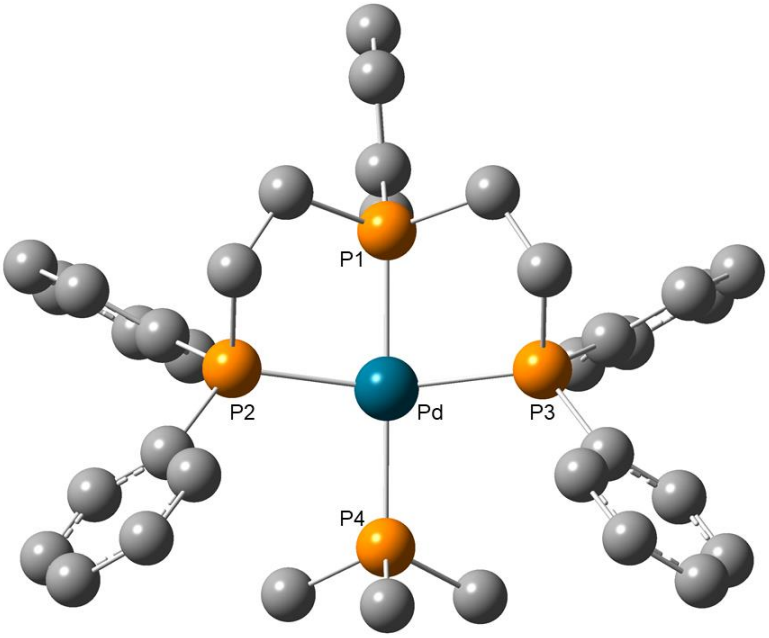

Figure A29. *Optimized structure of* $[Pd(PP_2)(PMe_3)]^{2+}$. *Hydrogen atoms, other than the metal hydrides have been omitted.*

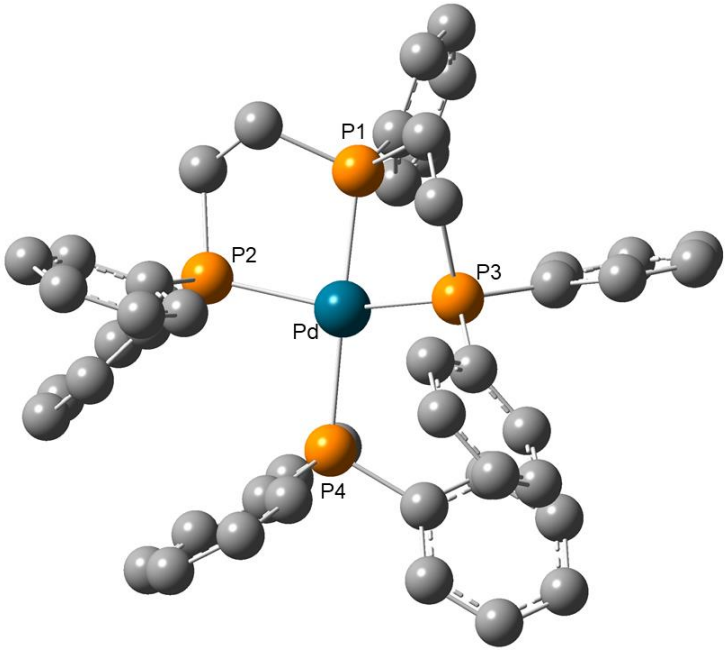

Figure A30. *Optimized structure of* $[Pd(PP_2)(PPh_2Et)]^{2+}$. *Hydrogen atoms, other than the metal hydrides have been omitted.*

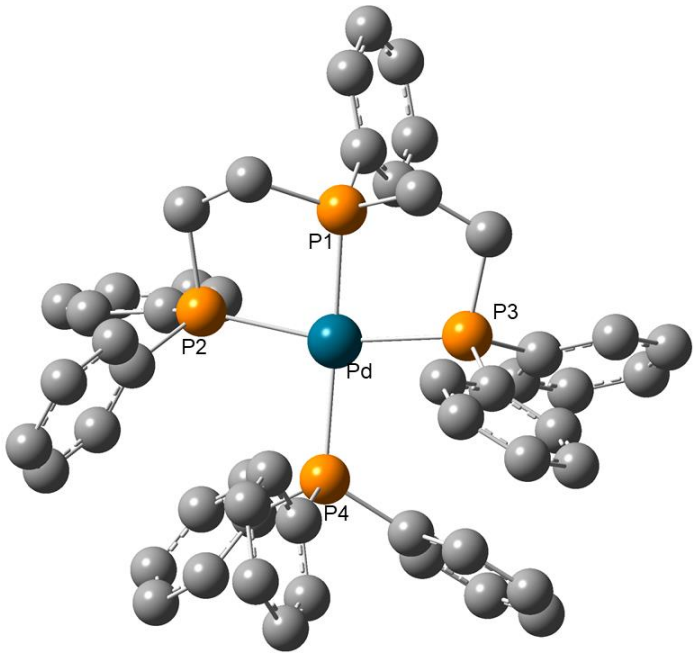

Figure A31. *Optimized structure of* $[Pd(PP_2)(PPh_3)]^{2+}$. *Hydrogen atoms, other than the metal hydrides have been omitted.*

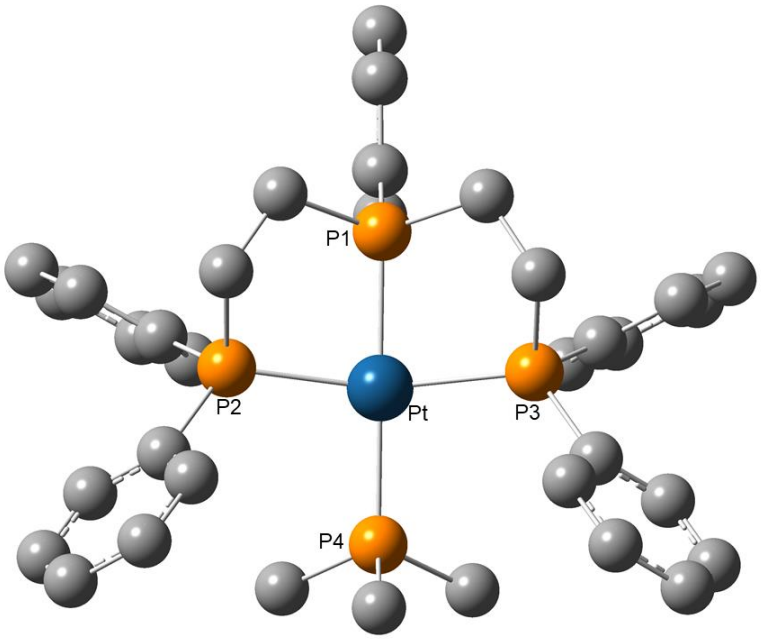

Figure A32. *Optimized structure of* $[Pt(PP_2)(PMe_3)]^{2+}$. *Hydrogen atoms, other than the metal hydrides have been omitted.*

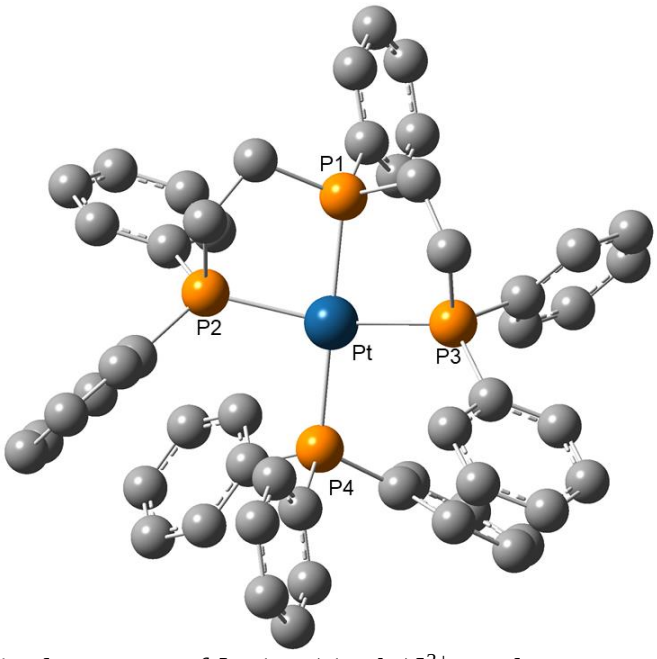

Figure A33. *Optimized structure of* $[Pt(PP_2)(PPh_3)]^{2+}$. *Hydrogen atoms, other than the metal hydrides have been omitted.*

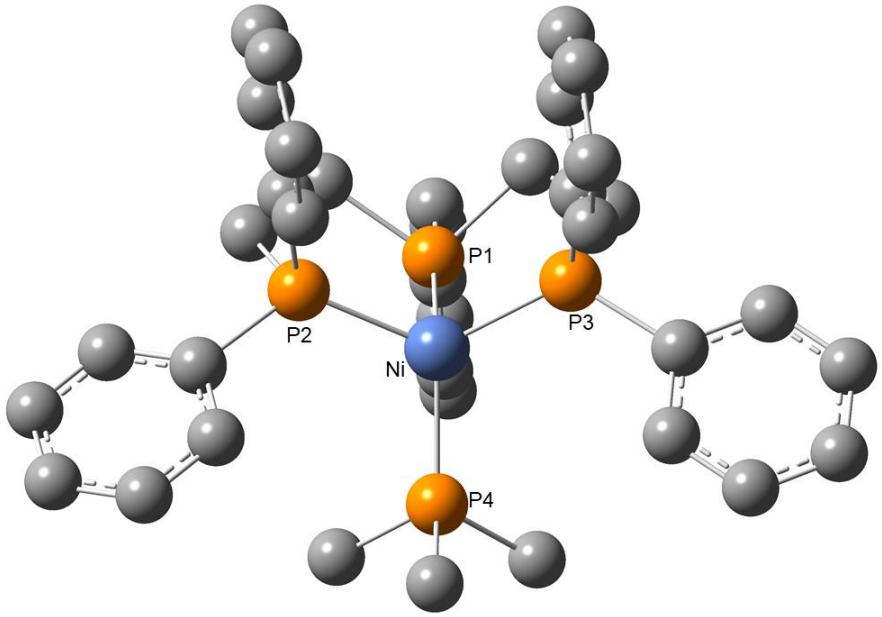

Figure A34. *Optimized structure of* $[Ni(PP_2)(PMe_3)]$. *Hydrogen atoms, other than the metal hydrides have been omitted.*

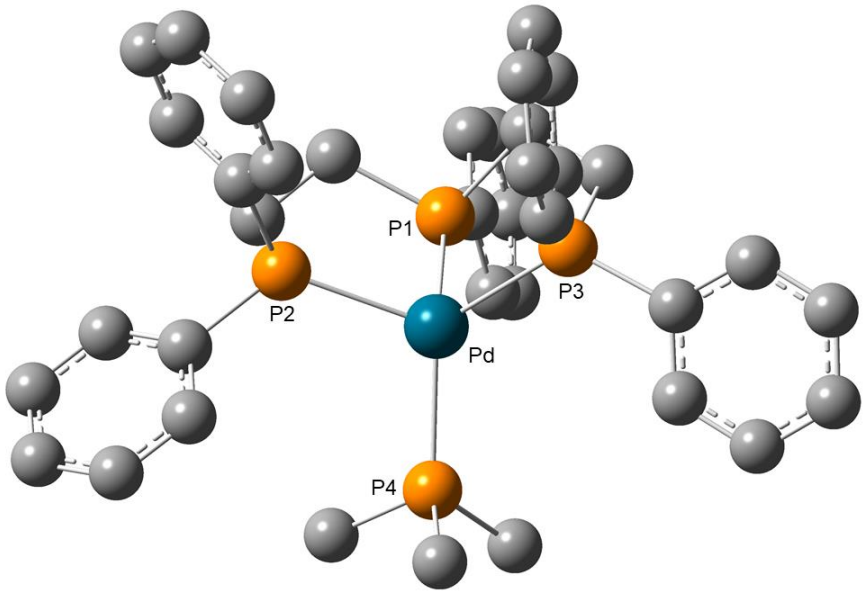

Figure A35. *Optimized structure of [Pd(PP$_2$)(PMe$_3$)]. Hydrogen atoms, other than the metal hydrides have been omitted.*

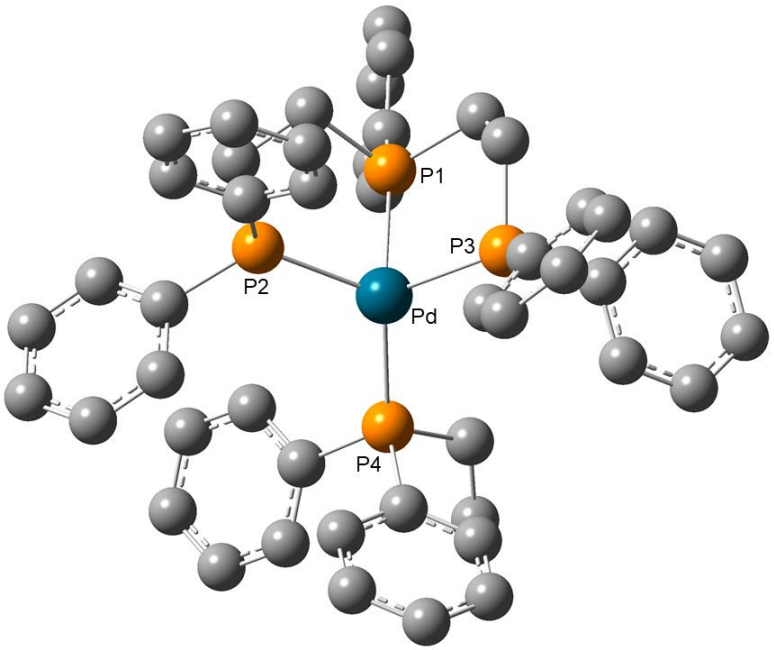

Figure A36. *Optimized structure of [Pd(PP$_2$)(PPh$_2$Et)]. Hydrogen atoms, other than the metal hydrides have been omitted.*

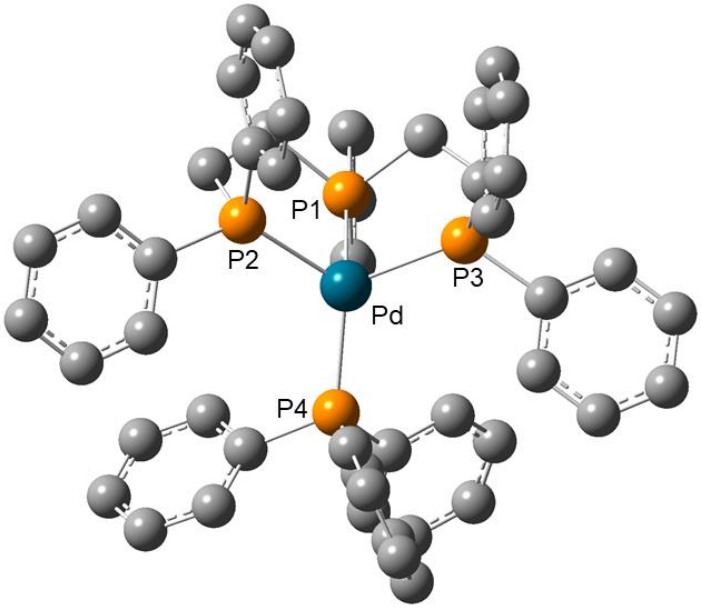

Figure A37. *Optimized structure of [Pd(PP$_2$)(PPh$_3$)]. Hydrogen atoms, other than the metal hydrides have been omitted.*

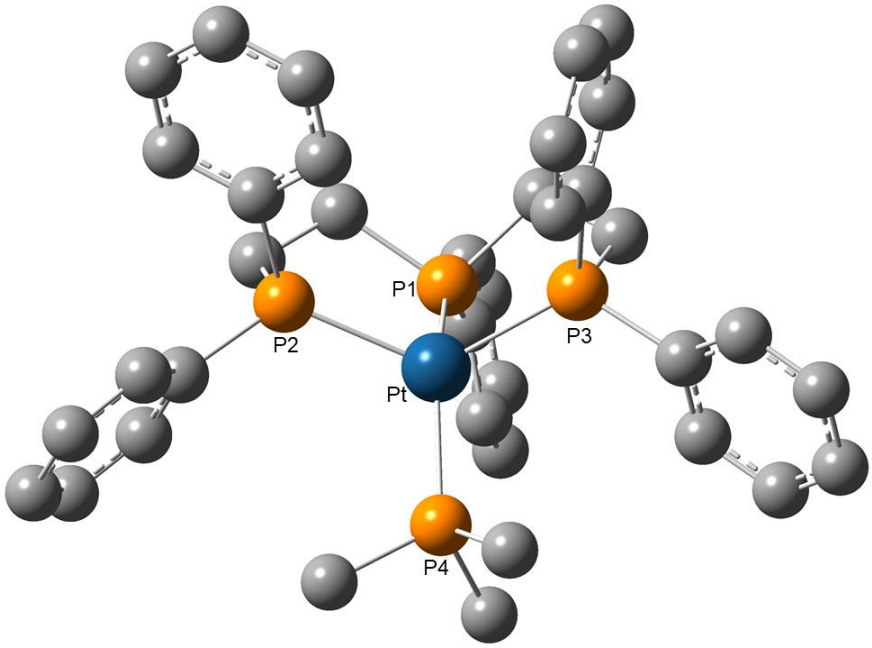

Figure A38. *Optimized structure of [Pt(PP$_2$)(PMe$_3$)]. Hydrogen atoms, other than the metal hydrides have been omitted.*

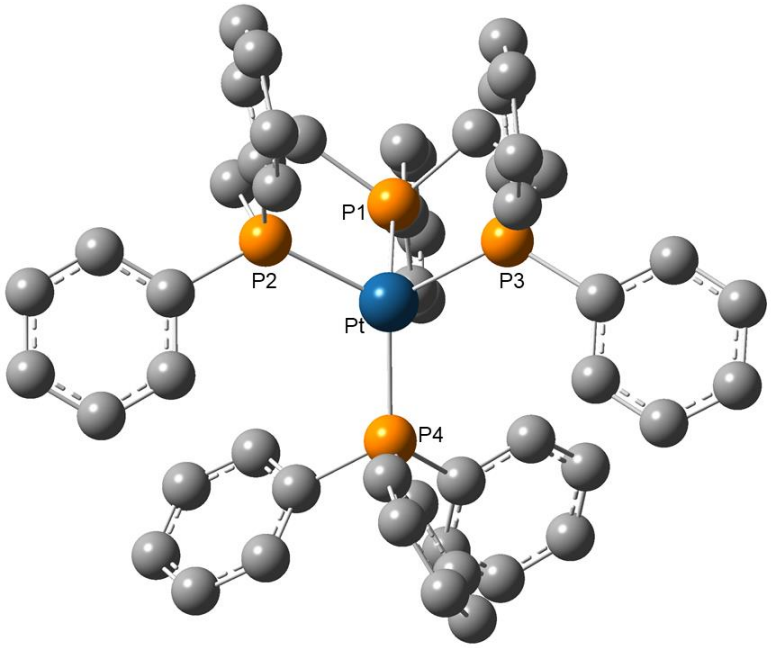

Figure A39. *Optimized structure of [Pt(PP$_2$)(PPh$_3$)]. Hydrogen atoms, other than the metal hydrides have been omitted.*

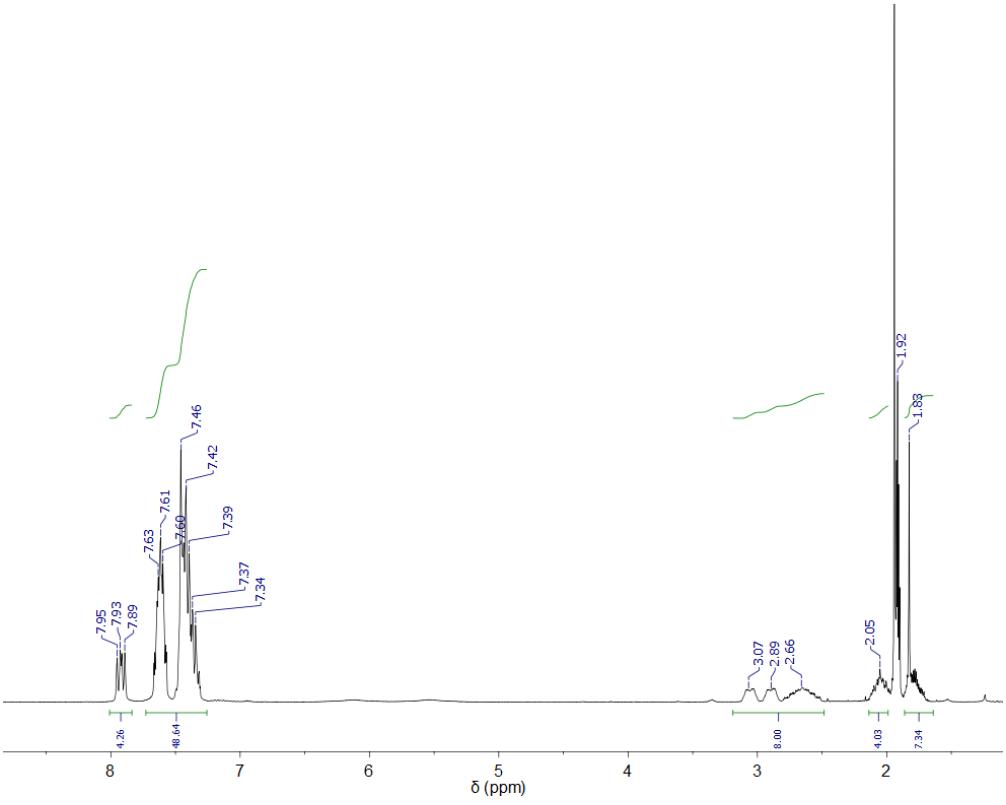

Figure A40. *^{1}H NMR spectrum of [Rh(PP$_2$)(MeCN)][BF$_4$] in CD$_3$CN (300 MHz)*

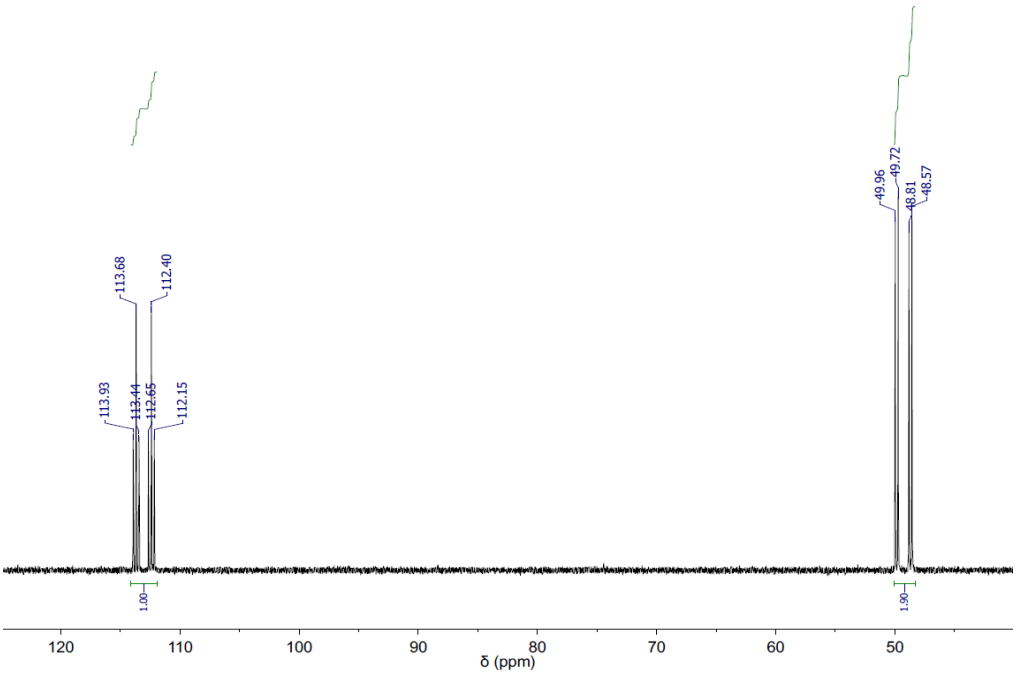

Figure A41. *^{31}P NMR spectrum of [Rh(PP$_2$)(MeCN)][BF$_4$] in CD$_3$CN (121 MHz)*

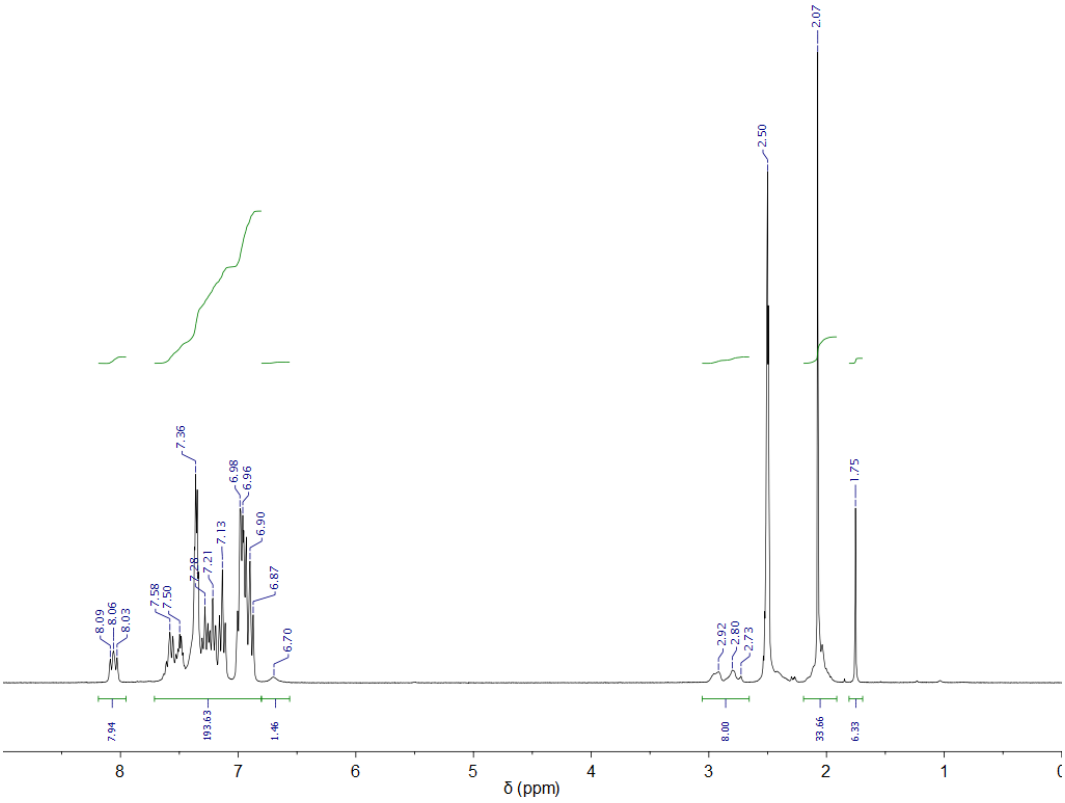

Figure A42. *^{1}H NMR spectrum of [Rh(PP$_2$)(PPh$_3$)][BF$_4$] in DMSO-d$_6$ (300 MHz)*

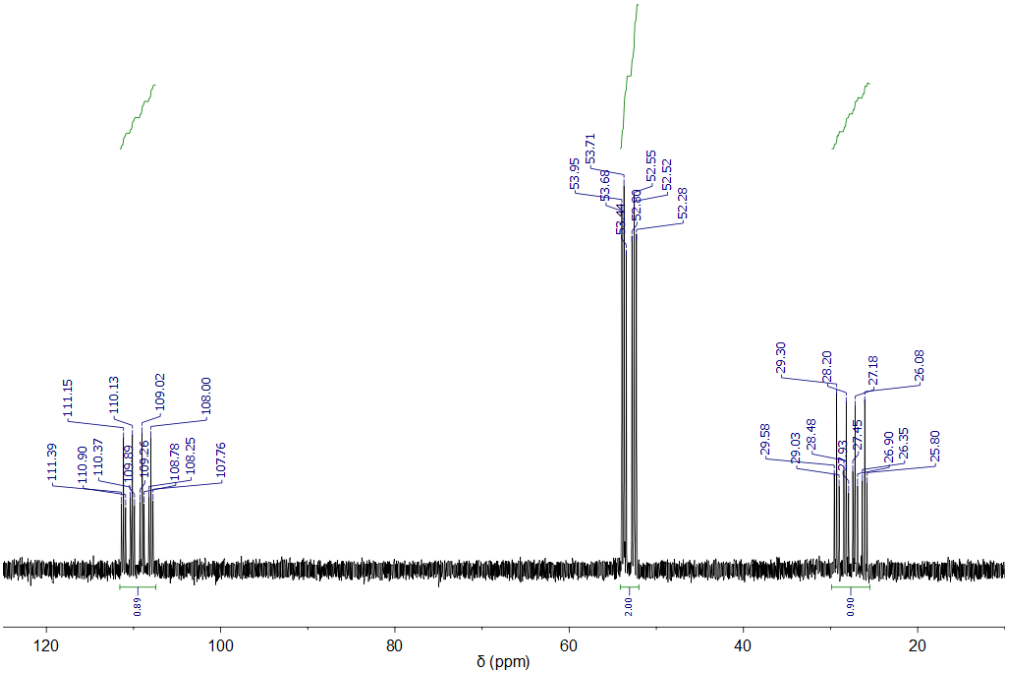

Figure A43. *^{31}P NMR spectrum of [Rh(PP$_2$)(PPh$_3$)][BF$_4$] in DMSO-d$_6$ (121 MHz)*

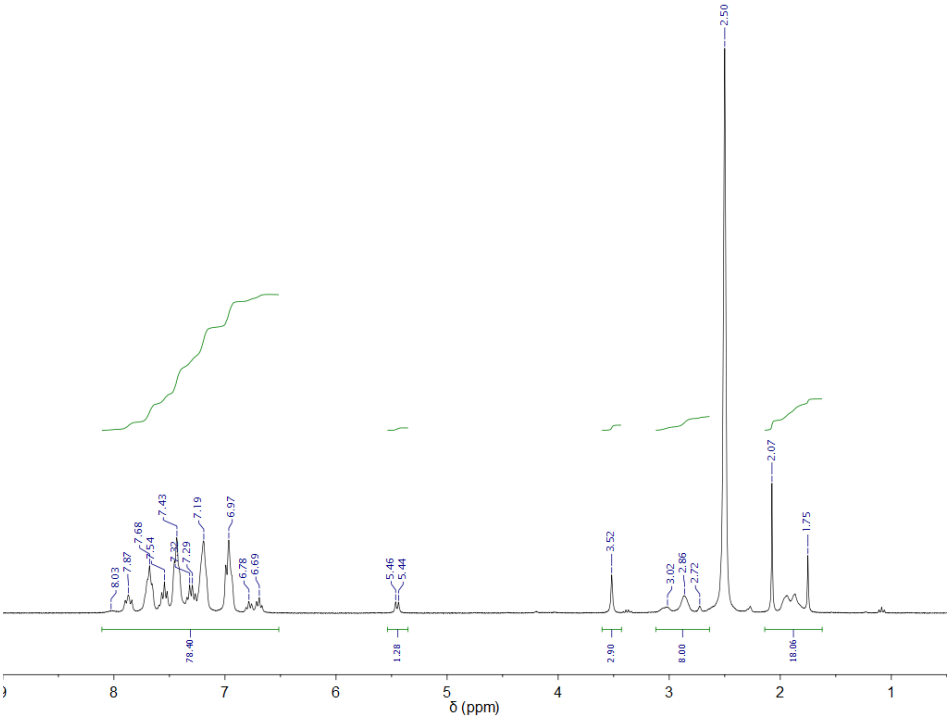

Figure A44. *^{1}H NMR spectrum of [Rh(PP$_2$)(L^{PhenH})][BF$_4$] in DMSO-d$_6$ (300 MHz)*

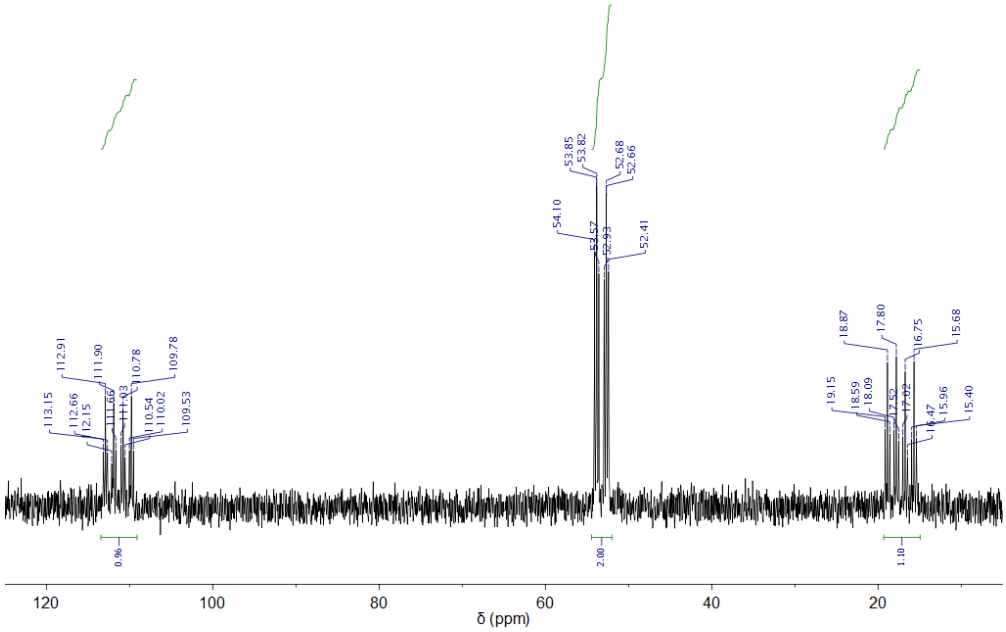

Figure A45. *^{31}P NMR spectrum of [Rh(PP$_2$)(L^{PhenH})][BF$_4$] in DMSO-d$_6$ (121 MHz)*

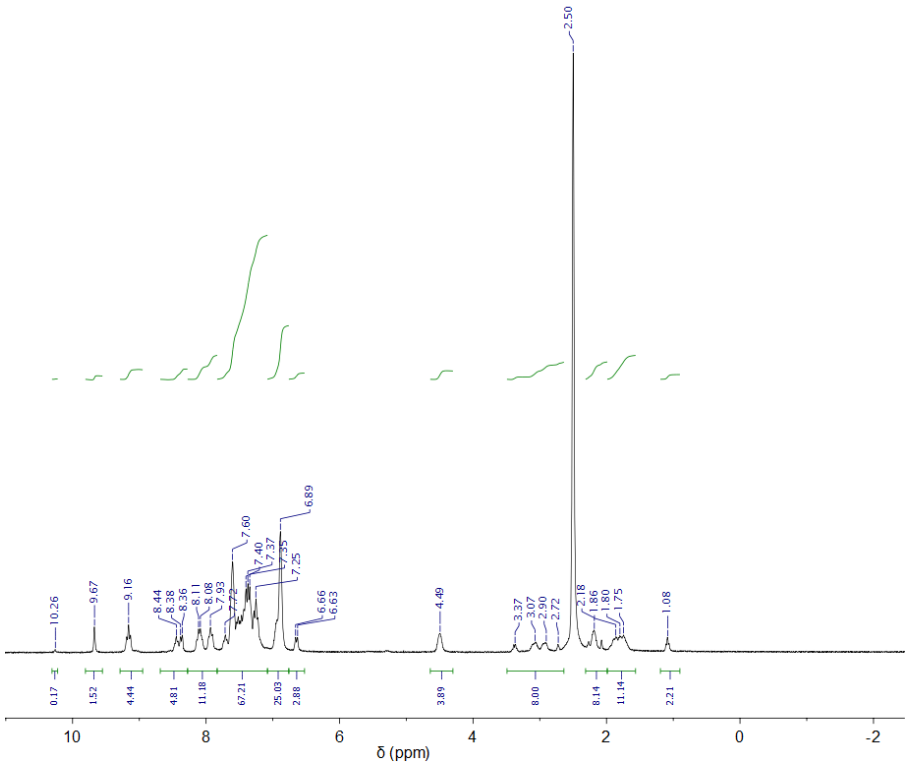

Figure A46. *^{1}H NMR spectrum of [Rh(PP$_2$)(L^{Phen+})][(SbF$_6$)(BF$_4$)] in DMSO-d$_6$ (300 MHz)*

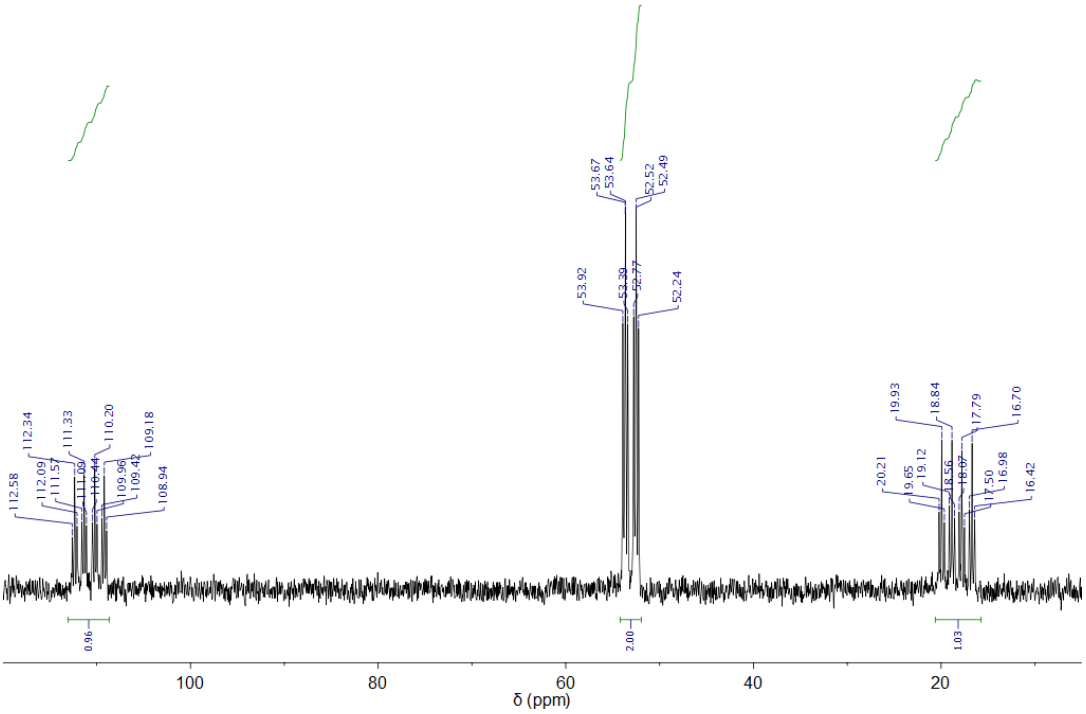

Figure A47. *^{31}P NMR spectrum of [Rh(PP$_2$)(L^{Phen+})][BF$_4$]$_2$ in DMSO-d$_6$ (121 MHz)*

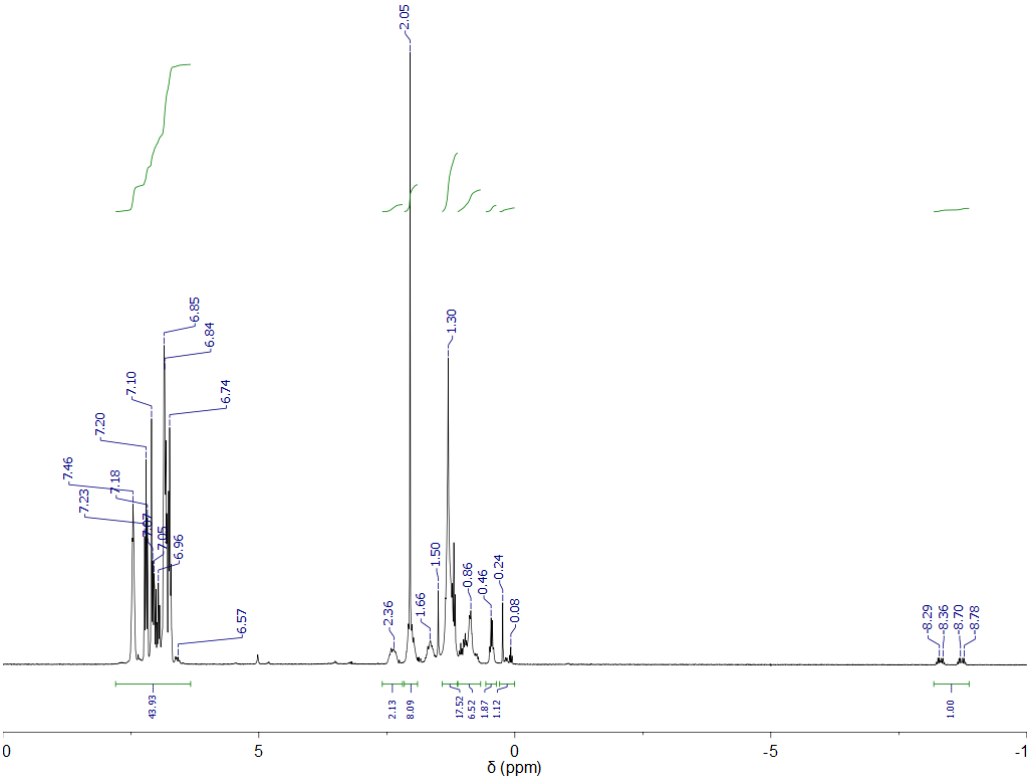

Figure A48. *^{1}H NMR spectrum of HRh(PP$_2$)(PPh$_3$) in C$_6$D$_6$ (300 MHz)*

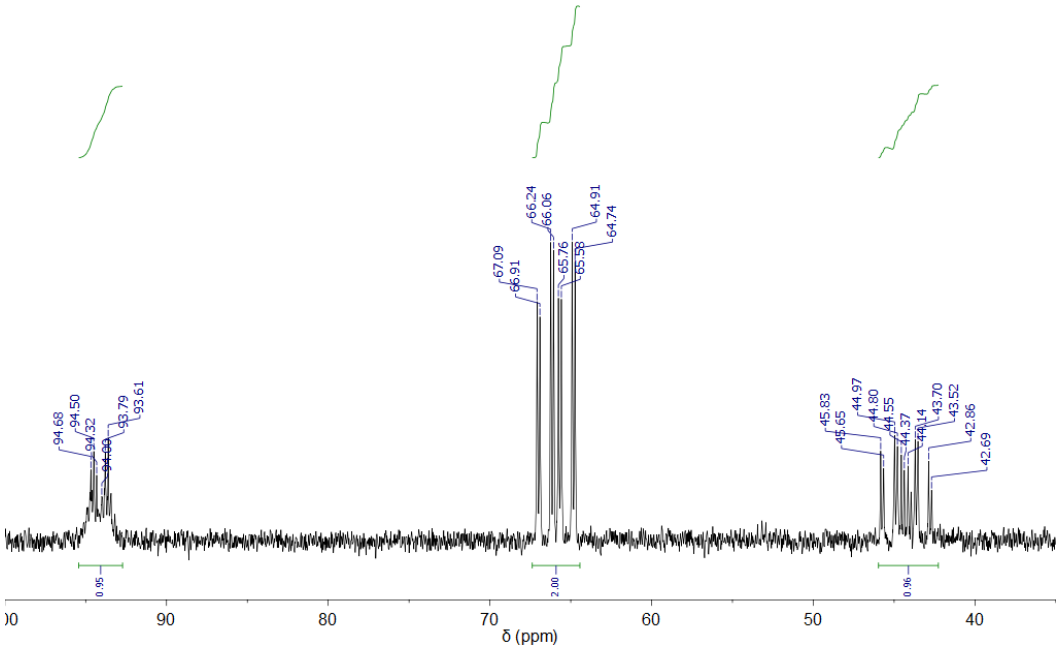

Figure A49. *^{31}P NMR spectrum of HRh(PP$_2$)(PPh$_3$) in C$_6$D$_6$ (121 MHz)*

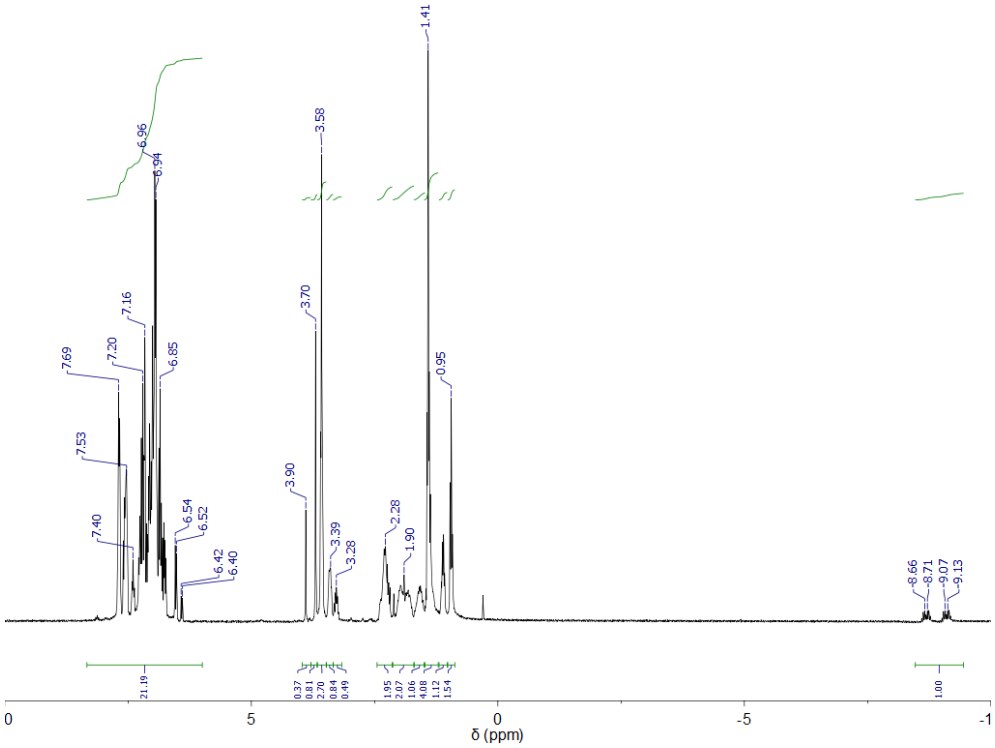

Figure A50. *^{1}H NMR spectrum of HRh(PP$_2$)(L^{PhenH}) in C$_6$D$_6$ (300 MHz)*

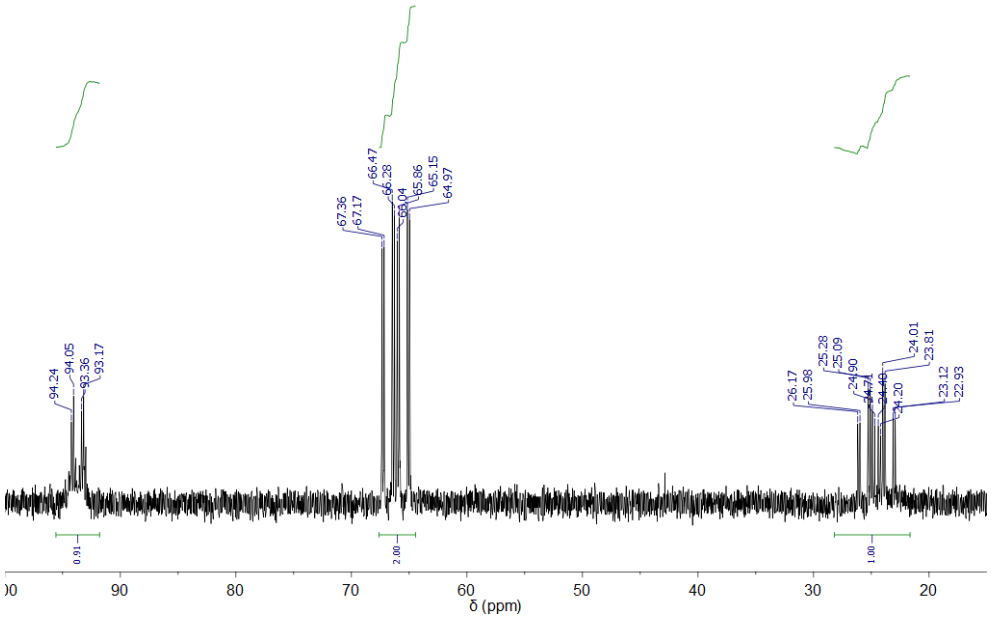

Figure A51. *^{31}P NMR spectrum of HRh(PP$_2$)(L^{PhenH}) in C$_6$D$_6$ (121 MHz)*

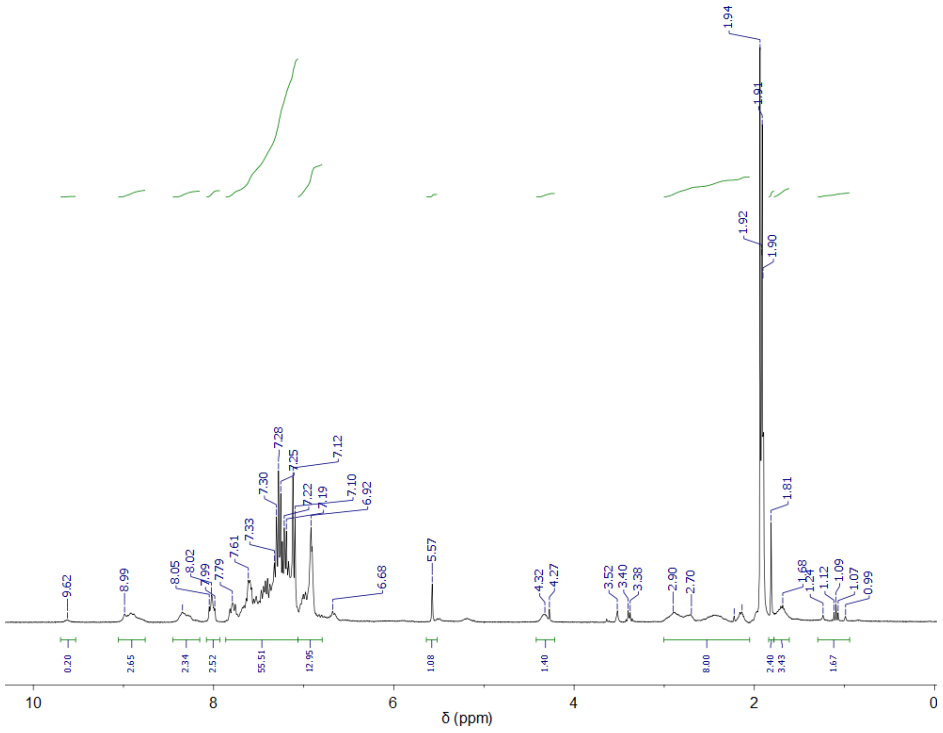

Figure A52. *^{1}H NMR spectrum for the reaction between [Rh(PP$_2$)(L^{PhenH})][SbF$_6$] and CPh$_3$(BF$_4$) in CD$_3$CN (300 MHz)*

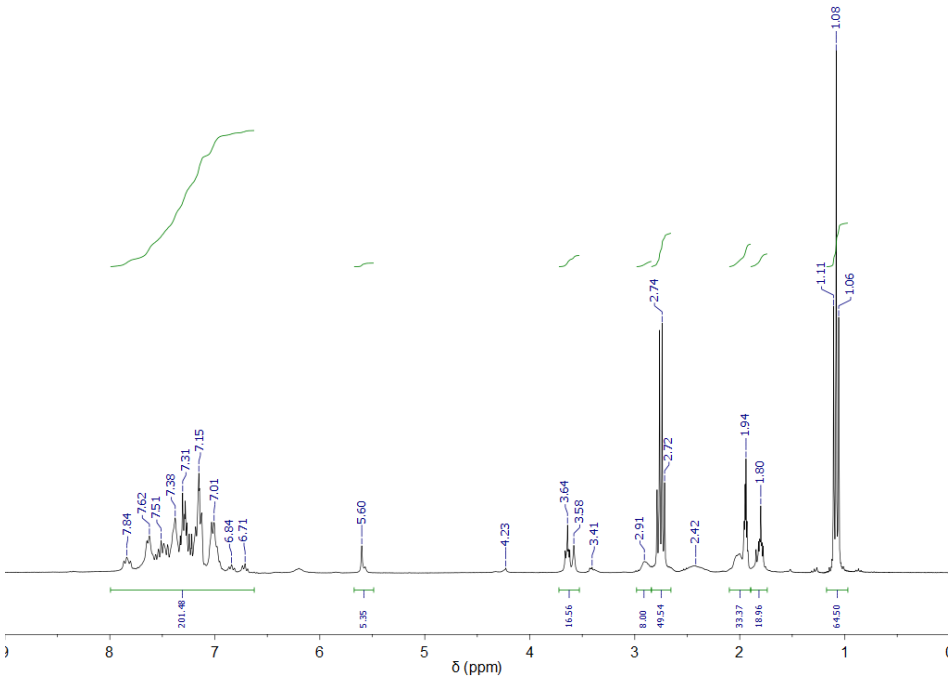

Figure A53. *^{1}H NMR spectrum for the reaction between [Rh(PP$_2$)(L^{Phen+})][(SbF$_6$)(BF$_4$)] and NEt$_3$ under H$_2$ and CO$_2$ in CD$_3$CN (300 MHz)*

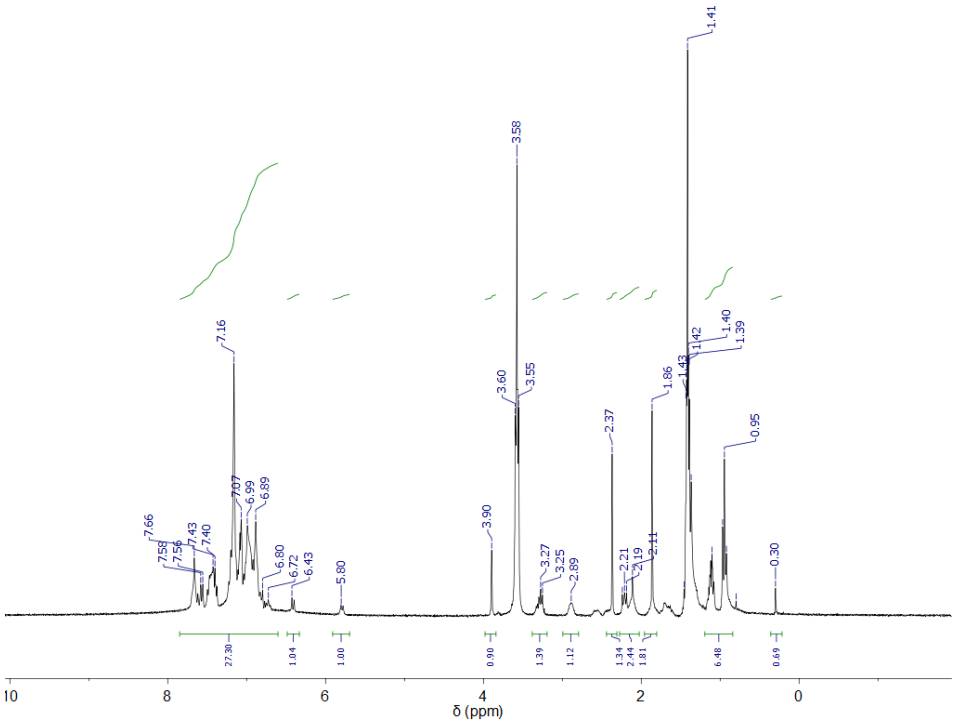

Figure A54. *^{1}H NMR spectrum for the reaction between HRh(PP$_2$)(L^{PhenH}) and H(DMF)OTf in C$_6$D$_6$ (300 MHz)*

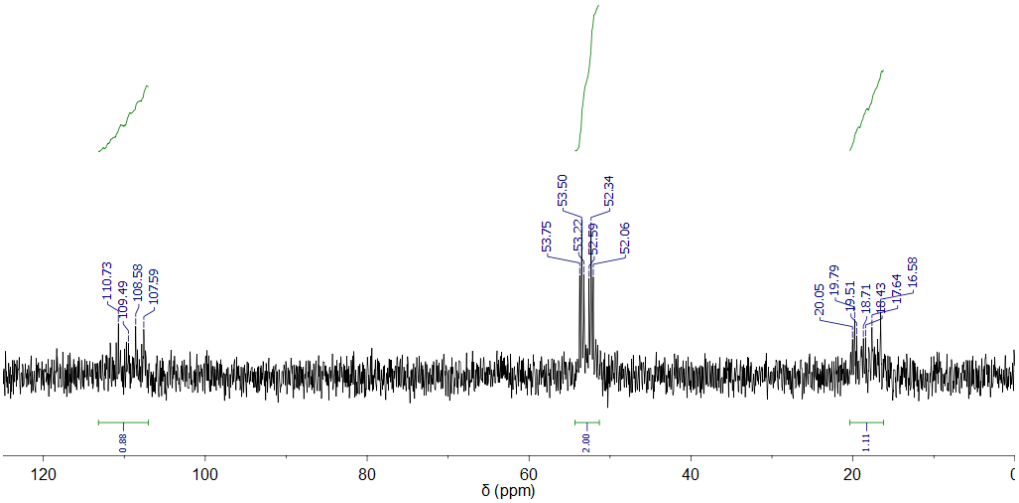

Figure A55. *^{31}P NMR spectrum for the reaction between HRh(PP2)(LPhenH) and H(DMF)OTf (121 MHz)*

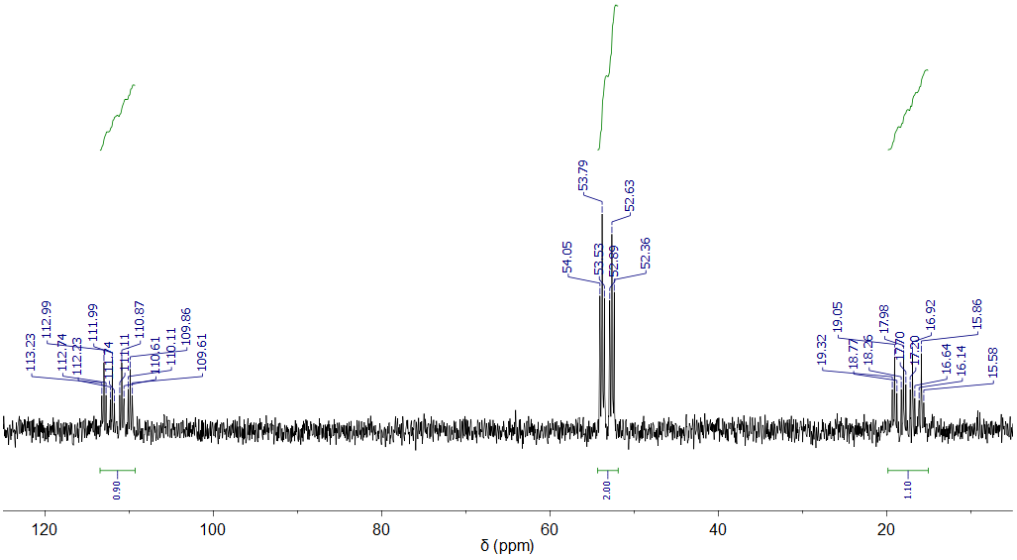

Figure A56. *^{31}P NMR spectrum for the reaction between [Rh(PP$_2$)(L^{PhenH})][BF$_4$] and H(DMF)OTf in 50% C$_6$D$_6$ and 50% DMSO-d$_6$ (121 MHz)*

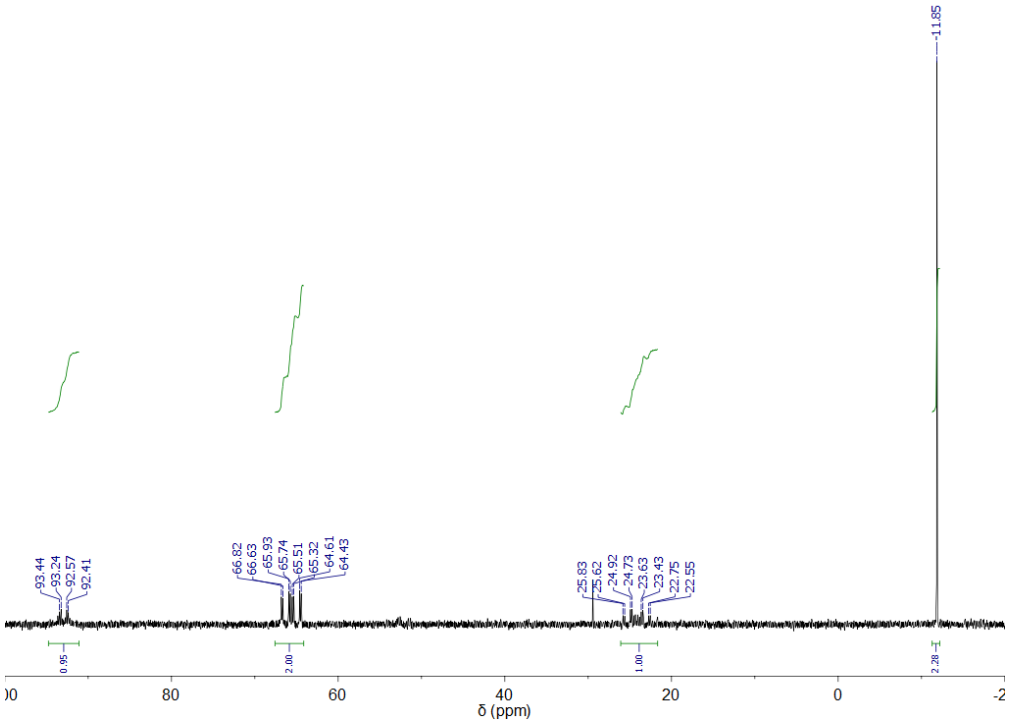

Figure A57. *^{31}P NMR spectrum for the reaction between [Rh(PP$_2$)(L^{PhenH})][SbF$_6$] and Verkade's base under H$_2$ and CO$_2$ in DMSO-d$_6$ (121 MHz)*

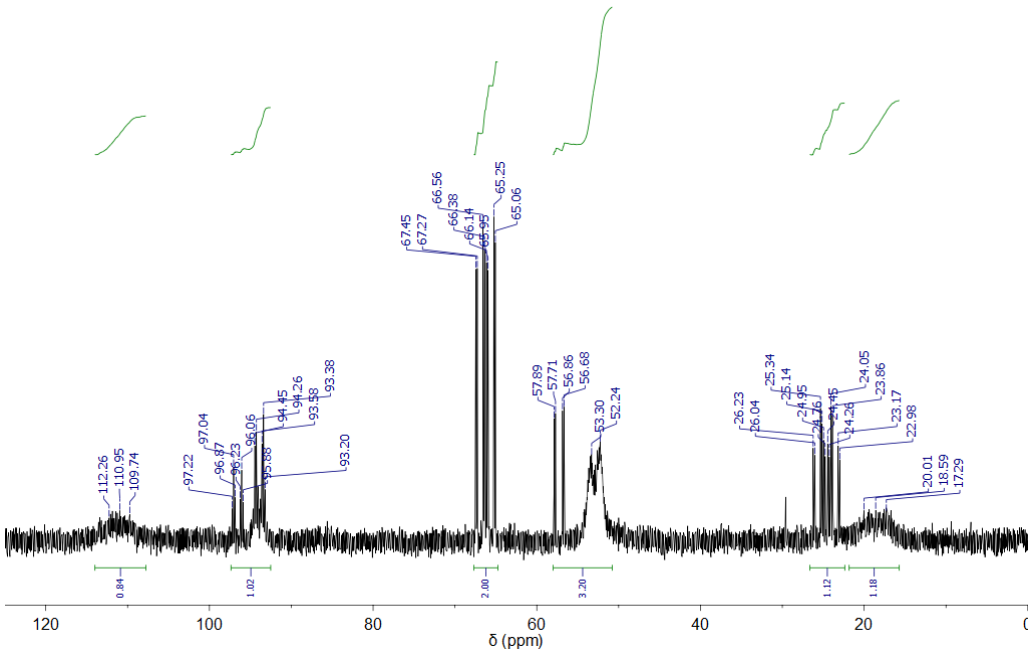

Figure A58. *^{31}P NMR spectrum for the reaction between [Rh(PP$_2$)(L^{PhenH})][SbF$_6$] and LiO^{t}Bu under H$_2$ in THF (121 MHz)*

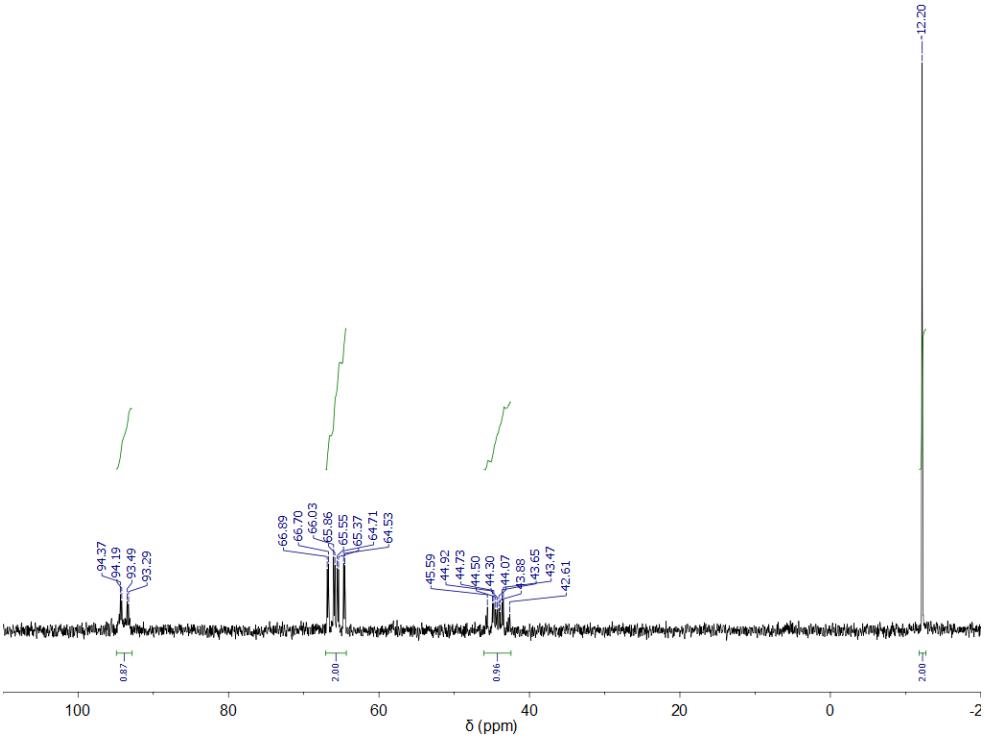

Figure A59. *^{31}P NMR spectrum for the reaction between [Rh(PP$_2$)(PPh$_3$)][BF$_4$] and Verkade's base under H$_2$ in THF (121 MHz)*

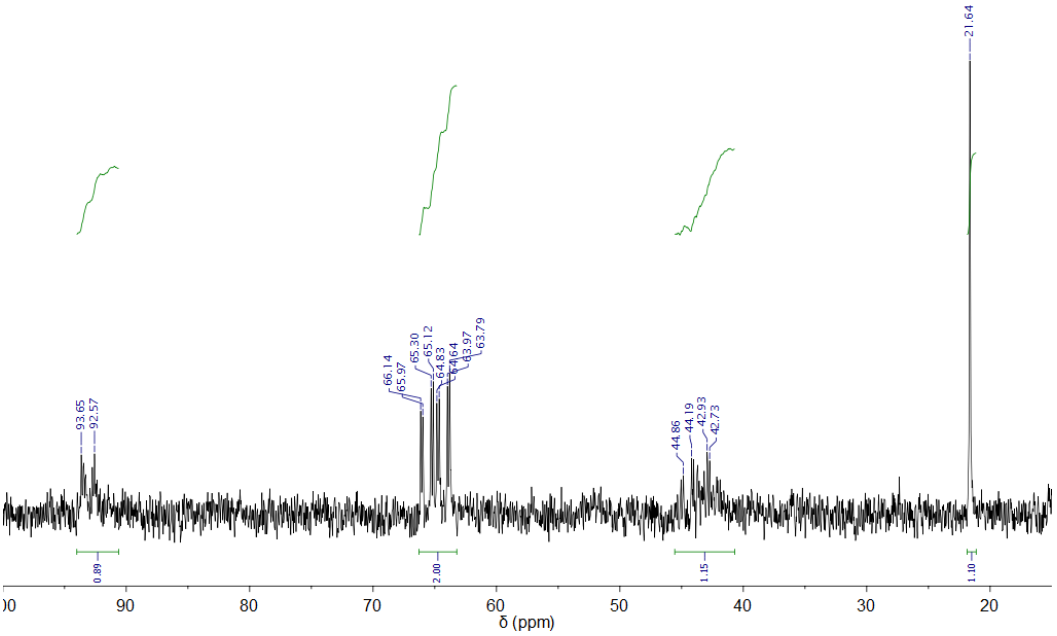

Figure A60. *^{31}P NMR spectrum for the reaction between [Rh(PP$_2$)(PPh$_3$)][BF$_4$] and P$_1$^{t}Bu under H$_2$ in THF (121 MHz)*

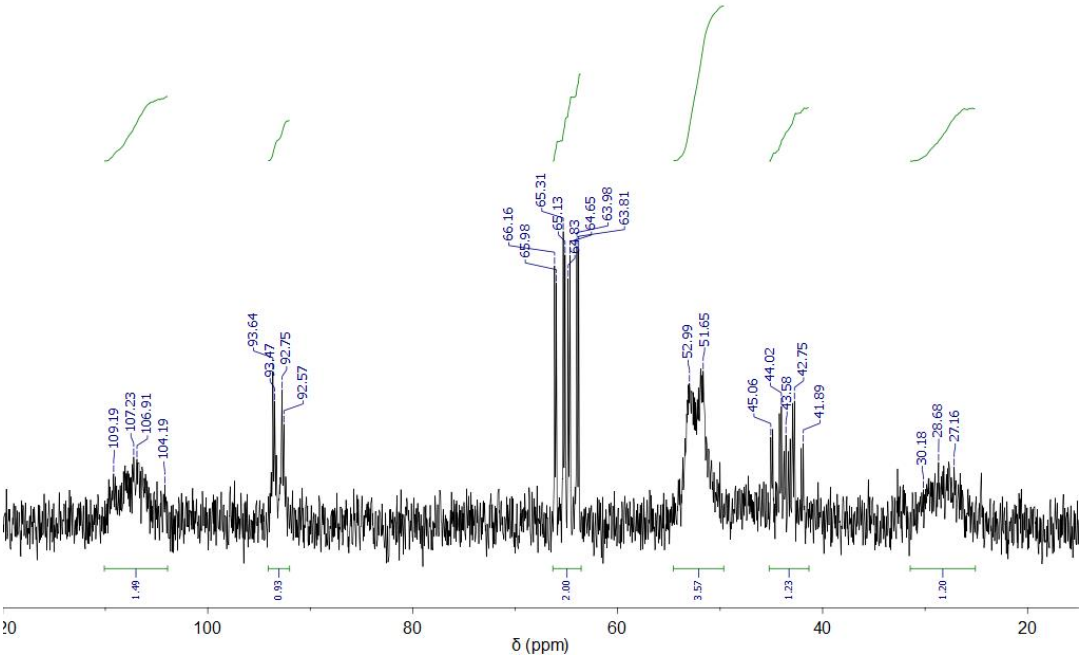

Figure A61. *^{31}P NMR spectrum for the reaction between [Rh(PP$_2$)(PPh$_3$)][BF$_4$] and LiO^{t}Bu under H$_2$ in THF (121 MHz)*

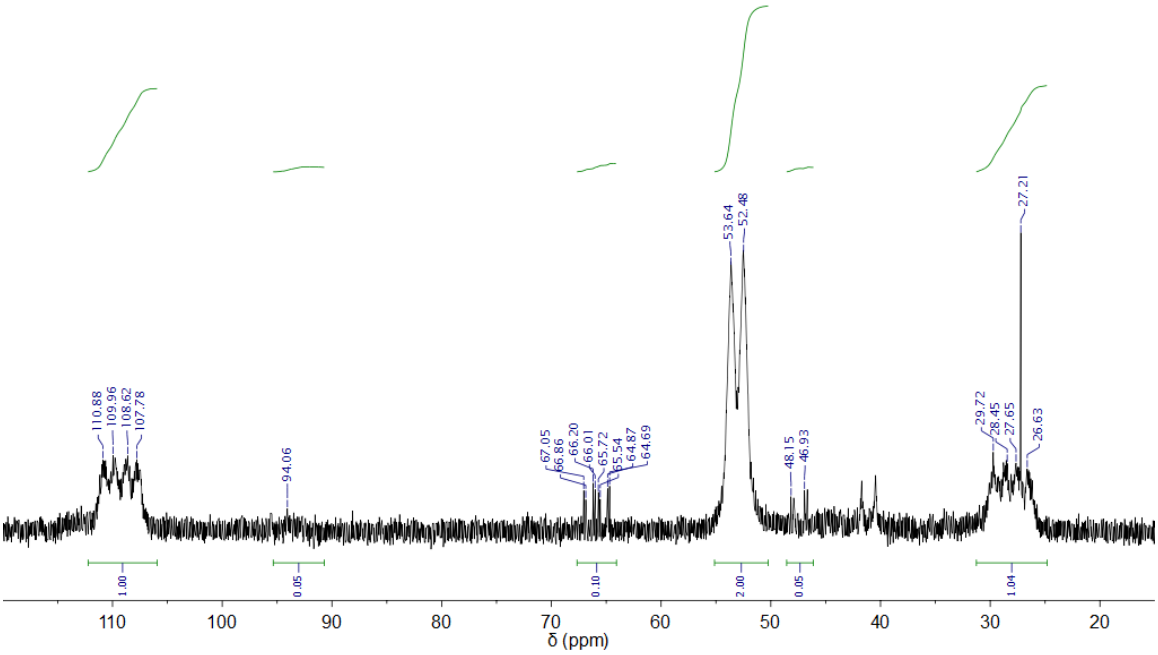

Figure A62. *^{31}P NMR spectrum for the reaction between [Rh(PP$_2$)(PPh$_3$)][BF$_4$] and DBU under H$_2$ in acetonitrile (121 MHz)*

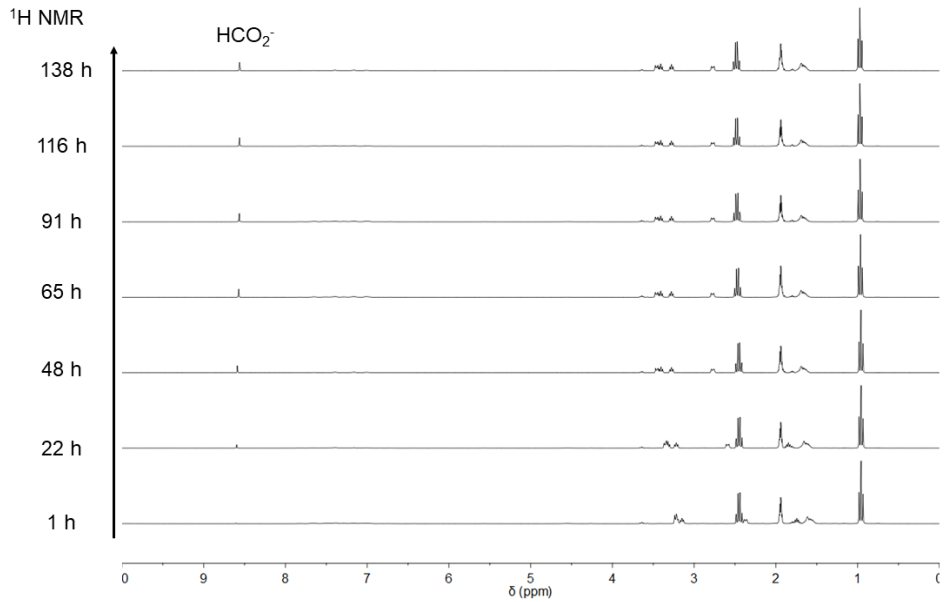

Figure A63. *Stacked ^{1}H NMR spectra for the reaction between [Rh(PP$_2$)(L^{PhenH})][SbF$_6$] and DBU under H$_2$ and CO$_2$ in CD$_3$CN (300 MHz)*

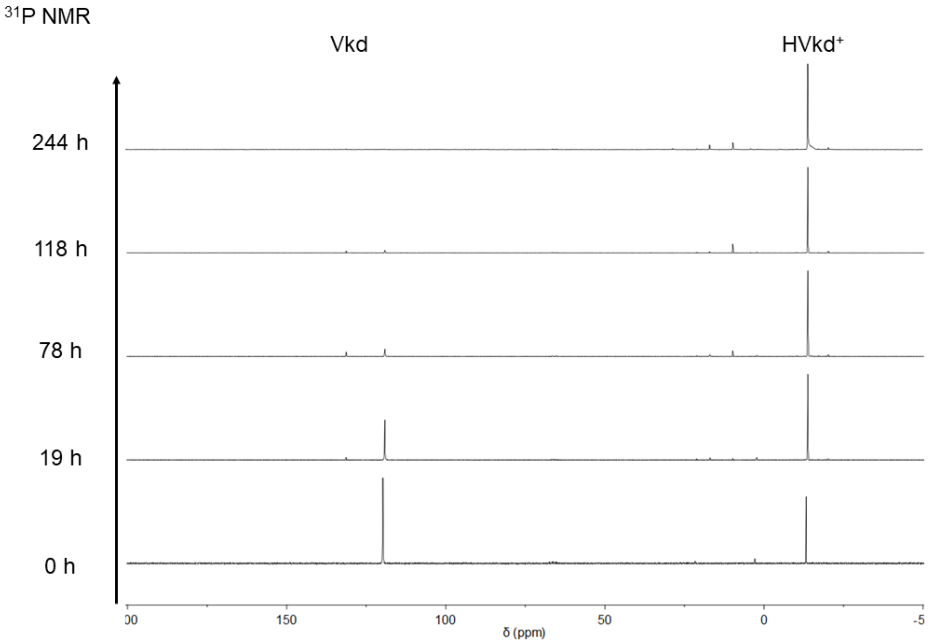

Figure A64. *Stacked ^{31}P NMR spectra for the reaction between [Rh(PP$_2$)(L^{PhenH})][BF$_4$] and Verkade's base under H$_2$ and CO$_2$ in THF (121 MHz)*

VITA

William Fernandez

EDUCATION

- M.S. student in Chemistry at Sam Houston State University, August 2018 – present. Thesis title: "Thermodynamic studies of hydride- and proton-donor abilities of heteroleptic transition metal complexes containing triphosphine and monophosphine ligands."

- Bachelor of Science (May 2018) in Chemistry, Sam Houston State University, Huntsville, Texas.

ACADEMIC EMPLOYMENT

- Graduate Teaching Assistant, Department of Chemistry, Sam Houston State University, May 2018 – present. Responsibilities include assisting professors with the preparation and presentation of undergraduate courses, grading and tutoring.

- Graduate Laboratory Assistant, Department of Chemistry, Sam Houston State University, May 2018 – present. Responsibilities include preparation of chemicals to be used for educational purposes and safe disposal and cleanup of used chemicals.

- Research Assistant to C. M. Zall, Department of Chemistry, Sam Houston State University, Fall 2018 – present. Research activities include researching the synthesis of mixed triphosphine/monophosphine rhodium complexes and finding optimal intermediates through computational study. Characterization of these complexes using multinuclear NMR spectroscopy and X-Ray diffraction.

PRESENTATIONS AT PROFESSIONAL MEETINGS

- W. Fernandez, D. L. Williams, C. M. Zall. "Structural and reactivity studies of rhodium hydrides containing mixed triphosphine and monophosphine ligands" Presented at the American Chemical Society (ACS) Southwest-Rocky Mountain Regional Meeting at El Paso, Texas, 11–15 November 2019. (Presented by W. Fernandez)
- W. Fernandez, D. L. Williams, C. M. Zall. *"Thermodynamic hydricities and acidities of transition metal hydrides containing mixed triphosphine and monophosphine ligands"* Presented at the 257th American Chemical Society National Meeting & Expo at Orlando, Florida, 31 March-3 April 2019. (Presented by W. Fernandez)
- I. Almaguer, A. Bui, W. Fernandez, and A. Villalta-Cerdas. *"Design of cooperative, project-based laboratory experiences to promote understanding of stoichiometry in college-level General Chemistry courses"* Presented at the 25th

Biennial Conference on Chemical Education, University of Notre Dame at South Bend, Indiana, 29 July-2 August 2018. (Presented by A. Bui)

- A. Bui, W. Fernandez, I. Almaguer, and A. Villalta-Cerdas. *"Design of cooperative, project-based laboratory experiences to promote understanding of stoichiometry in college-level General Chemistry courses"* Presented at the 11th Annual Undergraduate Research Symposium, Sam Houston State University, Huntsville, Texas, 28 April 2018. (Presented by W. Fernandez)
- A. Bui, W. Fernandez, I. Almaguer, and A. Villalta-Cerdas. *"Design of cooperative, project-based laboratory experiences to promote understanding of stoichiometry in college-level General Chemistry courses"* Presented at the 255th American Chemical Society National Meeting & Expo at New Orleans, Los Angeles , 18-22 March 2018. (Presented by W. Fernandez)
- C. M. Zall, N. Devi, and W. Fernandez. *"Incorporation of NADH-like hydride Relays Into Metal-Phosphine Catalysts for CO_2 Hydrogenation"* Presented at the 255th American Chemical Society National Meeting & Expo at New Orleans, LA, March 18-22, 2018. (Presented by C. M. Zall)

FELLOWSHIPS/AWARDS

- College of Science and Engineering Technology Graduate Achievement Scholarship, Sam Houston State University, Fall 2018, Spring 2019, Fall 2019, and Spring 2020
- Graduate Travel Fund, Sam Houston State University, Spring 2018
- Robert A. Welch Summer Fellowship, Summer 2017 and Summer 2018

PROFESSIONAL MEMBERSHIP

- American Chemical Society: Graduate student member